UNIVERSITY OF BELGRADE

FACULTY OF TECHNOLOGY AND METALLURGY

Aysha Ali Ahribesh

Synthesis, characterization and application of magnetic adsorbents based on sepiolite and zeolite

Doctoral Dissertation

Belgrade, 2017

UNIVERZITET U BEOGRADU

TEHNOLOŠKO-METALURŠKI FAKULTET

Aysha Ali Ahribesh

Sinteza, karakterizacija i primena magnetnih adsorbenata na bazi sepiolita i zeolita

doktorska disertacija

Beograd, 2017

Supervisor

Dr Rada Petrović, Professor

University of Belgrade, Faculty of Technology and Metallurgy

Committee Members

Dr Đorđe Janaćković, Professor
University of Belgrade, Faculty of Technology and Metallurgy

Dr Jelena Rogan, Associate Professor
University of Belgrade, Faculty of Technology and Metallurgy

Dr Slavica Lazarević, Research Associate
University of Belgrade, Faculty of Technology and Metallurgy

Dr Ljiljana Živković, Research Professor
University of Belgrade, Vinča Institute of Nuclear Sciences

Date of Defense:

Acknowledgements

First, thanks to Allah, whom, with his willing I am grateful for the opportunity to complete my thesis.

Also, I would like to express my deep sense of gratitude to my Thesis supervisor Prof. Dr. Rada Petrović for her permanent support, trust, precious advices and suggestions throughout this study. It was a great honor and pleasure to know her and to work with her.

I am also grateful to all members of the Department of Inorganic Chemical Technology.
I would also like to thank all my Professors who taught me at this faculty. I would like to express my great indebtedness to all my family, especially to my mother for her continuous support and encouragement. I like to convey many thanks to my father, my brother Milad.

I owe my loving thanks to my husband Abdelbast and my kids, Yusuf, Sarah and Nor. They have lost a lot, due to my research abroad. Without their encouragement and understanding, it would have been impossible for me to finish this work.

Finally, thanks to all of my friends, and everyone for their contribution by supporting my work.

Aysha Ali Ahribesh

List of figures

List of tables

Synthesis, characterization and application of magnetic adsorbents based on sepiolite and zeolite

Abstract

Magnetic nano-composite adsorbents have been attracting extensive attention recently owing to facilely recovering from liquid phases using an external magnetic field, which reduces the operational costs as compared with filtration and centrifugation. The magnetic composites are usually synthesized by deposition of magnetic nano-particles on a support, which should provide good dispersibility of the particles, preventing their agglomeration. In this dissertation, natural sepiolite (SEP), partially acid-activated sepiolite (ASEP), and natural zeolite (NZ) were used as supports to synthesize the magnetic nano-composites (MNCs) for the removal of Cd^{2+}, Cr(VI), phosphate and dyes (Reactive Orange 16 and Basic Yellow 28) from water. The goal of the dissertation was to analyze the influence of different synthesis conditions on the properties of the composites in order to obtain efficient magnetically separable adsorbent. The synthesis was performed by co-precipitation of Fe^{3+} and Fe^{2+} ions by strong (NaOH) or weak (NH_3) base in the presence of NZ or SEP or ASEP, whereas the base was added before (procedure 1) or after (procedure 2) adding of Fe^{3+} and Fe^{2+} in the support suspension. In addition, the molar ration Fe^{2+}/Fe^{3+} and the quantity of iron salts were also varied.

It was shown that the concentration of hydroxyl ions in the suspensions could decrease due to the interactions with the support functional groups, that caused in some cases the precipitation of $Fe(OH)_3$ instead of the Fe^{3+}/Fe^{2+} co-precipitation and the magnetite formation. Because of the strong interactions of ASEP with hydroxyl ions, it was not possible to synthesize the MNCs when NaOH or NH_3 was added to the support suspension before Fe^{3+} and Fe^{2+} adding, but only when NH_3 was added in the suspension of ASEP having Fe^{3+} and Fe^{2+} ions. On the other hand, the magnetic

composites with SEP and NZ were successfully prepared by both procedures, using both bases.

The synthesized composites contained individual or aggregated magnetite crystalliites, sizes about 10 nm. Sepiolite/zeolite structures were preserved in the composites, although some alkali leaching was occurred when NaOH was used for co-precipitation. The dispersibility of the magnetite particles depends on the type of the supported material, the type of base and the sequence of reagents mixing, while the ratio Fe^{2+}/Fe^{3+} did not have a significant influence. The best dispersibility was achieved when NH_3 was added in the SEP or NZ suspension containing Fe^{2+}- and Fe^{3+}-ions. Regardless of higher specific surface area of ASEP in comparison to SEP, magnetite dispersibility in ASEP-based composites is lower than in SEP-based composite because of stronger bonds between sepiolite fibers. Nevertheless, the specific surface area of ASEP-based MNC is higher than of SEP-based MNC, obtained at the same conditions.

The MNCs obtained by using NH_3 (NH_3-MNCs) and NaOH (NaOH-MNCs) differ among themselves by the type of oxidation during heating and the quantity of magnetite. Lower quantity of magnetite in NH_3-MNCs samples in comparison to NaOH-MNCs samples, synthesized at the same content of Fe^{2+}- and Fe^{3+} ions, is explained by different quantity of iron(III)-oxide, formed during synthesis. Regardless of higher quantity of magnetite, magnetization of NaOH-MNCs is lower than of NH_3-MNCs, which is a result of the higher quantity of amorphous magnetite formed as a layer on the support surface. At room temperature, all the samples show superparamagnetic behavior, which ensures that the composites do not retain magnetization when the magnetic field is removed.

The adsorption capacities of the composites are much higher for cations than for anions owing to higher affinity of both support and magnetite for cations. The capacities of the MNCs for Cd^{2+} at initial pH = 7 were higher than of pure compounds, as a result of lower aggregation of the compounds in the MNCs which provided higher accessibility of the surface to the ions. The main mechanism of the adsorption is the formation of inner-sphere complexes. The composites prepared by using NaOH had higher adsorption capacities for Cd^{2+} than composites NH_3-MNCs, while all MNCs had higher capacity than the previously synthesized composites SEP/NZ-iron(III)-oxide. The adsorption capacity of the MNCs decreased during storage as a consequence of

oxidation. Regardless of the low capacity of magnetite for cationic dye Basic Yellow 28, the magnetite caused just a small decrease of the adsorption capacity of sepiolite. Therefore, the composites can be used for efficient removal of Basic Yellow 28 from water and can be easily separated from water by magnetic separation.

Adsorption capacity of the composites for anions decreases with pH increase. At initial pH = 2, chromates adsorb dominantly by formation of outer-sphere complexes with protonated surface. The content of magnetite is the factor that determines the adsorption capacity, because the capacity of the support is negligible. The highest removal efficiency was achieved with the composite having the highest content of magnetite.

The adsorption of all asorbates onto the composites was best fitted with the Sips model. The pseudo-second-order model fitted the adsorption kinetics for both Cd^{2+} and chromates much better than the pseudo-first-order model. The adsorption capacity of the composites for Cd^{2+} ions increased with increasing temperature, indicating endothermic nature of the adsorption, while the adsorption of chromates is an exothermic process.

The results enable the optimization of the synthesis of magnetic composite adsorbents with a high adsorption capacity and high magnetization, which provides efficient treatment of water by the adsorbent and its subsequent removal by magnetic separation.

Key words: Magnetic nanocomposites, Zeolite, Sepiolite, Acid-activated sepiolite, Co-precipitation, Synthesis parameters; Adsorption, Metal ions, Phosphate, Dyes.

Scientific field: Technical engineering
Major in: Chemical engineering
UDK number: 544.723.21:549.623.8:549.67

Sinteza, karakterizacija i primena magnetnih adsorbenata na bazi sepiolita i zeolita

Izvod

Magnetni nano-kompozitni adsorbenti privlače veliku pažnju poslednjih godina zahvaljujući mogućnosti uklanjanja iz vode primenom magnetnog polja, što smanjuje operativne troškove u poređenju sa filtracijom i centrifugiranjem. Magnetni kompoziti se obično sintetišu deponovanjem magnetnih nano-čestica na nosač, koji obezbeđuje dobro dispergovanje čestica, sprečavajući njihovu aglomeraciju. U ovoj disertaciji, kao nosači za deponovanje magnetnih nano-čestica korišćeni su prirodni minerali zeolit (NZ) i sepiolit (SEP), kao i parcijalno kiselinski aktiviran sepiolit (ASEP), u cilju dobijanja magnetnih nano-kompozita (MNC) kao adsorbenata za uklanjanje Cd^{2+}, Cr(VI), fosfata i boja (Reactive Orange 16 i Basic Yellow 28) iz vode. Cilj ove disertacije je bio da se analizira uticaj različitih parametara sinteze na osobine kompozita da bi se dobio efikasan magnetno separabilni adsorbent. Kompoziti su sintetisani koprecipitacijom Fe^{3+}- i Fe^{2+}-jona korišćenjem jake (NaOH) ili slabe (NH_3) baze u prisustvu NZ ili SEP ili ASEP, pri čemu je baza dodavana pre (procedura 1) ili nakon (procedura 2) dodatka Fe^{3+} i Fe^{2+} u vodenu suspenziju nosača. Dodatno, variran je i molski odnos Fe^{2+}/Fe^{3+} i količina soli gvožđa.

Pokazano je da se koncentracija hidroksilnih jona u suspenziji smanjivala u većoj ili manjoj meri usled interakcije sa površinskim funkcionalnim grupama nosača, što je u nekim slučajevima dovodilo do precipitacije $Fe(OH)_3$ umesto koprecipitacije Fe^{3+}/Fe^{2+} i formiranja magnetita. Zbog jakih interakcija kisele površine ASEP sa hidroksilnim jonima, nije bilo moguće sintetizovati magnetne kompozite kada su NaOH ili NH_3 dodavani u suspenziju nosača pre dodatka Fe^{3+} i Fe^{2+}, već samo u slučaju kada je NH_3 dodavan u suspenziju ASEP sa Fe^{3+} i Fe^{2+} jonima. S druge strane, magnetni kompoziti sa SEP i NZ su uspešno sintetisani po obe procedure, korišćenjem obe baze.

Sintetisani kompoziti sadrže pojedinačne ili aglomerisane kristalite magnetita, veličine oko 10 nm. Nije došlo do narušavanja osnovne strukture sepiolita/zeolita u sintetisanim kompozitima, mada je korišćenje jake baze (NaOH) dovelo do izvesnog alkalnog izluživanja. Stepen dispergovanja magnetnih čestica zavisi od vrste nosača, vrste baze i redosleda mešanja reagenasa, dok odnos Fe^{2+}/Fe^{3+} nije imao velikog uticaja. Najbolja disperznost čestica magnetita je postignuta kada je NH_3 za koprecipitaciju dodavan u suspenziju SEP ili NZ sa Fe^{2+}- i Fe^{3+}-jonima. Bez obzira na veću specifičnu površinu ASEP u odnosu na SEP, disperznost magnetita u kompozitima sa ASEP je manja nego u kompozitima sa SEP usled jačih veza između vlakana sepiolita. Ipak, specifična površina ASEP-MNC je veća od specifične površine kompozita SEP-based MNC, dobijenog pri istim ostalim uslovima.

Kompoziti dobijeni korišćenjem NH_3 (NH_3-MNC) se razlikuju od kompozita dobijenih korišćenjem NaOH (NaOH-MNCs) po načinu oksidacije tokom zagrevanja i po količini magnetita. Manji sadržaj magnetita u uzorcima NH_3-MNC nego u uzorcima NaOH-MNCs, koji su sintetisani sa istom količinom jona Fe^{2+}- i Fe^{3+} se objašnjava prisustvom različitih količina gvožđe(III)-oksida, formiranog tokom sinteze. Bez obzira na veću količinu magnetita, magnetizacija kompozita NaOH-MNC je manja nego NH_3-MNC kompozita, što je verovatno rezultat prisustva veće količine amorfnog magnetita formiranog u obliku sloja na površini nosača. Svi magnetni kompoziti pokazuju superparamagnetno ponašanje na sobnoj temperaturi, što ukazuje da ne zadržavaju magnetizaciju u odsustvu magnetnog polja.

Sintetisani kompoziti imaju znatno veći adsorpcioni kapacitet za katjone nego za anjone, zahvaljujući velikom afinitetu i magnetita i nosača prema katjonima. Kapacitet svih sintetisanih MNC za Cd^{2+} na početnoj vrednosti pH = 7 je veći od kapaciteta čistih komponenti zahvaljujući manjem stepenu aglomeracije i time većoj dostupnosti površine. Dominantni mehanizam adsorpcije je formiranje kompleksa unutrašnje sfere. Kompoziti dobijeni korišćenjem NaOH imaju veći kapacitet adsorpcije od kompozita koji su dobijeni korišćenjem NH_3, pri čemu svi kompoziti imaju veći adsorpcioni kapacitet od kompozita SEP/NZ-gvožđe(III)-oksid, sintetisanih u prethodnim istraživanjima. Adsorpcioni kapacitet MNC se smanjuje sa vremenom usled oksidacije. Bez obzira na mali kapacitet adsorpcije čistog magnetita za katjonsku boju Basic Yellow 28, deponovanje magnetnih nano-čestica je u maloj meri smanjilo adsorpcioni

kapacitet sepiolita. Na taj način, dobijen je efikasam adsorbent za ovu boju, koji se može ukloniti magnetnom separacijom iz obrađene vode.

Adsorpcioni kapacitet kompozita za anjone se smanjuje sa povišenjem pH. Pri početnoj vrednosti pH = 2, hromati se adsorbuju dominantno formiranjem kompleksa spoljašnje sfere sa protonovanom površinom. Sadržaj magnetita je faktor koji određuje adsorpcioni kapacitet, jer je kapacitet nosača zanemarljiv. Najveći adsorpcioni kapacitet za hromate je imao kompozit sa najvećim sadržajem magnetita.

Proces adsorpcije se u svim slučajevima najbolje opisuje modelom Sipsa. Kinetika adsorpcije i Cd^{2+} jona i hromata se opisuje bolje modelom pseudo-drugog reda nego modelom pseudo-prvog reda. Adsorpcioni kapacitet kompozita za Cd^{2+} jone raste sa povišenjem temperature, što ukazuje na endoterman process, dok je adsorpcija hromatnih jona egzoterman proces.

Dobijeni rezultati omogućavaju optimizaciju procesa sinteze magnetnih kompozitnih adsorbenata velikog adsorpcionog kapaciteta i visoke magnetizacije, što obezbeđuje efikasan adsorpcioni tretman vode i magnetnu separaciju adsorbenta.

Ključne reči: Magnetni nano-kompoziti, zeolit, sepiolit, kiselinski aktiviran sepiolit, koprecipitacija, parametri sinteze, adsorpcija, joni metala, fosfati, boje.

Uža oblast: Tehnološko inženjerstvo
Uža naučna oblast: Hemijsko inženjerstvo
UDK broj: 544.723.21:549.623.8:549.67

Content

1. Introduction

Magnetite (Fe_3O_4) nanoparticles have a huge potential in the field of water treatment owing to their adsorption/reduction activities and the possibility to easily separate them from a treated water by applying an external magnetic field [1,2]. These advantages make magnetite appropriate for the removal of vast pollutants from contaminated waters, including different toxic cations and anions [3-6].

However, the strong tendency of the nanoparticles to aggregate and the chemical instability against oxidation reduce the surface area and the adsorption/reduction activities [7] that cause a decrease of the efficiency in the process of water pollutants removal. To prevent the aggregation of magnetite nanoparticles, different materials have been used as a support during magnetite synthesis, such as montmorillonite [7], zeolite [8,9], sepiolite [10,11], paligorskite [12], diatomite [2], pillared bentonite [13,14], activated carbon [15], microporous carbon [16], chitosan [17], cross-linked pectin [18] etc. In that way, the nanoparticles are dispersed in a solid matrix, precluding them from any local movement, as they are firmly embedded in the matrix. The magnetic properties of such composites depend on both the quantity of magnetite in the composite and the size of magnetite particles meaning that the magnetization is higher if the quantity of magnetite is higher and the magnetite particles are larger. On the other hand, the adsorption capacity of the composite is higher if the magnetite particles are smaller. Therefore, in order to obtain the composite with good magnetic and adsorption properties, it is necessary to increase the quantity of magnetite in the composite and to optimize the size of magnetite particles, as well as to prevent the magnetite oxidation [2,7].

The quantity of magnetite in the composite can be increased by using support materials with a high specific surface area and an appropriate porosity. Therefore, natural minerals zeolite and sepiolite are good candidates for magnetite particle supporting. Sepiolite is a fibrous, non-swelling clay mineral, with the ideal formula $Si_{12}Mg_8O_{30}(OH)_4(OH_2)_4 \cdot 8H_2O$. Structurally, sepiolite is formed by blocks and interior channels along the fiber direction, while each block consists of two SiO_4 tetrahedral sheets enclosing a central MgO_6 octahedral sheet. Natural zeolites are hydrated

aluminosilicate minerals that are characterized by cage like structure, high surface area and high cation-exchange capacities [19]. The specific surface area and the porosity of the minerals can be further increased by an acid activation due to the removal of mineral impurities and Al^{3+} or Mg^{2+} ions from the structure. It was shown that the degree of acid-activation could be controlled by the type and concentration of acid, as well as by the duration and temperature of the treatment. In the case of sepiolite, if the treatment is very aggressive, the octahedral Mg^{2+} cations are completely dissolved, while the tetrahedral sheets form a free amorphous silica gel, insoluble in the acid solution. However, by controlling the acid treatment, it is possible to increase the specific surface area and to preserve the sepiolite structure [20].

In this study, natural zeolite, natural sepiolite and the partially acid-activated sepiolite were used to prepare the magnetic nano-composites (MNCs) for the removal of cadmium (Cd^{2+}), hexavalent chromium (Cr(VI)), phosphate and dyes (Reactive Orange 16 and Basic Yellow 28) from water. For this purpose, a chemical co-precipitation method was used and the synthesis parameters were varied in order to obtain MNCs with a high adsorption capacity and good magnetic properties. In the case of pure magnetite synthesized by a co-precipitation method, the influence of different parameters, such as: iron salts concentration; the ratio of Fe^{2+}/Fe^{3+}; nature of the base used for the co-precipitation; the rate of the addition of the base solution; ratio of OH^-/($Fe^{2+} + Fe^{3+}$); temperature; and drying modality on the properties has been investigated [21-25]. On the other hand, the synthesis of sepiolite/zeolite MNCs was performed only under constant conditions [26,9,10], without examining the influence of synthesis parameters on the composites properties and the adsorption capacity. Therefore, the goal of this study was:

- to synthesize the magnetic composites on the basis of natural minerals sepiolite and zeolite for the removal of some cations and some anions from water;
- to investigate the influence of the synthesis parameters, such as the type and concentration of the base used for the co-precipitation, the order of the mixing of the reagents, ratio of Fe^{2+}/Fe^{3+} and quantity of iron salts on the properties and the adsorption capacities of the synthesized composites,
- to investigate the influence of the support type (natural zeolite, natural sepiolite or acid-activated sepiolite) on the adsorption capacity of the composites,

- comparison of the adsorption properties of the synthesized magnetic composites and composite based on sepiolite/zeolite and trivalent iron oxide;
- to examine the effect of contact time and temperature on the adsorption capacity of the synthesized composites.

THEORETICAL PART

2. Structure, properties, applications and modifications of sepiolite and zeolite

2.1. Structure, properties and applications of sepiolite

Sepiolite is a naturally occurring clay mineral of sedimentary origin. It is a non-swelling, lightweight, porous clay. The name comes from a perceived resemblance of the material to the porous bones of the cuttlefish or sepia [27]. The important deposits of sepiolite occur in southeastern United States, China, Senegal, Spain, and Ukraine.

2.1.1. Sepiolite structure

Chemically, sepiolite is a hydrated magnesium silicate with the ideal formula $Si_{12}Mg_8O_{30}(OH)_4(OH_2)_4 \cdot 8H_2O$ characterized by its fibrous morphology and intracrystalline channels. Sepiolite belongs to the phyllosilicate group because it contains continuous sheets composed of interconnected SiO_4^{4-} tetrahedrons. It differs, however, from the other layered silicates because of the lack of a continuous octahedral sheet (Fig. 1a) that caused fibrous morphology. Sepiolite structure can be considered to contain ribbons of a 2:1 phyllosilicate structure (Fig. 1b), each ribbon being linked to the next by inversion of SiO_4 tetrahedral along a set of Si-O-Si bonds. Ribbons extend parallel to the x-axis and have an average width along y-axis of three linked pyroxene-like single chains (Fig. 1a); in this framework, rectangular channels run parallel to the x-axis between opposing 2:1 ribbons. Because of the covalent link between different blocks, sepiolite has been described as non-swellable clay. As the octahedral sheet is discontinuous at each inversion of tetrahedra, oxygen atoms in the octahedra at the edge of the ribbons are coordinated to cations on the ribbon side only, and coordination and charge balance are completed along the channel by protons, coordinated water (H_2O_{coord}) and a small number of exchangeable cations. Also, a variable amount of zeolitic water (H_2O_{zeol}) is present in channels [28,29].
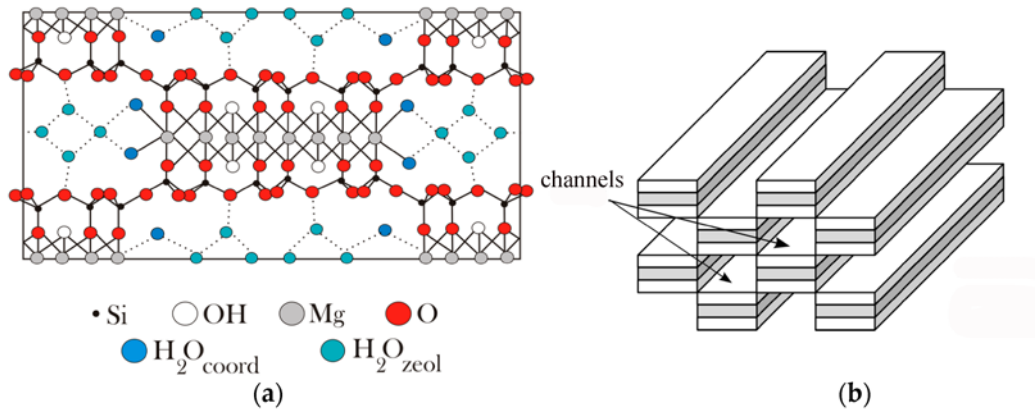
Fig. 1. Structure of sepiolite: a) unit cell of sepiolite, b) schematic representation of a sepiolite fiber [30].

As it can be seen from the Fig. 1a, there are three types of water in sepiolite structure: zeolitic water, bound or coordinated water and hydroxyl water. These types of water are removed at different temperatures: zeolitic water is removed by heating at temperatures up to 150 °C, while bound water is removed in two steps: one half of bound water is removed at ~ 300 °C and second half of bound water is removed at about 500 °C. The removal of zeolitic water does not influence the sepiolite structure, while the removal of bound water caused the structure folding (Fig. 2) [31-33]. In the structure of sepiolite, the hydrogen bridges between coordinated water and oxygen of the neighboring silica surface stabilize the structure. The loss of coordinated water molecules eliminates the bridge effect and permits the crystal to fold in order to satisfy the coordination of the octahedral magnesium by the oxygen of the neighboring silica surface.
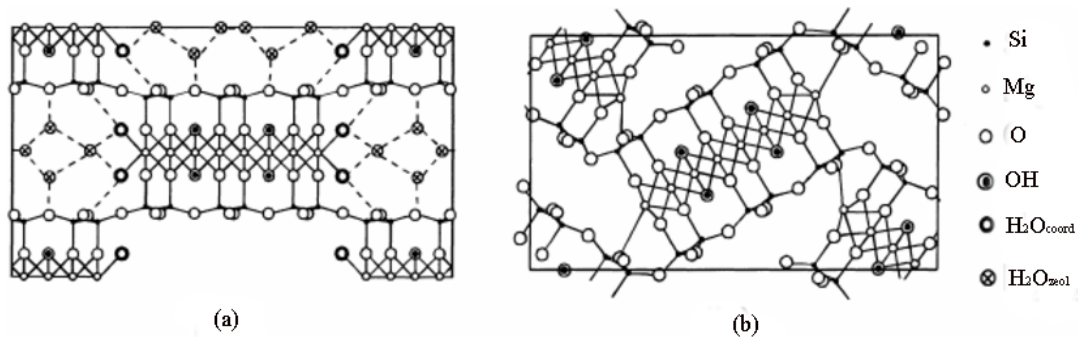
Fig. 2. Folding of sepiolite structure: a) unfolded structure, b) folded structure [33].

Heating of sepiolite at the temperatures around 800 °C causes the removal of hydroxyl groups, i.e. dehydroxylation, which is followed by formation of enstatite ($MgSiO_3$) and SiO_2 [31,32].

2.1.2. Sepiolite properties

Sepiolite is composed of elemental particles with fibre-like or needle-like shape. The dimensions of a single sepiolite fibre vary between 0.2-4 μm in length, 10-30 nm in width and 5-10 nm in thickness, with open channels of dimensions 3.6 Å x 10.6 Å running along the axis of the particle (Fig. 1). These particles are arranged forming loosely packed and porous aggregates, bundles (Fig. 3), with an extensive capillary network, which explains the high porosity. Sepiolite has the highest surface area of all the clay minerals, about 300 m^2/g. High specific surface area and the porosity of each sepiolite are the result of the sum of the intracrystalline or structural microporosity and the textural porosity (interfibre microporosity and mesoporosity), as well as macroporosity due to aggregation of bundles (Fig. 3). As a consequence, there is a hierarchical distribution of pore sizes which is different for each sepiolite.
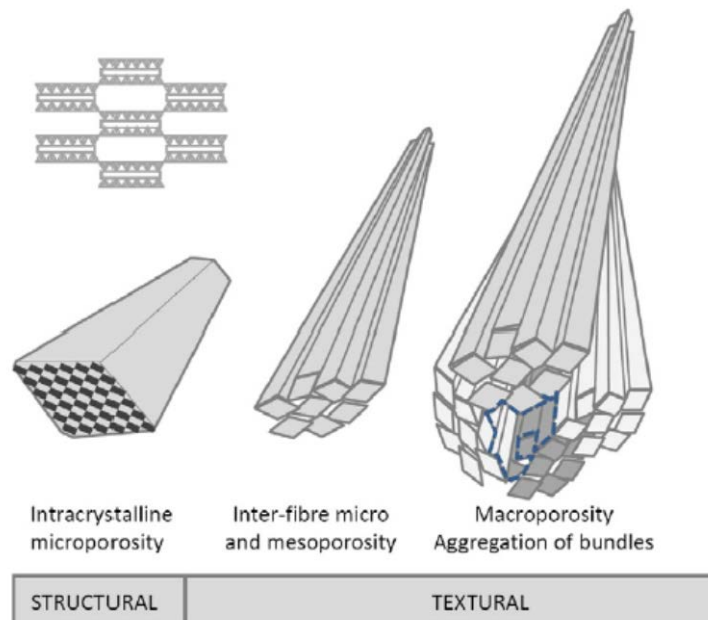
Fig. 3. Schematic representation of the hierarchical distribution of pores in sepiolite [34].

The structure of sepiolite includes three types of active adsorption sites: (a) oxygen ions on the tetrahedral sheets of the ribbons; (b) water molecules coordinated to Mg ions at the edges of structural ribbons (two H_2O molecules per Mg^{2+} ion) and (c) Si-OH (silanol) groups along the fibre axis. Silanol groups are formed by broken of Si-O-Si bonds at external surfaces, balancing their residual charge by accepting either proton or a hydroxyl group to form Si-OH groups. The relative abundance of these groups can be related to fibre dimensions and crystal defects, and increases with acid treatment [28,29].

Apart from the outstanding adsorptive capacity, sepiolite is also known for its colloidal properties. When dispersed in a liquid, it forms a structure of randomly intermeshed elongated particles, which is maintained by secondary bonds. Sepiolite exhibits a pseudoplastic and thixotropic behavior [29].

The cation exchange capacity of sepiolite is quite low; it ranges from 4 to 40 mmol M^+/100 g, but the higher values are probably related to impurities [35]. Usual impurities of sepiolite are quartz, feldspars, carbonates, gypsum, cristobalite, smectite, illite, kaolinite, chlorite and iron oxides.

2.1.3. Sepiolite applications

Sepiolite is used in numerous areas due to its high surface area, fibrous structure, porosity, crystal morphology and composition, surface activity, production of stable suspensions of high viscosity at low concentrations, etc. These properties provide the basis for a variety of catalytic, adsorptive and rheological applications for sepiolite [36,37]. Common industrial applications of sepiolite are listed in Table 1.

Table 1. Sepiolite characteristics and common industrial applications [37]

Characteristics	Applications
High liquid absorption, mechanical strength in wet conditions, non-flammability, chemical inertness	Adsorbent/absorbent in industry
Adsorption of active chemicals, effective release of the chemicals	Carrier for chemicals
Control of rheological properties in heat application systems, improving fire resistance	Bitumen
Stability, pseudo-plasticity and thixotropy in paints, adhesives, mastics and sealants	Rheological additives
Light weight, high liquid absorption, odor control	Cat and pet litter
Absorb moisture and odours	Household uses
Technological additive for animal feed	Animal feedstuffs

2.2. Structure, categorization, characterization, properties and applications of zeolite

Zeolites are microporous, aluminosilicate minerals. Natural zeolites occur in mafic volcanic rocks as cavity fillings, probably as a result of deposition by fluids or vapors. In sedimentary rocks zeolites occur as alteration products of volcanic glass and serve as cementing material in detrital rocks; they also are found in chemical sedimentary rocks of marine origin. Extensive deposits of zeolites occur in all oceans. Metamorphic rocks contain a sequence of zeolite minerals useful for assigning relative metamorphic grade; these minerals form at the expense of feldspars and volcanic glass [38].

Zeolites are the most important group of aluminum silicates. There are almost 40 types of natural zeolites and more than 150 types of synthetic zeolites manufactured [39,40]. Due to the large variability in chemical composition, a reliable classification in the zeolite family is possible only on the basis of structural considerations.

Common forms of zeolite are clinoptilolite, mordenite, phillipsite, chabazite, stilbite, analcime and laumontite, whereas offretite, paulingite, barrerite and mazzite are much rarer.

2.2.1. Zeolite structure

Structurally, zeolites are framework aluminosilicates consisting of infinity extending three-dimensional four-connected networks of AlO_4 and SiO_4 tetrahedra, which are liked to each other by sharing all of oxygen ions. Each AlO_4 thetrahedron in the framework bears a net negative charge, which is balanced by extra-framework cation. The framework structure contains channels or interconnected voids that are occupied by the cations and water molecules. The cations are mobile and ordinarily undergo ion exchange (exchangeable cations). The water may be removed reversibly, generally by the application of heat (heating to approximately 400 °C) [41].

The general chemical formula for zeolite minerals is:

$$M_{x/n}[Al_xSi_yO_{2(x+y)}] \cdot pH_2O \tag{1}$$

where: M is exchangeable cation (Na, K, Li and/or Ca, Mg, Ba, Sr), n is cation charge, y/x = 1 – 6, p/x = 1 – 4 [42]. The exchangeable cations compensate the negative charge of the framework due to the presence of Al^{3+} in tetrahedral position instead of Si^{4+}.

Aforementioned $[SiO_4]$ and $[AlO_4]$ tetrahedra are the basic structural building units of a zeolite framework, which is called the primary building units. In a zeolite structure, each (Al, Si) atom is coordinated to four oxygen atoms (Fig. 4a), with each oxygen atom bridging two (Al, Si) atoms (Fig. 4b) [43].
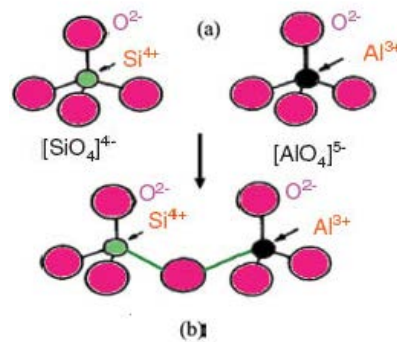
Fig. 4. a) AlO_4 or SiO_4 tetrahedron, b) The tetrahedra sharing common oxygen.

Groups of primary building units can be arranged to form polymeric subunits known as secondary building units (SBUs). The secondary building units shown in Fig. 5a are characteristic configurations of tetrahedral to be recurrent in many zeolite structures. In this figure, the atoms drown are the tetrahedral (T) atoms (the oxygen ions are not shown). One type of framework can comprise several SBUs. For example, the LTA (Linde Type A zeolite) framework contains five types of SBUs, including 4, 8, 4-2, 4-4, and 6-2 units, any of which can be used to describe its framework structure [43].

Secondary building units are combined to form cage-like units. Cages are generally described in terms of the n-rings defining their faces. For example, a truncated octahedron (sodalite unit (SOD) or β-cage), whose surface is defined by six 4-rings and eight 6-rings, would be designated as $[4^6 6^8]$ cage. Fig. 5b shows the cage-building units in the zeolite frameworks.
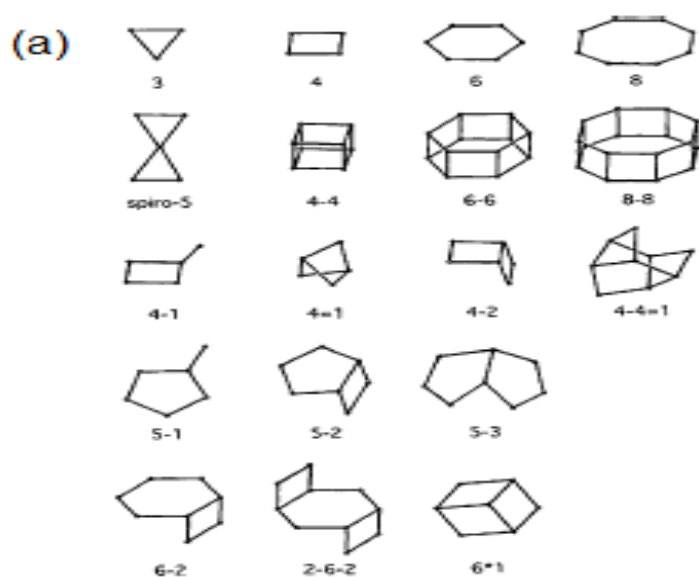
Fig. 5.a) Secondary building units in zeolite structure [43]
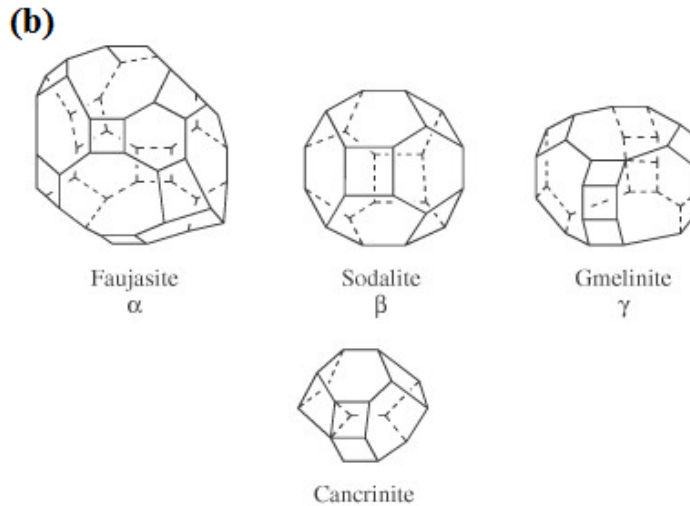
Fig. 5.b) Cage-building units [43].

Different zeolite frameworks may feature the same cage building unit, that is to say, the same cage-building unit may construct different framework types via different linkages. For example, starting from the SOD cage (Fig. 6), several structures can be obtained:

SOD - β-cages are linked by sharing 4-rings,

LTA - β-cages are arranged in a primitive cubic way, connecting the neighbors through double 4-rings,

FAU (Faujasite) and EMT (EMC-2) - the β-cages connect through double 6-rings, but the way β-cages arranged is different; for the FAU zeolite, β-cages are arranged in the same way as carbon atoms in the diamond structure. This is also one of the reasons for the excellent thermal stability of the FAU zeolite [43-45].
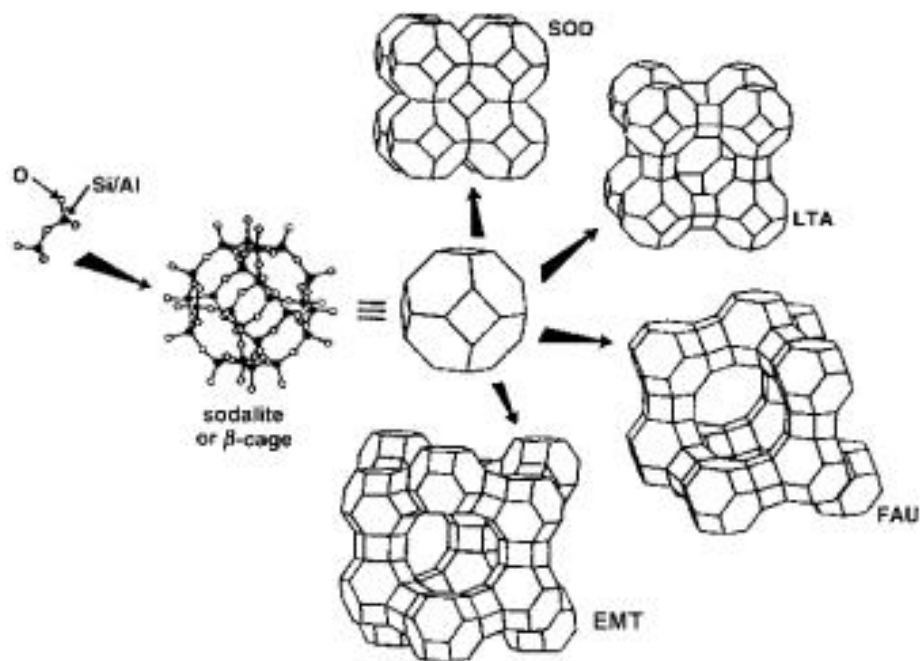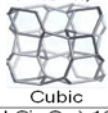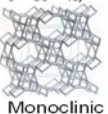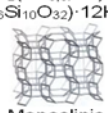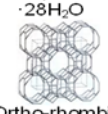
Fig. 6. The construction of four different zeolite frameworks built up from sodalite or β-cages [45].

2.2.2. Categorization and characterization of natural zeolites

Natural zeolites are divided into seven main groups (Table 2) according to their crystal structure, morphology, physically properties, ways of binding secondary units in the three-dimensional framework, the free pore volume and types of exchangeable cations in zeolite structure. These diverse types of zeolite are a reflection of the fascinating structures of these microporous materials [46].

Among the zeolites, clinoptilolite is the most abundant natural zeolite and is widely used in the world. A ratio between silicon and aluminium (Si/Al) of the clinoptilolite varies from 4.0 to 5.3. Sodium and potassium dominate among exchangeable cations of clinoptilolite [47].

Table 2. Categorization and structural properties of seven main groups of natural zeolites (channel dimensions in nm; free volume in cm^3 H$_2$O/cm^3 of zeolite) [46]

Zeolite	Primary cell formula, Structure Crystal system	Channel dimensions	Free Volume	Exchangeable cations
GROUP 1				
Analcime (ANA)	Na$_{16}$(Al$_{16}$Si$_{32}$O$_{96}$)·16H$_2$O Cubic	0,16 x 0,42	0,18	Na, K, Ca, Rb, Cs
Laumontite (LAU)	Ca$_4$(Al$_8$Si$_{36}$O$_{48}$)·16H$_2$O Monoclinic	0,40 x 0,53	-	K, Na, Ca
Phillipsite (PHI)	K$_2$(Ca$_{0,5}$,Na)$_4$·(Al$_6$Si$_{10}$O$_{32}$)·12H$_2$O Monoclinic	0,38 x 0,38	0,31	Na, K, Ca
GROUP 2				
Erionite (ERI)	NaK$_2$MgCa$_{1,5}$(Al$_8$Si$_{28}$O$_{72}$)·28H$_2$O Hexagonal	0,36 x 0,52	0,35	K, Na, Ca, Mg
GROUP 3				
Zeolite A	Na$_{12}$[(AlO$_2$)$_{12}$(SiO$_2$)$_{12}$]·27H$_2$O	-	0,47	-
GROUP 4				
Chabazite (CHA)	Ca$_2$(Al$_4$Si$_8$O$_{24}$)·12H$_2$O Hexagonal	0,38 x 0,38	0,47	Na, Ca, K
GROUP 5				
Natrolite (NAT)	Na$_{16}$[(AlO$_2$)$_{16}$(SiO$_2$)$_{24}$]·16H$_2$O Ortho-rhombic	0,25 x 0,41	0,23	Na, K, Ca
GROUP 6				
Mordenite (MOR)	Na$_3$KCa$_2$(Al$_8$Si$_{40}$O$_{96}$)·28H$_2$O Ortho-rhombic	0,65 x 0,70	0,28	Na, Ca, K
GROUP 7				
Heulandite (HEU)	(Na,K)Ca$_4$(Al$_9$Si$_{27}$O$_{72}$)·24H$_2$O Monoclinic	0,44 x 0,72	0,39	Na, K, Ca, Sr, Ba
Clinoptilolite (CLI)	(Na,K)$_6$(Al$_6$Si$_{30}$O$_{72}$)·20H$_2$O Monoclinic	0,44 x 0,72	0,34	Na, K, Ca, Sr, Ba

The clinoptilolite has framework structure that consists of three types of channels. The channels A (10-member ring) and B (8-member ring) are parallel to each other, while 8-member ring channel C intersects the channels A and B (Fig. 7a). Besides the compensating cations M, surrounded by water molecules in the channels, the H^+ ions may also be considered as exchangeable cations present in Si–OH and Al–OH. The structure of clinoptilolite is shown in Fig. 7b. [48,49].

a)   b)
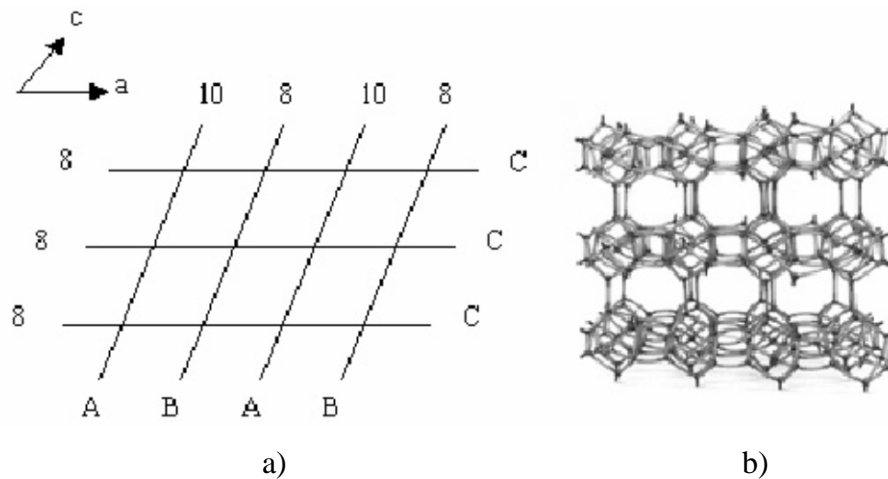
Fig. 7. a) Orientation of clinoptilolite channel axis, b) Model framework for the structure of clinoptilolite [48,49]

2.2.3. Properties and applications of natural zeolite

Natural zeolites are rarely pure and are normally contaminated to varying degrees by other minerals. Zeolites are commonly associated with minerals like calcite, pectolite, datolite, quartz and other zeolites. For this reason, naturally occurring zeolites are excluded from many important commercial applications where uniformity and purity are essential. In those cases where purity is required, synthetic zeolites are used [50].

Zeolites are white in color when free from iron and other impurities. Due to the presence of impurities, natural zeolites are usually light colored. The hardness is generally between 3.5 and 5.5 of Mohs scale [39,51].

Physical characteristics of some natural zeolites are shown in Table 3.

Table 3. Physical characteristics of some natural zeolites [52]

Zeolite	Porosity (%)	Heat stability	Ion exchange capacity (mmol M^+/100 g)	Specific gravity (g/cm^3)	Bulk density (g/cm^3)
Analcime	18	High	454	2.24-2.29	1.85
Chabazite	47	High	384	2.05-2.10	1.45
Clinoptilolite	34	High	216	2.15-2.25	1.15
Erionite	35	High	312	2.02-2.08	1.51
Heulandite	39	Low	291	2.18-2.20	1.69
Mordenite	28	High	429	2.12-2.15	1.70
Philipsite	31	moderate	331	2.15-2.20	1.58

Natural and synthetic zeolites are used commercially because of their unique adsorption, ion-exchange, catalytic properties [42], thermal stability, stability of the crystal framework structure when dehydrated [39], low density etc. These properties of a zeolite are dependent on the topology of its framework, size, shape, and accessibility of its free channels [53].

The most fundamental consideration regarding the adsorption of chemical species by zeolites is molecular sieving. Species with a diameter larger than a zeolite pore are effectively "sieved." This "sieve" effect can be utilized to produce sharp separations of molecules by size and shape.

The strong electrostatic field within a zeolite cavity results in very strong interactions with polar molecules such as water moleculs. Non-polar molecules are also strongly adsorbed due to the polarizing power of these electric fields. Thus, excellent separations can be achieved by zeolites even when no steric hindrance occurs.

Adsorption based on molecular sieving, electrostatic fields, and polarizability are always reversible in theory and usually reversible in practice. This allows the zeolite to be reused many times, cycling between adsorption and desorption. This accounts for the considerable economic value of zeolite in adsorptive applications [54].

Zeolites are widely used as adsorbents and ion-exchangers in water purification and softening, as molecular sieves and also for precise and specific separation of gases. Due to their micro-porous structure, zeolites can capture some ions while allowing

others to pass freely, allowing many fission products in nuclear industry to be efficiently removed from nuclear waste and permanently trapped. The high heat of adsorption and ability to hydrate and dehydrate while maintaining structural stability allow zeolites application as solar thermal collectors and for adsorption refrigeration. The largest single use of zeolite is the global laundry detergent market.

Development of many biochemical and biomedical applications of zeolites has been ongoing. Zeolites, especially a natural zeolite clinoptilolite, are used for a soil treatment. It provides a source of slowly released potassium. If previously loaded with ammonium, the zeolite can have a similar function in the slow release of nitrogen. Zeolites can also act as water moderators, in which they will absorb up to 55 % of their mass in water and slowly release it under the plant's demand [55,56].

2.3. Sepiolite and zeolite modifications

It was shown in recent studies that adsorption capacity and general physical and chemical properties of sepiolite and zeolite can be highly improved by various treatments such as acid/base treatment [20,57-62], heat treatment [60,63], surfactant modification [64], modification by metals oxides or hydroxides [19, 65-68], etc. For this dissertation, acid/base treatment and the modification by iron oxides/hydroxides are of particular importance.

2.3.1. Acid/base treatment

2.3.1.1. Treatment of sepiolite

Natural sepiolite minerals usually contain amounts of impurities, such as calcites, quartz, talcum and some other minerals. Besides, some carbonates adhere to the surface of the sepiolite, which can greatly reduce the specific surface area and restrict the applications of sepiolite in many fields. Hence, acid-activating treatment is adopted to purify the natural sepiolite [63]. In addition, acid treatment is used to increase the

surface area of sepiolite and to obtain solids with higher porosity and higher number of acidic centers [69].

During acid treatment of sepiolite, structural magnesium is removed and changed by H^+ ion. In that way, silanol groups are formed, which undergo the condensation reactions ana Si-O-Si bonds feormation. A possible reaction mechanism of the complete phenomenon of the acid dissolution of sepiolite is proposed and schematically summarized in Fig. 8 [57], where:

(a) the structure of original sepiolite,

(b) the structure in which the octahedral Mg-layer is eliminated by acid dissolution,

(c) the projection of the atoms of a unit cell after the acid-activation, and

(d) the structure after the condensation of silanol groups [57].
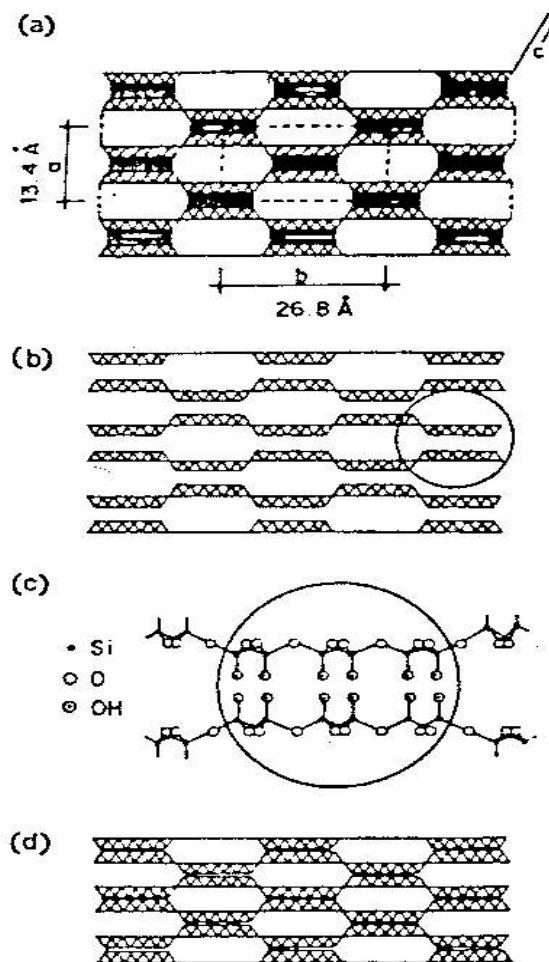
Fig. 8. Possible reaction mechanism of acid dissolution of sepiolite [57].

During acid treatments of sepiolite, variable amounts of structural Mg^{2+} ions can be removed, depending on the intensity of the acid treatment. If the treatment is aggressive enough, the octahedral cations are completely dissolved, while the tetrahedral sheets form free amorphous silica gel, insoluble in the acid solution [57]. It was shown [57] that the process of acid dissolution of sepiolite was controlled by the rate of diffusion of Mg^{2+} cations through a product layer consisting of amorphous silica. Dissolution rate increased with increase in temperature and acid concentration, and with decrease in particle size of sepiolite and sepiolite/acid solution ratio. The changes of texture of silicas (specific surface area and microporosity) obtained by acid dissolution of sepiolite depend on the reaction conditions (type and concentration of acid and reaction temperature). All investigations of the structural and textural changes of sepiolite under acid treatment [58- 60,69-71] show that the more intense the acid attack (higher concentration, higher temperature, stronger acid, longer treatment), the more affected the structure of the sepiolite. Generally, an important increase in the surface area of the solids obtained was observed. The modification in the micro- and mesoporosities together with particle disaggregation, surface cleaning and free silica generation contribute to the increase in surface area. The greatest surface area is observed when the octahedral layer is partially destroyed and microporosity is generated. During partial acid treatment [20], the crystal lattice of sepiolite and fibrous morphology is maintained, albeit with some decrease in crystallinity.

Treatment of sepiolite by base causes Si^{4+} leaching of from the structure. The comparison with the of Mg^{2+} leaching during acid-treatment showed that the amount of leached Si^{4+} was lower, indicating more tolerance of the sepiolite toward the base treatment [60]. While long-term treatment at room temperature did not cause any significant change, the treatments above 70 ºC decreased the surface area, which was explained by the partial destruction of nano-sized channels in the sepiolite, which were possibly related to the changes in its crystal structure or by the formation of Mg-rich compounds with low surface areas [60].

2.3.1.2. Treatment of zeolite

Zeolite structure and its chemical and physical properties can be modified with either inorganic acid (HCl, HNO$_3$…) or basis (NaOH, Ca(OH)$_2$). As for sepiolite, acid treatment is among the most common and simple methods for zeolite modification and its effectiveness depends on the chemical composition, structure, mineral purity, and the working conditions [46,61,62]. Generally, acid treatment changes the structure, resulting in an amorphization and an increase of the specific surface area and the micropore volume.

Usually, acid activation involves three steps [72]: removal of exchangeable cations (decationating), dealumination of framework (removal of Al from the zeolite framework and replacement of exchangeable cations by H$^+$), and formation of amorphous silicon-oxygen phase. The sequence and intensity of the steps are determined by treatment conditions and specific characteristics of minerals.

During the decationating process there is a replacement of exchangeable cations with hydrogen ions and a break of Si–O–Al bond followed by formation of new active centers—three-coordinated aluminum atoms and hydroxyl groups. These three-coordinated aluminum atoms polarize adjacent hydroxyl groups whose protons become able to participate in an exchange reaction with the cations of solution during sorption. Dealumination of the clinoptilolite framework may be represented as follows:

In addition to decationating and dealumination processes, there is an acid dissolution of impurities contained in zeolite, leading to opening of blocked active sites and, therefore, to an increase in effective surface and specific surface area, which is the reason for changes in adsorption properties of zeolite [72]. According to the Brønsted and Lewis theory, dissolution of natural zeolites in acid solution occurs as a result of the acidic/basic behaviour of the aluminosilicate structure in the presence of H$^+$ or OH$^-$ ions in the solution.

The extraction of framework silicon by treatment in alkaline solutions, referred to as desilication or base leaching, is a widely used method to prepare hierarchical porous zeolites. The controlled leaching of Si by OH$^-$ forms intracrystalline mesopores, which facilitate the access and diffusion of molecules in the zeolite [73]. Desilication of zeolite by alkaline treatment could deteriorate a crystallinity of zeolite, resulting in

decrease of Si/Al ratios [74]. Moreover, the desilication also created larger pores, allowing improved transport of molecules or ions in the zeolite. As in the case of acid treatment, the effects of alkaline treatment depend on the process conditions, especially on type and concentration of base and the length of the treatment. It was shown [73] that organic bases are intrinsically less reactive towards silicon dissolution than inorganic hydroxides. This makes the demetallation process highly controllable in comparison with the fast silicon dissolution kinetics in NaOH. The organic hydroxide is also less selective for silicon extraction, i.e. higher Al leaching compared to NaOH is observed and therefore higher Si/Al ratios in the mesoporous zeolites are attained. The differences in porosity and composition are determined by the nature of the cation in the organic base. In particular, the steric hindrance induced by the relatively bulky organic cation is responsible for this distinct demetallation mechanism.

2.3.2. Modification by iron oxides/hydroxides

Recently, zeolite and sepiolite have been modified by iron oxides/hydroxides. The zeolite–iron oxide/hydroxide and sepiolite–iron oxide/hydroxide systems were synthesized by adding natural sepiolite or zeolite to an iron nitrate or iron chloride aqueous solution under strongly basic conditions [66,75]. Such modification enhanced all properties responsible for better adsorption process such as specific surface area, the total pore volume, number of exchangeable sites, and surface charge [75-77]. It was shown that adsorption capacity of so-obtained Fe(III)-sepiolite [66,78] for Ni^{2+} and Co^{2+} ions is significantly higher than of untreated sepiolite as a result of higher specific adsorption and a higher ion exchange capacity. Similarly, adsorption capacity of Fe(III)-zeolite for Pb^{2+}, Cd^{2+}, and Zn^{2+} [65,79, 80] was much higher than that of untreated zeolite owing to the higher: specific adsorption caused by the new functional groups formed on the zeolite surface, ion exchange due to the presence of easily exchangeable ions, and hydroxide precipitation caused by higher point of zero charge of the Fe(III)-zeolite compared to natural zeolite.

Generally, different forms of iron have been identified in iron-modified zeolite (Fig. 9). These include isolated ions (a) either in framework positions (isomorphously

substituted) or (b) in cationic positions in the zeolite channels, (c) binuclear and, in general, oligonuclear iron complexes in extra framework positions, (d) iron oxide FeOx nanoparticles of size ≤ 2 nm, and (e) large iron oxide particles (Fe_2O_3) in a wide distribution (up to 25 nm in size) located at the surface of the zeolite crystals [75].
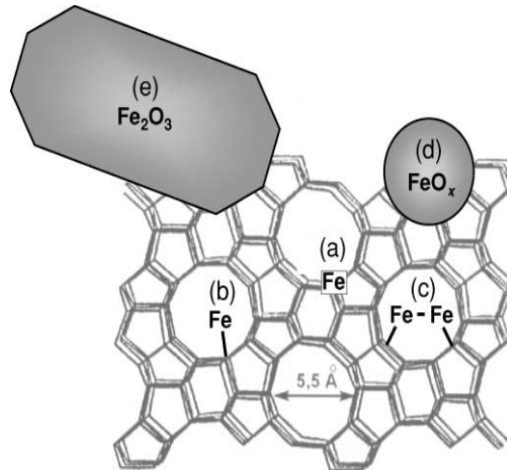
Fig. 9. Schematic presentation of the different iron species identified in iron-modified zeolite [75].

3. Synthesis, structure, properties and application of magnetite

Iron oxide is found in nature in different forms. Magnetite (Fe_3O_4), maghemite (γ-Fe_2O_3) and hematite (α-Fe_2O_3) are the most common among them [81]. Magnetite is a very common iron oxide mineral that is found in igneous, metamorphic, and sedimentary rocks. It is the most commonly mined ore of iron. It is also the mineral with the highest iron content (72.4%) and the most strongly magnetic mineral found in nature. [82]

3.1. Magnetite structure

Crystallographically, magnetite takes a cubic inverse spinel form. The oxygen ions form a close-packed cubic lattice with the iron ions located at interstices between the oxygen ions [81]. There are two different interstices, tetrahedral (A) and octahedral

(B), which the metal ions can take. The A sites are occupied by Fe^{3+} and the B sites are occupied by equal numbers of Fe^{2+} and Fe^{3+} (Fig. 10). The formula can be written as $[Fe^{3+}]\{Fe^{2+}Fe^{3+}\}O_4$, where [] and {} indicate tetrahedral and octahedral interstices, respectively.
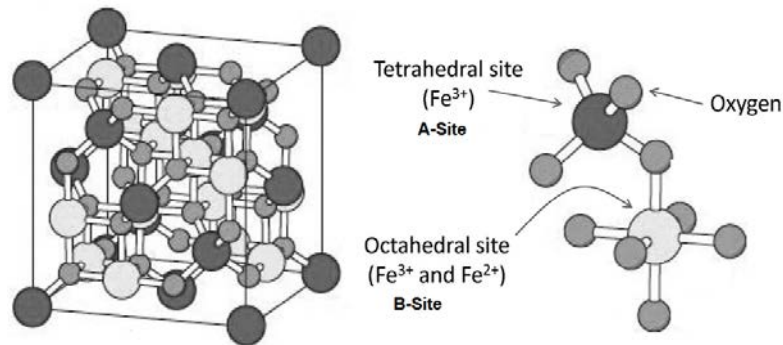
Fig. 10. The crystalline structure of magnetite [83].

3.2. Properties of magnetite

3.2.1. Magnetic properties

3.2.1.1. Types of magnetic materials

Magnetite is an example of a ferrimagnet. Ferrimagnets are similar in properties to ferromagnets with a magnetic structure comparable to an anti-ferromagnet (Fig. 11). In a simple ferromagnet (Fig. 11 a), the electron spins (and thus the magnetic moments) are aligned in one direction giving a large net magnetic moment in the material. In an anti-ferromagnet (Fig. 11 b), the spins are aligned so that the magnetic moments are of equal magnitude but point in opposite directions, giving a zero net magnetic moment. In ferrimagnets, the magnetic moments are aligned oppositely and have different magnitudes (Fig. 11 c) due to being made up of two different ions. Above a certain temperature, known as the Curie temperature (T_C), the alignment of the moments in ferromagnetic and ferrimagnetic materials is lost due to thermal energy and the material displays paramagnetic behavior: the magnetic moments are disordered in the absence of

an applied magnetic field and ordered in the presence of an applied magnetic field (Fig. 11 c) [84]. Diamagnetic materials are repelled by a magnetic field; an applied magnetic field creates an induced magnetic field in them in the opposite direction.

| a) | b) | c) | d) |
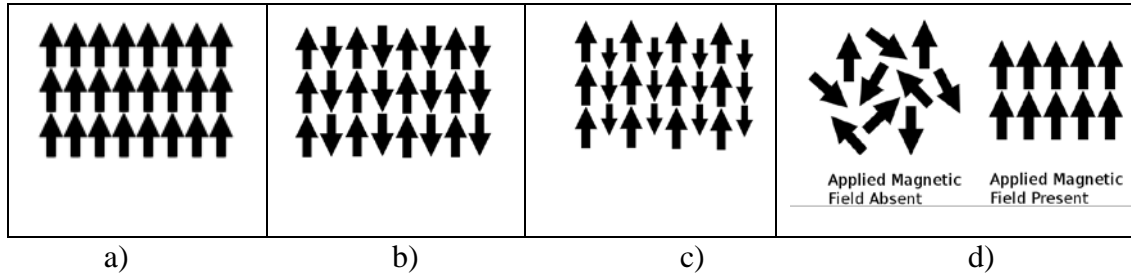
Figure 11. Orientations of magnetic moments in materials: a) ferromagnetism, b) anti-ferromagnetism; c) ferrimagnetism, d) paramagnetism [84].

3.2.1.2. Magnetic properties of magnetite

Magnetite electronic configuration consists of unpaired 3d electrons, which impart net magnetic moments. The spins of the tetrahedrally (A) coordinated Fe^{3+} and the spins of the octahedrally (B) coordinated Fe^{3+} and Fe^{2+} are antiparallel (Fig. 12). The magnitudes of spins of the tetrahedrally and octahedrally coordinated Fe^{3+} are equal (Fig.12), so that the magnetic moment of the unit cell only comes from the Fe^{2+} ions [85].
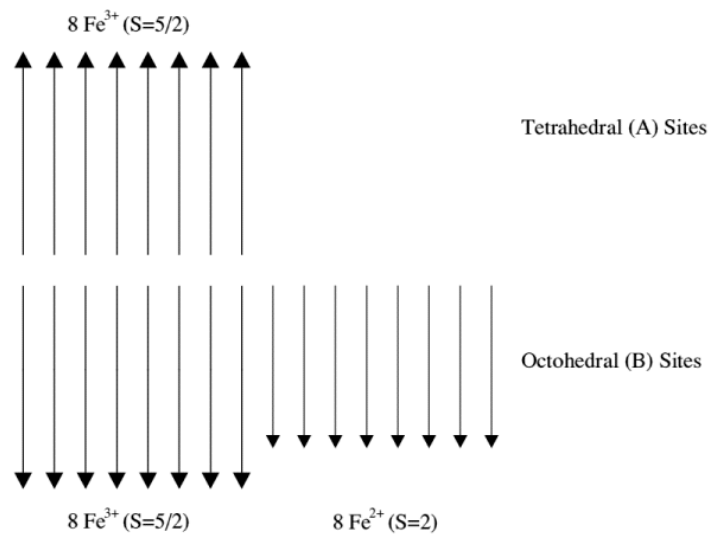
Fig. 12. Spin arrangements in magnetite [85].

Magnetite exhibits a variety of characteristics, depending on temperature [85]. There are three regions of temperature where magnetite behaves differently: (i) between 0 K and 119 K (the Verwey transition temperature), (ii) 120 K to 840 K (T_c, the Curie temperature) and (iii) above 840 K.

Above 120 K, electrons' moving from Fe^{2+} to Fe^{3+} in B sites is responsible for magnetite's large conductivity at these temperatures. As the temperature is lowered to region (i) there is a temperature, called the Verwey temperature (119 K), where a sudden change in behavior is seen. Between 120 K and 119 K there is a sharp drop in electrical conductivity of the order of 90 times. This change is associated with a change in crystal structure from cubic to a lower symmetry ordering, possibly orthorhombic. The iron ions on the B sites separate into either Fe^{3+} or Fe^{2+} ions (no longer enough thermal energy to allow electron hopping between ions), so there are now A sites with Fe^{3+} ions, B sites with Fe^{3+} ions and B sites with Fe^{2+} ions. In region (iii) magnetite simply behaves as a paramagnetic metal and this phase was not investigated [85].

3.2.1.3. The dependence of magnetization on magnetic field strength

The density of magnetic moments in a magnetic material is expressed by magnetization or magnetic polarization (M). Net magnetization results from the response of a material to an external magnetic field, together with any unbalanced magnetic dipole moments in the material itself (in ferromagnets and ferimagnets).

The relationship between magnetization (M) and magnetic field strength (H), so-called magnetization hysteresis loop, for different types of materials is illustrated schematically in Figure 13.

The parameters extracted from the hysteresis loop that are most often used to characterize the magnetic properties of magnetic materials are:

- the saturation magnetization Ms, where all moments align along the direction of applied field,
- the remanence magnetization M_R, which is remained in the material after applied field is removed, and

- the coercivity field H_C, which is the field required to bring the magnetization to zero.
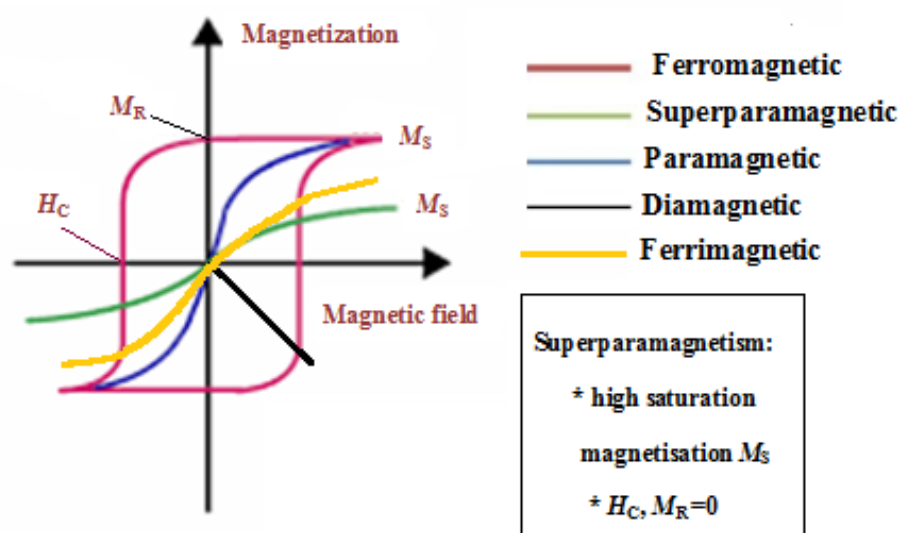
Fig. 13. Magnetization hysteresis loops of different magnetic materials [85].

Superparamagnetism is a form of magnetism, which appears in small ferromagnetic or ferromagnetic nanoparticles (size below about 50 nm in the direction under the influence of temperature [86]. The typical time between two flips is called the Néel relaxation time. In the absence of an external magnetic field, when the time used to measure the magnetization of the nanoparticles is much longer than the Néel relaxation time, their magnetization appears to be in average zero: they are said to be in the superparamagnetic state. In this state, an external magnetic field is able to magnetize the nanoparticles, similarly to a paramagnet. However, their magnetic susceptibility (the degree of magnetization of a material in response to an applied magnetic field) is much larger than that of paramagnets. In the Fig. 13, in contrast to the hysteresis observed in the case of ferromagnetic nanoparticles, the response of superparamagnetic nanoparticles to an external field also follows a sigmoidal curve, but shows no hysteresis.

3.2.1.4. The dependence of magnetization of superparamagnetic materials on temperature

Magnetic ions in the nanoparticle are locked together and produce a permanent magnetic dipole moment at any temperature. However, for temperatures higher than a so-called "blocking" temperature, T_B, the moment flips 180 degrees very rapidly and the resulting average moment is near zero. Only for temperatures below T_B does the moment stay fixed in one direction during the time of the measurement. Thus, the particles exhibit a ferromagnetic/ferrimagnetic-like response for temperatures below T_B, but possess a paramagnetic-like response above T_B. [87].

The blocking temperature can be determined from the magnetization vs. temperature exprements ($M(T)$ curves) for zero-field-cooling (ZFC) and filed-cooling (FC) conditions. In ZFC curve, magnetization increased with the temperature and than decreased, while magnetization decreased in FC curve (Fig. 14). The temperature at the peak point of ZFC curve is the blocking temperature [88]. The blocking temperature depends on the size of particles: TB is higher for large particles than for small particles. The particle size distribution also influence the shape of the $M(T)$ curve. Narrow peaks can be obtained for particles with narrow size distribution, while wide peaks for wide size distribution.
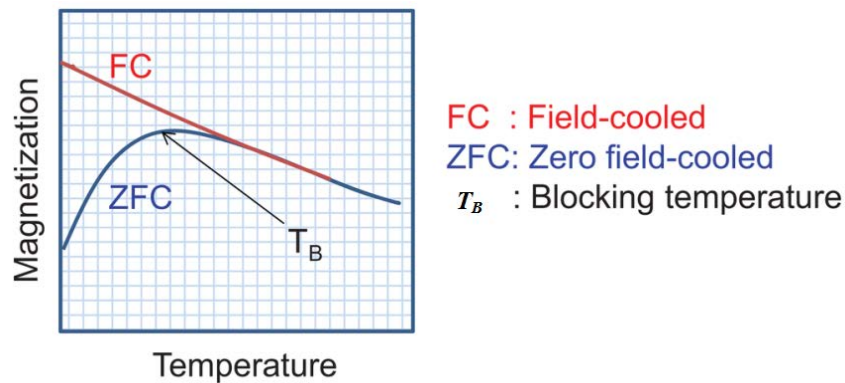
Figure 14. Experimental strategy for estimating the blocking temperature of magnetic nanoparticles [88].

Magnetization of superparamagnetic particles is described by the Langevin function (Eq. (2)):

$$M = M_s \left\{ coth\left(\frac{\mu H}{k_B T}\right) - \frac{k_B T}{\mu H} \right\}$$

(2)

where Ms saturation magnetization, μ the mean magnetic moment of a single particle, H is the applied field and $k_B T$ term corresponds to the thermal energy of the particles [89]. The Langevin relation considers each particle as a magnetic monodomain. The relationship between the mean magnetic moment of a particle and saturation magnetization of particles, as described by Eq. (2), can be used to calculate average particle size, D [89];

$$\mu = \frac{M_s \pi \rho D^3}{6}$$

(3)

where ρ is the density of the sample.

3.2.2. Other properties of magnetite

Natural and synthesized magnetite micro-scale crystals exhibit metallic luster and opaque jet-black color. Magnetite's density is established at 5.18 g/cm^3, slightly lighter than reddish-brown hematite (α-Fe$_2$O$_3$; 5.26 g/cm^3). At ambient temperatures, magnetite particles exhibit hardness of 5.5 (Mohs scale). Specific surface area of magnetite vary depending on synthesis method; however, typical micro-scale particles with approximate diameters of 0.2 µm exhibit surface areas of approximately 6 m^2/g. Magnetite particles are not porous. Standard Gibb's free energy of magnetite formation is - 1012.6 kJ/mol; therefore, formation of magnetite is thermodynamically favorable. Additionally, the standard enthalpy and entropy of magnetite formation are -1115.7 kJ/mol and 146.1 kJ/mol/K, respectively. Solubility products differ depending on the applicable dissolution reaction; however, magnetite dissolution is much faster than other pure ferric oxides [90].

Magnetite melting/boiling points are observed at 1590 and 2623 °C, respectively. Electrical conductivities range from 10^2–10^3 Ω^{-1}cm^{-1}, which evidence semi-conductor behavior of magnetite. This conductivity range borders conductor

(metallic) behavior. Semi-metallic behavior is further supported by magnetite's relatively low band gap (0.1 eV).

As magnetite particle diameters are decreased to the nano-scale, the structural, physical, thermal, electrical, and magnetic properties begin to change. Although many of these characteristic changes are described in the literature, some of nanoscale magnetite properties have not yet been explored.

Nano-scale magnetite still exhibits a face-centered cubic unit cell, although the unit cell volume is slightly larger. Electron probe analyses imply that oxygen concentrations within magnetite particles decline as particle size is reduced. Consequently, a relative decrease in iron valence is observed, generating greater ferrous ion presence. This structural change is insignificant to structural properties of magnetite, but some effect is observed on magnetic properties.

Owing to smaller particles, specific surface area of nano-magnetite is significantly larger than of micro-siyed magnetite (approximately 100 m^2g^{-1}). Magnetite nano-particles are assumed nonporous. Colloidal magnetite solutions are typically characterized by the jet-black color, hence no color change between bulk-scale and nano-scale magnetite is observed [90].

Magnetite readily oxidizes in air to maghemite (Eq. 4):

$$4\ FeO \cdot Fe_2O_3 + O_2 \rightarrow 6\ Fe_2O_3 \tag{4}$$

Magnetite and maghemite are similar in physical properties and crystalline structure. Both display ferrimagnetism, however maghemite has lower saturation magnetization. The difference in their magnetic response is because maghemite is structurally γ-Fe_2O_3, which is comprised solely of Fe^{3+} ions. In the crystalline structure, half of the Fe^{3+} ions are tetrahedrally coordinated and the other half are octahedrally coordinated [85].

At temperatures higher than 300°C, magnetite oxidizes to hematite, which is antiferromagnetic. Therefore, this conversion may be an important consideration in certain applications [85].

Magnetite surface chemistry plays an important role in magnetite applications. In aqueous systems, the Fe atoms coordinate with water, which dissociates readily to leave the iron oxide surface hydroxyl functionalized. Surface hydroxyl groups are amphoteric and may be protonated or deprotonated, depending on pH of solution. The

pH value where the surface displays an equal number of negative and positive surface charges is the point of zero charge, PZC. The PZC of magnetite depends on the powder properties, but usually is in the range 6.4-6.8 [91].

3.3. Applications of magnetite

Among all iron oxides, Fe_3O_4 presents the most interesting properties for applications: (*i*) it is magnetic, (*ii*) it contains Fe^{2+} in the structure which is an important electron donor, (*iii*) the octahedral site in the magnetite structure can easily accommodate both Fe^{2+} and Fe^{3+}, producing a very interesting redox chemistry within the solid structure [92,93].

An important application of magnetite is as an adsorbent for drinking water decontamination due to magnetite nanoparticles possess strong adsorption/reduction activities, and magnetic property to be easily separated and collected by an external magnetic field; these features make it suitable for the adsorption/reduction of quite a few heavy metal ions (e.g. Ni(II), Cu(II), Cd(II), Zn(II), Cr(VI), etc.).

Magnetite is also of great importance in environmental studies, as it is a common product of Fe^{3+} oxide reduction by biological and abiotic mechanisms, and can form by Fe^{2+} oxidation.

Magnetite is used in several medicinal and industrial processes as a ferrofluid; ferofluids are colloidal suspensions containing nanoscale magnetite particles; in the presence of strong magnetic fields, the ferrofluid will grow "spikes" along magnetic field lines. The great potential is in a diverse number of biomedical applications due to the guidable nature: retinal detachment therapy, cell separation methods, tumor hyperthermia, improved magnetic resonance imaging (MRI) contrast agents and as magnetic field-guided carriers for localizing drugs or radioactive therapies [85].

There are many other applications of magnetite nano particles: low-friction seals, dampening and cooling agents in loudspeakers, magnetically active membrane biological reactor, regenerant solution, controlled microfluidic flow etc. Clearly, nano-scale magnetite offers potential for creation of novel technology in multiple fields of study [90].

3.4. Synthesis of magnetite nanoparticles

The applications of magnetite nanoparticles depend on the preparation method, which, in turn, influences particle size and shape, size distribution, agglomeration and surface chemistry of the material [21].

Various methods for magnetite synthesis have been developed, such as micro-emulsion method, thermal decomposition of organic iron precursors in organic solvents, co-precipitation process, sol-gel method, solvothermal method, hydrothermal synthesis, electrochemical synthesis, ultrasonic chemical co-precipitation, gas/aerosol-phase methods, polyols method [81,94], etc.

3.4.1. Magnetite synthesis by the co-precipitation method

Co-precipitation from a solution of ferrous/ferric mixed salts has been widely used to produce magnetite nanoparticles for engineering application because of ease of implementation, large volume capability, and economy.

There are two methods of adding precursors [95] in the technique of co-precipitation from a solution of ferrous/ferric mixed salt to synthesize magnetite:

(i) Normal co-precipitation and (ii) reverse co-precipitation.

In the first case, the pH value gradually increases by dropping alkali solution into the mixed metals solution. In the second case, the mixed metals solution is directly dropped into an alkaline solution. Consequently, the pH value, a critical factor in synthesis of magnetite, can be easily controlled at high values.

In the co-precipitation method, according to reaction (5), the initial molar ratio of $Fe^{2+}:Fe^{3+}$ is considered to be 1:2. However, because Fe^{2+} oxidizes to Fe^{3+} in air and the oxidation rate is almost independent of the Fe^{2+} concentration, the $Fe^{2+}:Fe^{3+}$ ratio of the system reduces from the initial value (1:2).

$$Fe^{2+} + 2Fe^{3+} + 8OH^- \rightarrow Fe_3O_4 + 4H_2O \qquad (5)$$
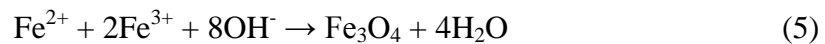
To solve this problem, some researchers synthesized magnetite nanoparticles by increasing the initial molar ratio of $Fe^{2+}:Fe^{3+}$ to more than 1:2 [95]. Generally, the

reaction is performed under inert (N_2 or Ar) atmosphere, using degassed solutions to avoid uncontrollable oxidation of Fe^{2+} to Fe^{3+} [21].

The following reactions are proposed for the mechanism of magnetite formation [21]:

$$Fe^{3+} + 3OH^- \rightarrow Fe(OH)_3(s) \tag{6}$$

$$Fe(OH)_3(s) \rightarrow FeOOH(s) + H_2O \tag{7}$$

$$Fe^{2+} + 2OH^- \rightarrow Fe(OH)_2(s) \tag{8}$$

$$2FeOOH(s) + Fe(OH)_2(s) \rightarrow Fe_3O_4(s) + 2H_2O \tag{9}$$

An overall reaction is:

$$2Fe^{3+} + Fe^{2+} + 8OH^- \rightarrow 2Fe(OH)_3 \cdot Fe(OH)_2(s) \rightarrow FeOOH \cdot Fe(OH)_2(s) +$$

$$+ H_2O \rightarrow Fe_3O_4(s) + 4H_2O \tag{10}$$
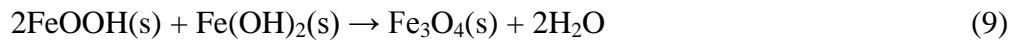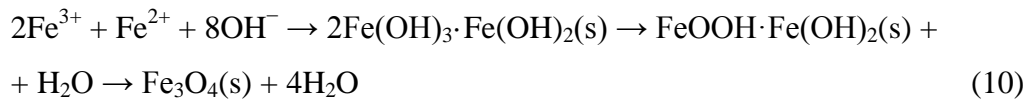
Briefly, the ferric and ferrous hydroxides are precipitated firstly. These reactions are very fast. Secondly, the ferric hydroxide decomposes to FeOOH. Finally, a solid state reaction between FeOOH and $Fe(OH)_2$ takes place, which produces magnetite.

3.4.2. Factors influencing the properties of magnetite nanoparticles synthesiyed by the co-precipitation method

The properties of magnetite nanoparticles, such as particle size, specific surface area, morphology and magnetization, are strongly depended on the synthesis conditions. The influence of different parameters, such as: iron salts concentration; the ratio of Fe^{2+}/Fe^{3+}; nature of the base used for the co-precipitation; the rate of the addition of the base solution; ratio of $OH^-/(Fe^{2+} + Fe^{3+})$ and temperature on the magnetite properties has been investigated [21-25,96].

Mascolo et al. [21] synthesized magnetite by co-precipitation reaction in a large pH range (10.0–13.0) at room temperature, by slow or fast addition of base (NaOH, KOH or $(C_2H_5)_4NOH$) in the reaction mixture. The reverse co-precipitation was also applied. It was shown that the size reduction of magnetite nanoparticles, precipitated with a certain base, was affected by both pH and the slow or fast addition of the basic solution to the solution of mixed Fe^{2+} and Fe^{3+} ions. As the amount of base and pH

increases, the nanoparticles size decreased. A further reduction of magnetite size was achieved by the change of the precipitating base, in accordance with the following sequence: $[(C_2H_5)_4NOH$ (6.5nm) < KOH (7.1nm) < NaOH (11nm)]. It was found that samples exhibit superparamagnetic properties and lower saturation magnetization had samples with smaller particles (crystallites). The agglomeration of individual nanoparticles appears to be responsible for the formation of mesoporous structures, which are affected by pH, nature of alkali, slow or fast addition of alkaline solution and drying modality of the synthesized powders. The degree of agglomeration, determined by the interface area among the individual particles, affects the value of saturation magnetization. Its reduction with the decrease of magnetite particle size becomes less marked for less agglomerated particles.

Gnanaprakash et al. [23] investigated the effect of temperature (30 or 60 ºC) and initial pH of iron salt solutions prior to alkali addition (0.7-6.7) on formation of magnetite nanoparticles during co-precipitation. It was found that the formed nanoparticles were 100 % spinel iron oxide (magnetite) when the initial pH was below 5. The content of magnetite decreased with the temperature and pH increasing. These results show that the initial pH and temperature of the iron salt solution before initiation of the precipitation reaction are critical parameters controlling the composition and size of the nanoparticles.

The impact of parameters of co-precipitation process on the properties of the superparamagnetic iron oxide nanoparticles was also investigated by Roth et al. [22]. Particle of different sizes and saturation magnetizations were achieved by variation of iron salt concentration, reaction temperature, ratio of hydroxide ions to iron ions and ratio of Fe^{3+}/Fe^{2+}. The results revealed that the particles' saturation magnetization could be enhanced by the employment of high iron salt concentrations and a molar ratio of Fe^{3+}/Fe^{2+} below 2:1. Furthermore, it was shown that the particle size could be increased by higher iron salt concentrations and a ratio of hydroxide ions to iron ions of 1.4:1.Overall results indicate that the saturation magnetization is directly related to the particle size.

The effects of surfactant, temperature, time, solvent and magnetic field on the morphology and particle size of the magnetite nanoparticles prepared by a coprecipitation method were investigated in the research of Nabiyouni et al. [24]. In all

various conditions, nanoparticles with average diameters less than 100 nm were synthesized, which exhibited ferrimagnetism behavior at room temperature. Bigger particles were obtained with anionic than cationic surfactant, by prolonged time of synthesis and with higher quantity of solvent.

Valenzuela et al. [96] studied the influence of the stirring velocity on the size of the magnetite nanoparticles synthesized by the co-precipitation method, where ammonia was added in deoxygenated aqueous solutions of Fe^{2+}/Fe^{3+} (molar ratio 1:2) at 20 ^{0}C. Two stirring conditions were applied: mechanical stirring (homogenizer) at different velocity and magnetic stirring. Then suspensions obtained were aged and digested at 80 ^{0}C under a gentle magnetic stirring. Superparamagnetic nanoparticles of magnetite with a mean diameter of 10 nm and narrow size distribution were obtained by using a homogenizer at a stirring velocity of 10,000 rpm. At this stirring velocity, the mean diameter of the nanoparticles was smaller than the values obtained by vigorous magnetic stirring. A decrease in stirring velocity resulted in a larger size of particles (~19 nm) and a wider size distribution. At 18,000 rpm, in addition to magnetite, goethite is also synthesized in the form of nanoparticles and nanorods. An increase in the precursor solution's temperature by high stirring velocities initially promotes the partial thermal oxidation of magnetite to goethite, generating goethite nanorods by the hydrothermal process. If the temperature highly increases, the final product is a non-magnetic mixture of iron oxide, hematite and goethite instead of magnetite.

The influence of processing conditions on the crystallite size and magnetic properties of Fe_3O_4 nanoparticles was studied by Upadhyay et al. [25]. The samples were prepared by (i) reverse co-precipitation method, at Fe^{2+}/Fe^{3+} ratio 1:2, at room temperature or at 100 ^{0}C, and (ii) modified co-precipitation method, using only Fe^{2+} ion and KNO_3 as an oxidizing agent, at different reaction times. It was found that the crystallite size and lattice parameter increased as the temperature and the reaction time increased. Larger magnetite nanoparticles were obtained via oxidation method. Magnetically, the synthesized nanoparticles are ranging from superparamagnetic to multi domain state. Magnetic parameters of the samples show a strong dependence on average crystallite size.

Overall results indicate that the saturation magnetization of the magnetite synthesized by co-precipitation method is directly related to the size of magnetite

crystallites, which can be controlled by the type and quantity of base used for co-precipitation, the temperature and duration of the synthesis, the type and velocity of stirring, and concentration of solvent. In addition, saturation magnetization is also related to phase composition, i.e. the quantity of other iron phases than magnetite, which can be influenced by the quantity of iron salt, ration Fe^{2+}/Fe^{3+}, temperature and pH of the iron salts solution.

4. Water pollution

Water pollution is the contamination of water bodies (rivers, lakes, oceans, and groundwater), very often by human activities when pollutants are directly or indirectly discharged into water bodies without adequate treatment to remove harmful compounds. The specific contaminants leading to pollution in water include a wide spectrum of chemicals, pathogens, and physical changes such as elevated temperature and discoloration.

Water pollution can be caused in a number of ways, one of the most polluting being city sewage and industrial waste discharge. Indirect sources of water pollution include contaminants that enter the water supply from soils or groundwater systems and from the atmosphere via rain.

The contamination of water resources has important repercussions for the environment and human health. For example, water pollution by heavy metals represents a serious problem for a variety of living species due to their toxicity, persistency and bioaccumulation tendency [80]. Pollution of water bodies with dyes causes, in addition to visual pollution, changes in the biological cycles of the aquatic biota, particularly affecting the photosynthesis and oxygenation processes of the water body, for example by hindering the passage of sunlight through the water. Moreover, some classes of dye, especially azo dyes and their byproducts, may be carcinogenic and/or mutagenic [97]. A major impact on the quality of natural water, especially lakes and streams, has also phosphates, which caused the eutrofication due to over-production of algae and water weeds.

4.1. Polution by cadmium

Cadmium is a relatively rare metal with atomic number 48. It prefers oxidation state +2 in most of its compounds. In its pure state, cadmium is silvery white with a bluish color, insoluble in water and not flammable [98]. Pure cadmium does not exist in nature, but it is present as oxide, sulfide, sulfate, carbonate and chloride [99].

Cadmium is used in the production of inks and dyes, as well as in many industrial applications such as metal plating, engraving and soldering. It is also used in plastics and production of nickel–cadmium batteries, which are in widespread use in cell phones, portable computers, and in many toys. Also, cadmium is present in trace amounts in food [99].

Common sources of cadmium in natural waters are fertilizer, fungicides, pesticides, soil and air pollution [67]. Cadmium also appears in industries as an inevitable by-product of zinc, lead and copper extraction. Naturally, a very large amount of cadmium is released into the environment, about 25,000 tons a year. About half of this cadmium is released into rivers through weathering of rocks and some of it into air through forest fires and volcanoes. The rest of the cadmium is released through human activities, such as manufacturing [99].

Cadmium is one of the most toxic heavy metals. It accumulates in the body and has varying degrees of toxicity where it replaces the body's stores of the essential zinc in the liver and kidneys [99]. According to the world health organization, intake of dietary cadmium should not exceed 7 micrograms per kilogram of body weight, per week.

Health effects that can be caused by cadmium are: high blood pressure, diarrhea, stomach pains and severe vomiting, osteoporosis due to depletion of calcium, bone fracture, reproductive failure and possibly even infertility, damage to the central nervous system and destruction of red blood cells, damage to the immune system; psychological disorders, possibly DNA damage or cancer development, etc. [100].

As cadmium is presents stably in the environment with great difficulty for microbiological degradation, it is necessary to eliminate them from wastewaters by using some effective methods before their discharge into environmental systems. Several methods have been employed to remove cadmium ions from wastewater, which

include precipitation, flotation, ion exchange, membrane-related process, electrochemical technique and biological process [101]. Low efficiency performance particularly when used on very small concentration of cadmium ions, the necessity of using expensive chemicals in some methods as well as accompanying disposal problem are among the drawbacks of these conventional methods. In regards of its simplicity and high-efficiency characteristics even for low concentrations, adsorption is looked upon as a good technology.

4.2. Pollution by hexavalent chromium

Chromium is the earth's 21st most abundant element (about 122 ppm) and the sixth most abundant transition metal. The principal chromium ore is ferric chromite, $FeCr_2O_4$, while crocoite, $PbCrO_4$, and chrome ochre, Cr_2O_3 are less common. Chromium occurs mainly in +III and +VI oxidation states, whereby chromium(VI) compounds are more toxic than Cr(III) due to their high water solubility and mobility [102]. Cr(VI) compounds include a large group of chemicals with varying chemical properties, uses, and workplace exposures [103].

Although chromium(VI) is dangerous and toxic, it's useful in industrial applications. Major industrial sources of Cr(VI) to environment are effluents from electroplating, metal finishing, magnetic tapes, pigments, leather tanning, wood protection, chromium mining and milling, brass, electrical and electronics' equipments manufactures and catalysis [104]. In natural waters, chromium(VI) is present also due to erosion of chromium deposits found in rocks and soils. In uncontaminated waters, the concentration of chromium is extremely low (< 1 $\mu g/dm^3$).

Hexavalent chromium exists in water primarily as hydrogen chromate ion ($HCrO_4^-$) and chromate ion (CrO_4^{2-}), depending on the pH: $HCrO_4^-$ predominates at pHs between 1.0 and 6.0, and CrO_4^{2-} at pHs above about 6.0 [102]. At pHs less than about 1.0, H_2CrO_4 is dominant species. The dichromate ion ($Cr_2O_7^{2-}$) forms when the concentration of chromium exceeds approximately 1 g/dm^3.

Single exposures to hexavalent chromium compounds can cause irritation and inflammation of the nose and upper respiratory tract, irritation of the skin and eye

damage from splashes. Repeated exposure to hexavalent chromium compounds can cause: damage to the nose, including ulcers and holes in the flap of tissue separating the nostrils (the nasal septum); inflammation of the lungs; allergic reactions in the skin and respiratory tract; kidney damage and cancer of the lung [105].

Several treatment technologies have been developed to remove chromium from water and wastewater. Common methods include chemical precipitation, ion exchange, membrane separation, ultrafiltration, flotation, electrocoagulation, solvent extraction, reduction, reverse osmosis, dialysis/electrodialysis, adsorption/filtration, flocculation, chelation etc. [102]. Chemical precipitation has traditionally been the most used method. The disadvantage of precipitation is the production of sludge, which constitutes a solid waste a disposal problem. Ion exchange is considered a better alternative. However, it is not economically appealing because of high operational costs. Adsorption is a promising process for removal of Cr(VI) because of its economic efficiency, simplicity of design, low cost and high selectivity.

4.3. Pollution by phosphates

Phosphates exist in three forms in aqueous systems: orthophosphate, metaphosphate (or polyphosphate) and organically bound phosphate. Orthophosphate are produced by natural processes, but major man-influenced sources include: partially treated and untreated sewage, runoff from agricultural sites, and application of some lawn fertilizers. Orthophosphate is a readily available to the biological community and typically found in very low concentrations in unpolluted waters. Polyforms are used for treating boiler waters and in detergents. In water, they are transformed into orthophosphate and available for plant uptake. The organic phosphate is the phosphate that is bound or tied up in plant tissue, waste solids, or other organic material. After decomposition, this phosphate can be converted to orthophosphate [106].

Phosphates stimulate the growth of plankton and aquatic plants, which provides food for larger organisms. Initially, this increased productivity will cause an increase in the fish population and overall biological diversity of the system. But, as the phosphate loading continues and there is a build-up of phosphate in the lake or surface water ecosystem, the aging process (eutrophication) of lake or surface water ecosystem will be

accelerated. In situations where eutrophication occurs, the excessive inputs, usually a result of human activity and development, appear to cause an imbalance in the "production versus consumption" of living material in an ecosystem. This overproduction can lead to a variety of problems ranging from anoxic waters to toxic algal blooms and decrease in diversity, food supply, and habitat destruction. Some blue-green algae can at times produce toxins, which are harmful to humans, pets, and farm animals [106].

Controlling phosphorous discharged by municipal and industrial wastewaters is a key factor in preventing eutrophication of surface waters. Phosphorus removal from wastewater can be achieved either through chemical removal, advanced biological treatment or a combination of both [107]. The chemical removal of phosphorus involves the addition of calcium, iron and aluminum salts to achieve phosphorus precipitation by various mechanisms. Biological phosphorus removal is dependent upon the uptake of phosphorus in excess of normal bacterial metabolic requirements and is proposed as an alternative to chemical treatment. Adsorption technology, owing to its simplicity, efficiency and cost-effectiveness, has been increasingly challenged lately.

4.4. Pollution by dyes

Many industries such as textile, leather, food processing, dyeing, and cosmetics generate massive amount of wastewater, and dye chemicals represent one of the most prominent contaminants contained in the wastewater effluents. The presence of dye in the water bodies increases the chemical oxygen demand as well as adversely influences the metabolic functions of phytoplankton and aquatic plants by interfering with photosynthesis [108]. Intense exposure to dyes leads to have increased heartrate, vomiting, shock, Heinz body formation, cyanosis, jaundice, quadriplegia, and tissue necrosis in humans [109]. It is noteworthy that some dyes are highly toxic and mutagenic, and also decrease light penetration and photosynthetic activity, causing oxygen deficiency and limiting downstream beneficial uses such as recreation, drinking water and irrigation.

Dyes are organic compounds with a complex chemical structure, which includes a group of atoms known as chromophores, responsible for the dye color. These chromophore-containing centers are based on diverse functional groups, such as azo, anthraquinone, methine, nitro, arilmethane, carbonyl and others. In addition, electrons withdrawing or donating substituents so as to generate or intensify the color of the chromophores are denominated as auxochromes.The most common auxochromes are amine, carboxyl, sulfonate and hydroxyl [97].

Dyes are persistent in the environment owing to their high stability to light, temperature, water, detergents, chemicals, soap and other parameters such as bleach and perspiration. The synthetic origin and complex aromatic structure make them more recalcitrant to biodegradation [97]. Therefore, to safeguard environment and human health, it is necessary to monitor and regulate the concentration of dyes in waste effluents before they are discharged into the environment [110].

There are four commonly used methods for the treatment of textile wastewater: physical methods include membrane technology; chemical methods include photochemical oxidation and coagulation processes; biological methods include anaerobic/aerobic sequential processes and physico-chemical processes. Among the physico-chemical processes, adsorption technology is known to be one of the extremely useful technologies, because of its high efficiency, good benefit/cost ratio, the availability of different adsorbent types and the possibility of reusing the adsorbent and/or adsorbate [111]. By proper selection of the adsorbent, the adsorption can be a simple, environmental friendly and low cost operation of high efficiency [112].

5. Application of adsorption for the water pollutants removal

5.1. Adsorption from liquid phase on a solid surface

The adsorption is a mass transfer process by which a substance (adsorbate) is transferred from the liquid phase to the surface of a solid (adsorbent), and becomes bound by physical and/ or chemical interactions. The adsorption process is referred to as physical adsorption if the attraction between the solid surface and the adsorbate is

physical in nature, where the attractive forces are Van der Waals forces, which are weak, and the resulting adsorption is reversible in nature. On the other hand, if the attraction forces between adsorbate and the solid surface arise due to chemical bonding, the adsorption process is called chemisorption; the bonding in this case is strong, and it is difficult to remove chemisorbed species from the solid surface.

A great variety of materials applies as adsorbents for the removal of different pollutants from water The most important properties for an adsorbent is the porous structure resulting in high surface area; a highly porous solid may be carbonaceous or inorganic in nature, synthetic or naturally occurring, and in certain circumstances may have true molecular sieving properties [113].

There are three main steps involved in adsorption from liquid phase onto a solid adsorbent (Fig. 15): (1) the transport of an adsorbate from the bulk of the liquid to the boundary layer (film) around the adsorbent particle; (2) the transport of an adsorbate through the boundary layer, (3) internal diffusion through the adsorbent pores, and (4) adsorption on the adsorbent's particle surface.
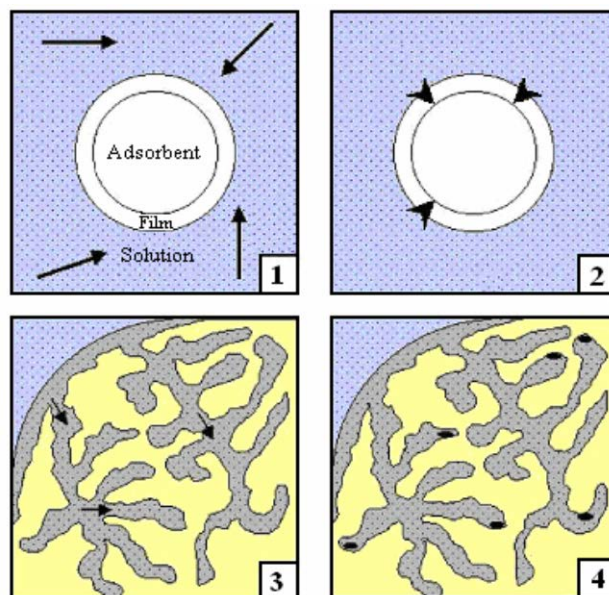
Fig. 15. Schematic illustration of adsorption steps [113].

5.2. Factors influencing the adsorption process

The most important factors affecting adsorption are [114]:

Nature of adsorbate and adsorbent: The nature of the adsorbent has a profound effect on the process of adsorption, because it determines the type of adsorbate that will be adsorbed. Activated carbon, metal oxides, silica gel, zeolite, and clay are commonly used adsorbents.

Specific surface area and pore sizes of the adsorbent: The surface area determines the number of adsorption sites and generally, the greater the specific surface area of the solid, the greater would be its adsorption capacity. Pore size is the factor which determines the accessibility of the sites for adsorbates. Generally, there is an inverse relationship between the pore size and surface area: the smaller the pores for a given pore volume, the greater the specific surface area. However, the pores should be large enough to allow the adsorbate to enter them.

Particle size of the adsorbent: Smaller particle sizes reduce internal diffusional and mass transfer limitation to the penetration of the adsorbate inside the adsorbent particle. The use of adsorbents in the nanoscale strongly enhances the adsorption efficiency because of the high exposed surface able to interact with the adsorbate.

Activation of adsorbents: Different methods are applied for specific surface area increasing or for change of chemical nature of adsorbent surface. Specific surface area can be increased:
- by making the surface of the adsorbent rough,
- by dividing the adsorbent into small fine pieces or grains,
- by removing the compounds already adsorbed,
- by physical (thermal methods) or chemical (acid or base) activation.

The properties of adsorbents can be tailored for specific applications through surface functionalization, by using different compounds: surfactants, silanes, oxides etc. In that way, adsorption capacity for specific adsorbate can be significantly increased.

Adsorbent dosage: In many instances, higher adsorbent dosages yield higher uptakes and higher percentage removal efficiency. Increase in adsorbent dosage generally increases the amount of solute adsorbed due to the increase in surface area and the number of binding sites.

Solubility of the adsorbate: Solubility of an adsorbate is an important factor affecting adsorption. In general, the extent of adsorption of a solute is inversely proportional to its solubility in the solvent (water) from which adsorption occurs. Such effect of solubility on adsorption might be expected since, in order for adsorption to occur, solute-solvent bonds must first be broken. The greater the solubility, the bonds are stronger and hence the smaller the extent of adsorption. However, there are exceptions since many compounds are difficult to adsorb even though they are slightly soluble. Some compounds which are very soluble may be adsorbed readily.

Polarity of adsorbate: A general rule is that polar surfaces prefer polar adsorbates and non-polar surfaces prefer non-polar adsorbate.

Contact Time: Sufficient contact time is required to reach adsorption equilibrium and to maximize adsorption efficiency.

Temperature: In adsorption process, temperature does take effect in rate of adsorption and the extent to which adsorption occurs. Generally, adsorption rates increase with increase in temperature. However, since the adsorption is generally an exothermic process, an increase in temperature normally leads to a decrease in the adsorbed amount. However, the influence of temperature on the adsorption from a liquid phase can be more complicated because different processes are include in adsorption process.

pH of solution: pH usually plays major role in the adsorption process because it affects: the solution chemistry of adsorbate, the activity of the functional groups of the adsorbent, solubility of the adsorbate and degree of ionization of the adsorbate during adsorption.

5.3. Adsorption of ionic species from water onto solid surfaces

Adsorption of ionic species on the active sites of the solid surface results in the formation of outer- and inner-sphere complexes. *Outer-sphere* complexes occur if at least one water molecule is interposed between the surface functional group and the bound ion (Fig. 16). On the contrary, *inner-sphere* complexes occur when water molecules are not interposed between the bound ion and the functional group of the

adsorbent and the adsorbate forms a direct coordinate-covalent bond with surface functional groups on the variable charge surface [115,116]. The formation of inner-sphere complexes are usually denoted as specific adsorption, while the formation of outer-sphere complexes belongs to the non-specific adsorption processes.
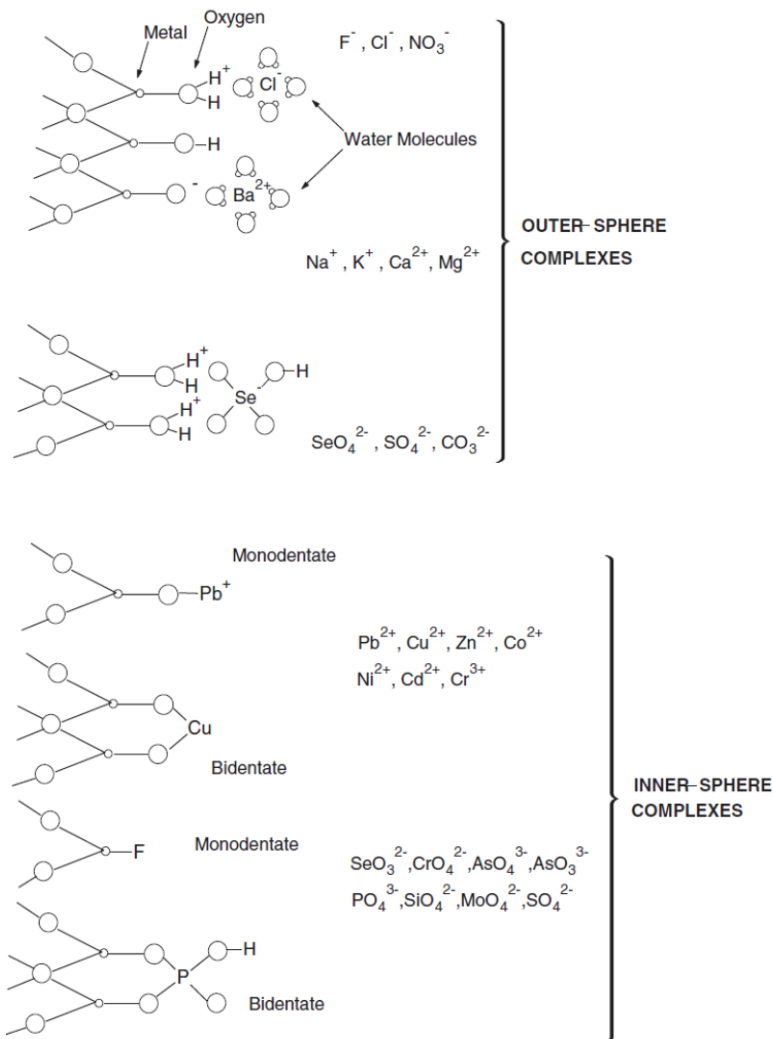
Fig. 16. Schematic presentation of different types of adsorption complexes that can be occurred on solid surfaces [115].

Outer-sphere complexes are formed through electrostatic interactions between metal ions and oppositely charged solid surface. At the earlier adsorption stages, outer-sphere complexes are formed at the external surface sites, while, as ions concentration

increases, the ions are forced into internal surface sites forming also inner-sphere complexes. These inner complexes are more stable compared to the outer-sphere complexes due to the formation of covalent bonds or combinations of covalent and ionic bonding [116]. On the other hand, outer-sphere complexation is usually rapid and reversible, while inner-sphere complexation is slower and may be irreversible [116].

During the formation of inner-sphere complexes, protons are released and the process causes a total decrease in solution pH. The adsorption will be strongly pH dependent, where adsorption of cations generally increases, while the anions adsorption decreases with increasing pH. In addition, the metals can be transferred from the bulk solution to the solid phase due to precipitation on the mineral's surface. Mineral addition in electrolyte solution can reduce metal solubility and enhance metal precipitation on the mineral surface even in a non-saturated environment. At low surface coverage complexation tends to dominate, while as the surface coverage increases nucleation occurs and results in the formation of distinct entities or aggregates on the surface; as loading increases further, surface precipitation becomes the dominant mechanism. Precipitation mostly depends on solution pH and initial metal concentration. Moreover, co-precipitation of metals may play an important role in the surface precipitation mechanism. Surface precipitation is favored by the pH increase. [116]. Hence, the addition of minerals that significantly increases the pH enhances metal removal from the bulk solution.

5.4. Adsorption equilibrium

Knowledge of adsorption equilibrium is necessary to estimate the maximum capacity of an adsorbent, as well as to characterize the molecular forces involved in this process. Adsorption equilibrium is a dynamic concept achieved when the rate at which adsorbate species adsorb onto a surface is equal to the rate at which they desorb [117]. The adsorbent 'affinity' for the adsorbate determines adsorbate distribution between the adsorbent and liquid (water) phase.

The adsorption equilibrium relates the amount of solid-bound adsorbate (q_e) and its portion remaining in the solution (residual, final or equilibrium concentration, c_e) at a constant temperature:

$$q_e = f(c_e) \tag{11}$$

The adsorption equilibrium relationship given by Eq. 11 is termed an adsorption isotherm. Typically, this dependence is obtained by gathering the adsorption capacity data at a fixed temperature and various adsorbate concentrations and the data are plotted as an isotherm, i.e. loading versus concentration at constant temperature.

Many theoretical and empirical models have been developed to represent the various types of adsorption isotherms. At present, there is no single equation that satisfactorily describes all mechanisms and shapes [118]. Langmuir, Freundlich and Sips models are some of the equations that find common use for describing adsorption isotherms [42].

5.4.1. Langmuir model

In 1916 Langmuir proposed the monolayer adsorption theory. The assumptions made in the derivation of the Langmuir model are:
- Adsorption sites on adsorbent surface have the same adsorption energy
- One adsorption site is occupied by one adsorbed molecule
- There is no lateral interaction between adsorbed molecules
- Adsorption is complete when a monolayer is formed,
- Adsorption takes place only at specific localized sites on the surface and the saturation coverage corresponds to complete occupancy of these sites [119].

The Langmuir isotherm is usually described by:

$$q_e = \frac{q_m K_L c_e}{1 + K_L c_e} \tag{12}$$

where:

q_e is the amount of the adsorbate adsorbed per unit mass of adsorbent at equilibrium,

c_e is the equilibrium concentration of the adsorbate in the bulk solution,

q_m is the maximum adsorption capacity (monolayer capacity) and

K_L is the constant related to the free energy of adsorption.

5.4.2. Freundlich model

The empirical model developed by Freundlich in 1906 [120], can be applied to multilayer adsorption, as well as for adsorption at heterogeneous surfaces [121]. The Freundlich relation is an exponential equation that assumes that concentration of adsorbate on adsorbent surface increases by increasing the adsorbate concentration in the liquid phase [116, 117]. It is represented by the equation:

$$q_e = K_f \; c_n^{1/n} \tag{13}$$

where:

k_F is a constant which indicates the relative adsorption capacity of the adsorbent; it is a function of energy of adsorption and temperature;

n is a sorption intensity parameter, where the strength of adsorption bonds is higher when n is higher; values of n > 1 represent favorable nature of adsorption.

5.4.3. Sips model

Sips isotherm is a combined form of Langmuir and Freundlich expressions deduced for predicting the heterogeneous adsorption systems and circumventing the limitation of the rising adsorbate concentration associated with Freundlich isotherm model. At low adsorbate concentrations, it reduces to Freundlich isotherm; while at high concentrations, it predicts a monolayer adsorption capacity, characteristic of the Langmuir isotherm. Generally, the equation parameters are governed mainly by the operating conditions such as the alteration of pH, temperature and concentration [122].

The Sips isotherm is described by:

$$q_{\mathrm{e}} = \frac{q_m \cdot K_{\mathrm{S}} \cdot c_{\mathrm{e}}^{1/n_{\mathrm{s}}}}{1 + K_{\mathrm{S}} \cdot c_{\mathrm{e}}^{1/n_{\mathrm{s}}}} \qquad (14)$$

where:

K_{a} is the Sips equilibrium constant and

n_{S} is the index of heterogeneity.

5.5. Adsorption kinetics

Kinetic performance of a given adsorbent is of a great significance for the practical applications. The kinetic parameter, that is helpful for the prediction of adsorption rate, gives important information for design of adsorption systems [123]. Residence time required for completion of adsorption may be established according to kinetic analysis [124]. To describe the rate of an adsorption process, three kinetic models are usually used.

5.5.1. Pseudo-first order equation model

The Largergren model [125], proposed in 1898, is widely used for adsorption kinetics. It can be represented by the equation:

$$\frac{\mathrm{d}q_{\mathrm{e}}}{\mathrm{d}t} = k_1(q_{\mathrm{e}} - q_{\mathrm{t}}) \qquad (15)$$

where:

q_{e} and q_{t} are adsorption capacity at equilibrium and at time t, respectively and

k_1 is the pseudo-first order rate constant of adsorption.

After integration and applying of boundary conditions: from t = 0 and $q_t = 0$ to t = t to $q_t = q_t$, equation (15) becomes:

$$\log(q_e - q_t) = \log q_e - \frac{k_1 t}{2.303} \tag{16}$$

5.5.2. Pseudo-second order model

If the adsorption involves rather complex interactions and the effects of transport phenomena and chemical reactions that are not experimentally inseparable, the pseudo second order model is used [126]. This model is based on the assumption that the adsorption capacity is proportional to the number of the active sites [127].

The model is expressed as:

$$\frac{dq_t}{dt} = k_2(q_e\text{-}q_t)^2 \tag{17}$$

where k_2 is the pseudo-second order rate constant of adsorption.

After integration and applying of boundary conditions: from $t = 0$ and $q_t = 0$ to t = t to $q_t = q_t$, equation (17) becomes:

$$\frac{t}{q_t} = \frac{1}{k_2 q_e^2} + \frac{t}{q_e} \tag{18}$$

5.5.3. Intra-particle diffusion model

The overall adsorption rate is shown to be controlled by one or more steps, e.g., film or external diffusion, pore diffusion, surface diffusion, and adsorption on the pore surface, or a combination of more steps [112].

In order to assess the extent to which diffusion, as the rate-controlling step, participates in the adsorption process, the intra-particle diffusion model, proposed by Weber and Morris [128] was used:

$$q_t = k_{td}\, t^{1/2} + C \tag{19}$$

where:

k_{td} is the intra-particle diffusion rate constant, and

c is a constant that gives information about thickness of the boundary layer.

This model considered the intra-particle diffusion as the rate controlling step when the value of c is close to zero [112].

5.6. Adsorption thermodynamics

5.6.1. Influence of temperature on adsorption

A number of adsorption studies deals with the influence of temperature on the adsorption. Temperature increase results in changes related to both kinetics and equilibrium due to:

- increase in the kinetic energy which facilitates the access of the adsorbate to the active adsorption sites,

- decrease in the mass transfer resistance; the increase in temperature causes a decrease in the thickness of the boundary layer surrounding the adsorbent, so that the mass transfer resistance of the adsorbate in the boundary layer decreases; it results in an increase in the diffusion rate of the adsorbate in the adsorbent,

- lowering of pH_{PZC}; the resulting decrease in surface charge at constant pH lead to a decrease in electrostatic repulsion; However, at very high temperatures physical damage to the adsorbent can occur, reducing its adsorption capacity [129,130].

In most cases, it is desirable to evaluate the adsorption capacity of an adsorbent at room temperature, since at higher temperature the operational cost of the process increases.

Most studies of cations adsorption show that an increase in temperature enhances the adsorption process. In the anion adsorption case, there are several studies on the adsorption on oxide mineral with respect to temperature dependence. It is

generally expected that an increase in temperature causes a decrease in adsorption capacity because of the change in charge [130].

5.6.1. Evaluation of thermodynamic parameters

Thermodynamic parameters of adsorption, free energy of adsorption (ΔG^o), enthalpy (ΔH^o) and entropy (ΔS^o), are calculated by using the thermodynamic equilibrium constant k_a, which has also been derived in different ways in the literature [131].

According to thermodynamic law, $\Delta G°$ of adsorption is calculated as follows:

$$\Delta G^o = -RT \ln k_a \tag{20}$$

where:

T is the absolute temperature,

R is the gas constant and

k_a is thermodynamic equilibrium constant.

The relationship of $\Delta G°$ to enthalpy ($\Delta H°$) and entropy ($\Delta S°$) of adsorption is expressed as:

$$\Delta G^o = \Delta H° - T \Delta S^o \tag{21}$$

According to Liu [131], k_a can be obtained using Langmuir constant k_L, as follows:

$$k_a = \frac{k_L}{\gamma_e} \cdot (c_s) \tag{22}$$

where:

γ_e is the activity coefficient of the adsorbate at the adsorption equilibrium, and

c_s is the molar concentration of the standard reference solution (1 mol/dm^3)

In the case of a dilute solution of charged adsorbate (e.g., heavy metal ions), the activity coefficient in Eq. 22 would be close to unity, thus Eq. 22 can be reduced to:

$$\Delta G^{o} = -RT \ln k_{L} \tag{23}$$

The substitution of Eq. 23 into Eq. 21 gives:

$$\ln k_{L} = -\frac{\Delta H^{o}}{RT} + \frac{\Delta S^{o}}{R} \tag{24}$$

By plotting $\ln k_{d}$ *vs* $1/T$, the enthalpy ($\Delta H°$) and the entropy ($\Delta S°$) of adsorption are determined from the respective slope and intercept of the straight line of (Eq. 24). It was concluded [131] that the thermodynamic equilibrium constant of adsorption can be reasonably approximated by the Langmuir equilibrium constant for neutral adsorbates or adsorbates with very weak charge and also for a dilute solution of charged adsorbate. In this case, the Langmuir equilibrium constant can be applied for determination of $\Delta G°$. It was stated that special attention should be given if the equilibrium constants derived from other adsorption isotherm equations.

In 1987, Khan and Singh [132] proposed the method used to calculate thermodynamic parameters (Eq. 28) by using distribution coefficient (k_{d}):

$$k_{d} = \frac{q_{e}}{c_{e}} \tag{25}$$

It was proposed that at very low concentrations of absorbate, k_{d} is equal to the thermodynamic equilibrium constant k_{a}. Thus, k_{d} value is obtained by plotting (q_{e}/c_{e}) against c_{e} and extrapolating c_{e} to zero. The data fitline intersection with the vertical axis gives the value of k_{d}. So obtained value is used for $\Delta H°$ and $\Delta S°$ determination according to Eq. 25 [80].

6. Synthesis, properties and application of magnetic composite adsorbents

Recently, magnetic separation technology has attracted much attention and made progress in water treatment because of improvement material performance as an adsorbent, and its easy and fast separation.

Owing to adsorption/reduction activities and the possibility to easily separate from a treated water by applying an external magnetic field, magnetite nanoparticles have a huge potential in the field of water treatment [1,2] for the removal of different pollutants from contaminated waters, including lead [3,133,134], cadmium [4], hexavalent chromium [3,133], arsenic [6] and phosphates [135]. However, nanoparticles of magnetite tend to aggregate and oxidize in air, which decreases the efficiency in the process of water pollutants removal. To prevent the aggregation of magnetite nanoparticles, magnetic adsorbents are prepared by loading magnetic nanoparticles on the surface of carrier. At present, many kinds of materials have been used as carrier to prepare magnetic composite adsorbents for different contaminants removal from water. In most cases, the composites were synthesized by co-precipitation method, by adding base in deoxygenated suspension of the support with Fe^{2+} and Fe^{3+} ions.

Besides by co-precipitation method, Yuan et al. [7] synthesized montmorillonite-supported magnetite nanoparticles also by loading montmorillonite in synthesiyed magnetite hydrosol. Co-precipitation was performed by dropping the suspension of montmorilonite in alkaline solution into the ferric chloride/ferrous chloride solution, without changes the parameter of synthesis (one ratio Fe^{2+}/Fe^{3+}, one ratio iron salts/montmorilonite etc.). It was shown that montmorillonite-supported magnetite nanoparticles exist on the surface or inside the interparticle pores of the clay. The supported magnetite nanoparticles synthesized via hydrosol method were shown to be better dispersive than those synthesized via co-precipitation method and the unsupported magnetite nanoparticles. The Cr(VI) uptake was mainly governed by a physico-chemical process, which included an electrostatic attraction followed by a redox process in which Cr(VI) was reduced into trivalent chromium. It was shown that the adsorption of Cr(VI) was highly pH-dependent and the kinetics of the adsorption followed the pseudo-second-order model. The adsorption data fit well with the Langmuir and Freundlich isotherm equations. The montmorillonite-supported magnetite nanoparticles showed better adsorption capacity per unit mass of magnetite (15.3 mg/g) than unsupported magnetite (10.6 mg/g), and were more thermally stable than the unsupported sample.

Nourmohamadi et al. [136] synthesized Fe_3O_4/bentonite magnetic composite by using NH_3. As in other composites, magnetite particles were less aggregated then in pure magnetite. The composite was used for the copper removal from wastewater.

Commercial NaY zeolite was used to obtained zeolite/magnetite composite [9] by co-precipitation method, by adding NaOH in the suspension of NaY in iron salt solution. Just one sample was prepared and used for the removal of Cu^{2+}, Cr^{3+} and Zn^{2+} from water. It was shown that the main magnetic phase formed is maghemite, not magnetite. It was suggested to selectively reduced maghemite to magnetite in order to enhance the magnetization of the composites. This increase in magnetization might be of importance to improve the magnetic separation of the adsorbent from its medium. The composites showed high adsorption capacities for the Cu^{2+}, Cr^{3+} and Zn^{2+} in aqueous solution and no reduction of the adsorption was produced by the formation of the composite. In addition, the magnetic composites showed good chemical resistance in a wide pH range 5–11. The same synthesis procedure was applied for the synthesis of zeolite composite for the removal of pharmaceutical compounds from aqueous solution [137]. As in previous case, just one sample was prepared, without varying the synthesis parameters.

Magnetic zeolite nanocomposite was successfully synthesized also by a two sequential steps method [138]. In the first step, nanocrystalline zeolite A was synthesized; then, magnetite nanocrystals were prepared in the presence of nanozeolite. The magnetic measurements showed that composite has sufficiently magnetic properties to be attracted by a magnetic field. The composite was used for the removal of Cs^+ and Sr^{2+} ions. This nanocrystalline zeolite composite showed higher adsorption capacity for the ions than microcrystalline zeolite composite. Adsorption of the ions was fast and experimental kinetic data were well fitted with pseudo-second-order kinetic model.

In addition, magnetic zeolite composites with different ratio zeolite/magnetite were synthesized by adding previously synthesized Fe_3O_4 in the precursor of zeolite [139]. The addition of Fe_3O_4 makes the zeolite with good magnetic susceptibility and good magnetic stability regardless of the Fe_3O_4 loading, confirming the considerable separation efficiency. Additionally, Fe_3O_4 loading had alittle effect on removal of heavy metal by magnetic zeolite (Cu^{2+} and Pb^{2+}).

Sepiolite was also used as a support for magnetite [10] and the composite adsorbents obtained by co-precipitation method was used for atrazine removal from water. The co-precipitation was performed in air, by adding ammonia in the sepiolite suspension with iron salts. Synthesis parameters were not changed and just one sample was prepared. It was shown that magnetite particles were uniformly distributed in sepiolite matrix and the composite had higher specific surface area than pure sepiolite. Magnetic hysteresis loop measurements indicate that composite had relatively high saturation magnetization, low remanent magnetization and small coercivity, which ensures separation by external magnetic field. The adsorption experiments show that the composite possessed high adsorption capacity for atrazine and the adsorption process followed the Langmuir isotherm model. Similar method of synthesis was applied for the sepiolite-magnetite composite which was used for the removal of Cd^{2+} and Co^{2+} ions [26], and the composite [140] used for safranin dye removal from water.

Slightlly modified co-precipitation method was used for magnetite/paligorskite composite synyhesis [12]. Fe^{3+} ions were firstly adsorbed on palygorskite nanoparticles and then Fe^{2+} ions were added, followed by ammonia addition for co-precipitation. All characterizations confirmed the palygorskite nanoparticles' surface modification by magnetite particles, which gave them a superparamagnetic behavior with high saturation magnetization. Despite the reduction of their specific surface area after surface modification of the palygorskite, which should result in reduced absorptive potential of this clay, the magnetic nanoparticles are easily removed from the medium by a simple magnetic separation procedure, proving that magnetic palygorskite nanoparticles can be effectively used to remove methylene blue from contaminated wastewaters.

Magnetite composites were also prepared with activated carbon, at different ration magnetite/activated carbon [15] and with different bases [16]. It was shown that magnetic nanoparticles were successfully decorated on the surface of the activated carbon via precipitating mixture of ferrous and ferric chloride by NaOH or NH_3 [16]. The two precipitating agents cause significant differences on activated carbon. NaOH results a decrease in the surface area and a slight increase in the alkalinity of the sample, while NH_3 causes a collapse in the texture and a significant surface acidity of the sample. The saturation magnetization of the sample obtained with NH_3 was much lower.

It was shown that the impregnation with magnetite decreases the adsorption capacity of activated carbon for the Reactive Black 5 dye.

In adition to standard co-precipitation methods of the composites synthesis, some modifications of the synthesis were applied in order to improve dispersity of magnetite particles and general properties of the composites. For example, sepiolite-supported magnetite nanocomposite with excellent dispersity was successfully prepared by a facile, robust and time-saving microwave-assisted co-precipitation of Fe^{2+} and Fe^{3+} in the mixed solvent of water and ethylene glycol [141]. The composite exhibited excellent removal ability to low concentrations of Cr(VI) and the removal capacity (33.4 mg/g, per unit mass of magnetite) at pH 3.0 was higher than that of the unsupported magnetite nanoparticles (22 mg/g). In addition, magnetic sepiolite nanofibers were prepared by thermal decomposition of organic iron precursors [11]. The obtained composites had a high specific surface area, high loading amount, the non-aggregated nature of magnetite nanocrystals, good dispersion and magnetic properties, which make them promising for use as a separable adsorbent for As(III) removal with high adsorption capacity and magnetic separation properties.

Regardless of some improvements in the synthesis of magnetic composites, it is obvious that co-precipitation method was not optimized, i.e. the synthesis was performed usually under constant conditions, without examining the influence of synthesis parameters on the composites properties and the adsorption capacity.

EXPERIMENTAL PART

7. Experimental procedure

7.1. Materials

Natural sepiolite (SEP) from Andrići (Serbia), natural zeolite (NZ) from Slanci locality (Serbia), and acid-activated sepiolite (ASEP), prepared according to the previous study [20], were used as the starting materials. Briefly, ASEP was prepared by 10 h stirring of dispersion of 10 g of sepiolite in 100 cm^3 of 4 M HCl solution, at the room temperature. The solid was then separated from the liquid phase by centrifugation and washed with distilled water until Cl$^-$ ion free. The obtained sample was dried at 110 °C for 2 h.

The reagent grade chemicals such as NaOH, $FeCl_3 \cdot 6H_2O$, $FeSO_4 \cdot 7H_2O$, $Cd(NO_3)_2$, $K_2Cr_2O_7$, KH_2PO_4, Basic Yellow 28 and C.I. Reactive Orange 16 were used without any further purification. Structures of dyes Basic Yellow 28 and C.I. Reactive Orange 16 are shown in Fig. 17.

a)   b)
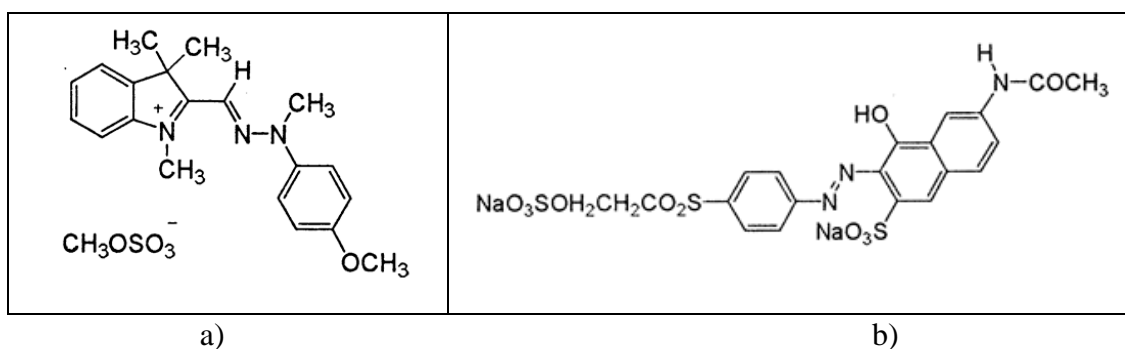
Fig. 17. Structure of dye: a) Basic Yellow 28, b) C.I. Reactive Orange 16.

7.2. Preparation of magnetic nanocomposites and pure magnetite

The sepiolite-magnetite and zeolite-magnetite composites were prepared by the precipitation of magnetite onto the SEP, NZ and ASEP surfaces.

Two procedures were applied for the MNCs synthesis:

Procedure 1: 5 g of SEP or ASEP or NZ powder was first added into 500 cm^3 of 1 M NaOH or NH$_3$ solution under stirring to make a suspension, which was further kept under a N$_2$ atmosphere for 30 min. After dissolving 4.51 g of $FeCl_3 \cdot 6H_2O$ and 2.31 g

$FeSO_4 \cdot 7H_2O$ (molar ratio of $Fe^{2+}:Fe^{3+} = 1:2$) in 100 cm^3 of distilled water that was deoxygenated by bubbling N_2 gas for 30 min, the solution was kept under a N_2 atmosphere in a water bath at ~ 60 ^oC. Then, the suspension of SEP or ASEP or NZ in NaOH solution was dropped into the solution, followed by the stirring of the mixture for 2 h at the same temperature. The SEP-based composites were prepared also using 1.5 M NaOH solution and with different quantity of iron salts in order to obtain composite with 50 % more (6.77 g $FeCl_3 \cdot 6H_2O$ and 3.46 g $FeSO_4 \cdot 7H_2O$) or 50 % less (2.25 g $FeCl_3 \cdot 6H_2O$ and 1.15g $FeSO_4 \cdot 7H_2O$) magnetite.

Procedure 2: First, 4.51 g of $FeCl_3 \cdot 6H_2O$ was dissolved in 500 cm^3 deionized water and then 5 g of SEP, ASEP or NZ was added, followed by treatment in an ultrasonic bath for 15 min. The dispersion was bubbled by a N_2 gas for 30 min before the solution of 2. 31 g of $FeSO_4$.$7H_2O$ in 100 cm^3 deoxygenated water was added. The mixture was stirred for 30 min under a N_2 atmosphere and then placed in a water bath, at ~ 60 ^0C, followed by the drop wise addition of the NaOH or NH_3 solution (25%) until a black precipitate was formed. The suspension was aged for 2 h at the same temperature. The synthesis with NH_3 was repeated with ratio $Fe^{2+}/Fe^{3+} = 1:1.5$ for all supported materials, SEP, ASEP and NZ.

The pure magnetite was synthesized by the following procedure: the solution of 4.51 g of $FeCl_3 \cdot 6H_2O$ and 2. 31 g of $FeSO_4 \cdot 7H_2O$ in 100 cm^3 deionized degassed water was kept under a N_2 protection in a water bath at ~ 60 ^oC and NaOH solution (25 %) was added drop wise until a black mixture was formed (~ 15 cm^3). The mixture was stirred and aged for 2 h at 60 ^oC.

In all cases, after magnetic separation or filtration, the solid phase was washed three times with deoxygenated deionized water (100 cm^3) and finally with ethanol (50 cm^3). The drying was performed under vacuum at 60 ^oC until constant mass.

Schematic presentation of the procedures used for the composite synthesis is given in Fig. 18.

Procedure 1

5 g SEP/ASP/NZ in 500 cm^3 of NaOH or NH$_3$ solution

↓ dropping into

100 cm^3 of Fe^{2+} + Fe^{3+} solution (N2 treated) in water bath (60 ºC)

↓

stirring for 2 h at 60 ºC

↓

magnetic separation and/or filtration

↓

washing with water and etanol

↓

vacuum drying at 60 ºC

Procedure 2

5 g SEP/ASP/NZ in 500 cm^3 of Fe^{3+} solution (N$_2$ treated) + 100 cm^3 of Fe^{2+} (N2 treated)

↓

stirring for 30 min at 60 ºC

↓

addition of NaOH or NH$_3$

↓

magnetic separation and/or filtration

↓

washing with water and etanol

↓

vacuum drying at 60 ºC

Figure 18. Schematic presentation of the procedures used for the composite synthesis

A qualitative assessment of the magnetization of the composites was demonstrated by a hand-held magnet. Examples of the magnetization assessment are shown in Fig. 19.
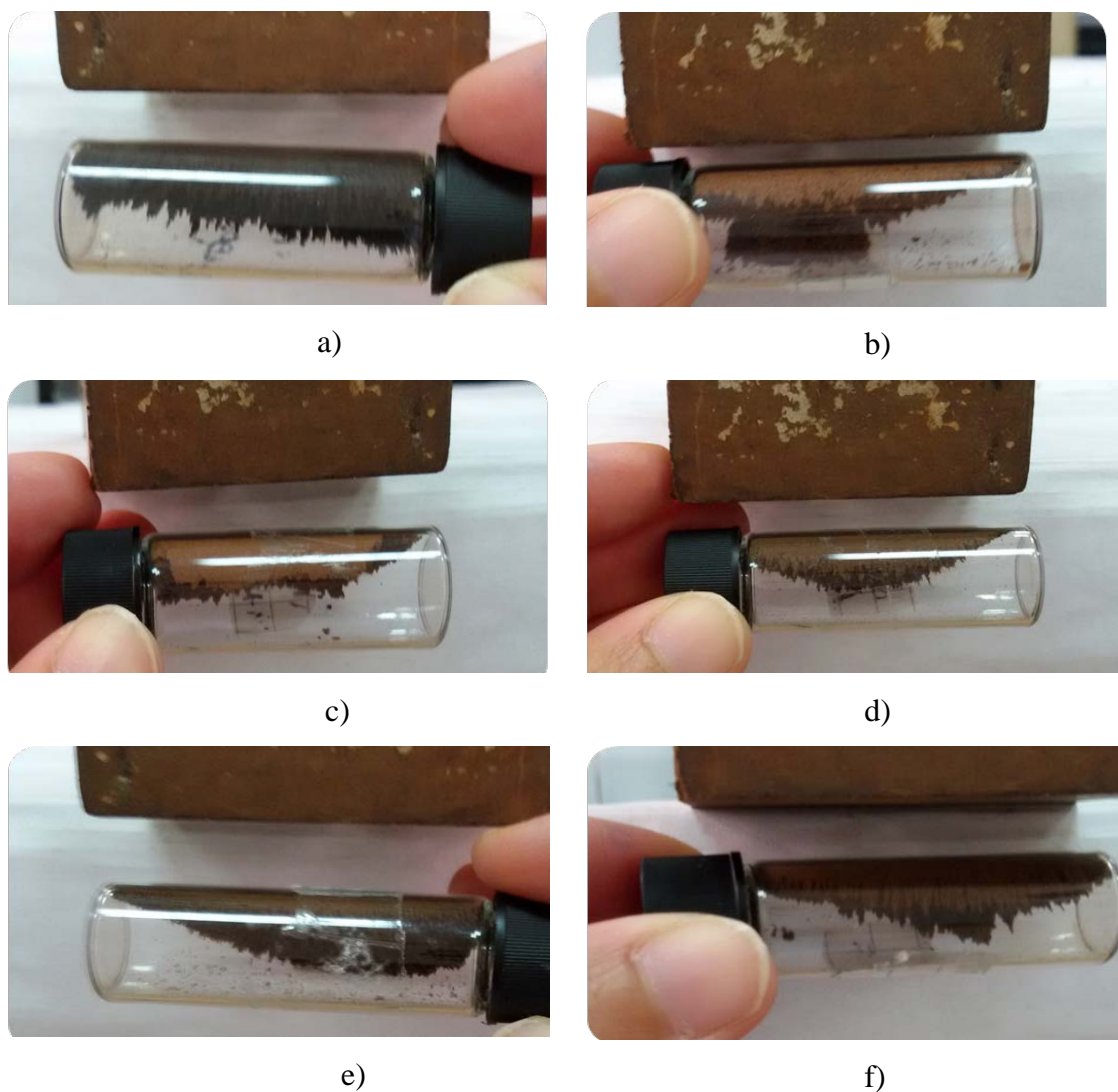
Fig. 19. A qualitative assessment of the magnetization of the: a) pure magnetite, b) SEP-M(1)NaOH(1:2), c) NZ-M(1)NaOH(1:2), d) SEP-M(2)NH$_3$(1:2), e) ASEP-M(2)NH$_3$(1:2), f) NZ-M(2)NH$_3$(1:2).

7.3. Characterization

The X-ray diffraction (XDR) analysis of the samples was carried out with an ITAL STRUCTURES APD 2000 diffractometer using CuKα radiation, in the 2θ angle range from 5° to 50°, with a 0.02° step. The average crystallite sizes of the compounds in the composites were calculated by applying the Scherer equation [142]:

$$D = \frac{k\lambda}{\beta \cos\theta} \qquad (26)$$

where: D - crystallite size, k - a dimensionless shape factor, λ - X-ray wavelength, θ - diffraction angle, and β - the peak width at the half-maximum height after subtraction of the instrument broadening.

The FTIR analysis was performed on a MB BOMAN HARTMANN 100 instrument in the wave number range from 4000 to 400 cm^{-1}. The samples were prepared by the KBr method, with a sample to KBr ratio of 1:150.

The particles morphology of the samples was observed by a Tescan MIRA3 field emission gun scanning electron microscope (FESEM), with electron energies of 20 kV in a high vacuum. The samples were sputter-coated with an Au-Pd alloy to ensure the surface conductivity.

The TEM analysis of samples was performed on a JEOL T-100 instrument. The samples were ultrasonically dispersed in ethanol to form a dilute suspension. A drop of the suspension was applied onto a holy carbon film supported by a copper-mesh TEM grid and air-dried at room temperature.

The specific surface area (S_{BET}) and the pore size distribution of the samples were determined using the nitrogen adsorption–desorption isotherms obtained by a Micrometrics ASAP 2020 instrument. Before the sorption measurements, the samples were degassed at 150 °C for 10 h under reduced pressure. The S_{BET} of the samples were calculated according to the BET method [143], taking into account the linear part of the nitrogen adsorption isotherm. The volume of the mesopores and the pore size distribution were analyzed according to the Barrett, Joyner and Halenda (BJH) method [144], from the desorption isotherm. The volume of the micropores was calculated according to the α-plot analysis [145].

The differential thermal and thermo-gravimetric analyses were conducted on an SDT Q600 TGA/DSC instrument (TA Instruments), at a heating rate of 20 °C/min, with less than 10 mg of the sample. The analyses were done in air, with a flow rate of 100 cm^3/min.

The magnetic measurements were performed using a Quantum Design MPMS XL-5 SQUID magnetometer. The DC magnetization measurements were carried out as a function of temperature (T = 5-300 K) in the magnetic field of 100 Oe. The

magnetization *vs.* magnetic field strength measurements (hysteresis) were performed at temperatures 5 K and 300 K in the fields up to 50 kOe.

The point of zero charge (PZC) was determined by a batch equilibration method [20,78], in KNO_3 solutions having concentration of 0.1 M, 0.01 M or 0.001 M. The initial pH values (pH_i) of KNO_3 solutions (20 cm^3) were adjusted by addition of 0.1 M HNO_3 or 0.1 M KOH, in the pH range from 3 to 9. Then 0.02 g of the sample was added to the solution and kept under constant stirring for 24 h at 25 ºC. Finally, the samples were filtrated and the pH values of the filtrates (pH_f) were measured. The PZC was determined from the pH_f *vs.* pH_i dependence as the pH value of a plateau [20,78].

7.4. Adsorption experiments

The adsorption experiments were performed by batch technique to investigate the removal of Cd^{2+}, chromates (Cr(VI)), phosphates, Basic yellow 28 dye and C.I. Reactive Orange 16 dye onto pure compounds and MNCs. The solutions were prepared by dissolving $Cd(NO_3)_2$, $K_2Cr_2O_7$, KH_2PO_4, Basic Yellow 28 and C.I. Reactive Orange 16, respectively, in deionized water. The general method used for the adsorption experiments is described as follows: 20 cm^3 of solution was placed in 50 cm^3 reagent bottle, the pH value was adjusted and then the constant amount of adsorbent (0.02 g) was added to each bottle, followed by shaking for a given period of time.

For the purpose of determining the adsorption isotherms, solutions of different concentrations were prepared and equilibrated with an adsorbent at 25 ^{o}C for 24 h, at the initial pH value (pH_i) of 7.0 ± 0.1 (Cd^{2+}), 2.0 ± 0.1 (chromates), 5.0 ± 0.1 (phosphate), 5.0 ± 0.1 (Basic Yellow 28) and 4.0 ± 0.1 (C.I. Reactive Orange 16).

The effect of temperature on Cd^{2+} and Cr(VI) adsorption was conducted for some samples by determining the adsorption isotherms at different temperatures, under the same conditions as those employed for the determination of the adsorption isotherms at 25 ^{o}C.

The amounts of ions retained by the adsorbents at equilibria, q_e (mg/g), were calculated using the equation:

$$q_e = \frac{c_i - c_e}{m} \cdot V \qquad (27)$$

where c_i is the initial metal ion concentration (mg/dm^3), c_e is the equilibrium concentration (mg/dm^3) of metal ions in the solutions, V is volume of solution (dm^3) and m is mass of the adsorbent (g).

The kinetics analysis of the Cd^{2+} adsorption was done using solution of 100 mg/dm^3 concentration. For the kinetic analysis of Cr(VI) adsorption, solutions of 40 mg/dm^3 concentration was used. The suspensions of adsorbent in ion solutions were equilibrated for different time intervals and the amounts of ions retained by the adsorbents at time t, q_t (mg/g), were calculated using the equation:

$$q_t = \frac{c_i - c_t}{m} \cdot V \qquad (28)$$

where and c_t (mg/dm^3) is the metal ion concentration in the solution after time t.

After adsorption of Cd^{2+} and Cr(VI), the adsorbent was separated from the suspension using filter paper, whereas in the case of adsorption of dye centrifugation was used. The final solution pH (pH$_f$) was measured using a pH meter (Ino Lab WTW series pH 720). The initial concentrations of Cd^{2+} and Cr(VI), as well as the concentrations after the adsorption, were determined using the atomic absorption spectrometer (AAS) (Perkin Elmer 730). The concentrations of phosphate, Basic yellow 28 and C.I. Reactive Orange 16 were determined by UV–Vis spectroscopy (Shimadzu 1800 instrument). The solutions for analysis by UV–Vis spectroscopy were prepared by passing through a syringe filter (pore size of 0.22 μm). Absorbance measurements were made at 880 nm (for phosphate), 439 nm (for Basic Yellow 28) and 493 nm (for C.I. Reactive Orange 16).

The adsorption equilibrium data were fitted to the Langmuir (Eq. 12), Freundlich (Eq. 13), and Sips (Eq. 14) isotherms. The adsorption isotherms constants were determined by non-linear regression analysis using the OriginPro 8.5.

The adsorption kinetics data were analyzed by the pseudo-first (Eq. 15) and pseudo-second order (Eq. 16) kinetics models.

Thermodynamic parameters of adsorption were calculated by using equations 21 – 25.

8. Results and discussion

8.1. A qualitative assessment of the magnetization

A qualitative assessment of the magnetization of the composites and the synthesis conditions are systematized in Table 4.

Generally, for the magnetite synthesis by a co-precipitation (Eq. 5 - 10) it is necessary to prevent Fe^{2+} oxidation and to provide enough OH^- ions for Fe^{2+} and Fe^{3+} co-precipitation [21]. During the synthesis of the composites and pure magnetite, a nitrogen bubling provided an inert atmosphere to prevent the oxidation, while the quantity of OH^- ions was optimized by the pH value adjustment using NaOH or NH_3. When a support like sepiolite or zeolite is present in the reaction mixture, the pH value is determined not just by the quantity of base added, but also by the interaction of the surface functional groups of the support with H^+ (at pH < pH_{pzc}) or OH^- (at pH > pH_{pzc}) ions from the solution [20].

In the Procedure 1 of the composite synthesis (Figure 18, Table 4), the suspension of a support was stirred with base, before the mixture of Fe^{2+} and Fe^{3+} was added. The idea was to form, in that way, negatively charged sites on the support surface, which can attract Fe^{3+} and Fe^{2+} in order to ensure magnetite precipitation directly on the surface, providing a better dispersion of the magnetite particles. In the case of ASEP as the support, because of a high interaction of the acid functional groups with OH^- ions, there was not enough OH^- ions in the solution for magnetite formation and the red material without magnetite properties was formed (Table 4), probably the $Fe(OH)_3$/ASEP composite. As the solubility of $Fe(OH)_3$ is much lower than of $Fe(OH)_2$, when there was not enough OH^- ions for Fe^{3+}/Fe^{2+} co-precipitation, $Fe(OH)_3$ was precipitated. The increase of the concentration of the NaOH/NH_3 solution did not provide conditions for magnetite synthesis, probably because ASEP reacted with base at very high concentrations. Thus, the composites with ASEP formed by the Procedure 1 were without magnetic properties (samples ASEP-M(1)NaOH(1:2) and ASEP-M(1)NH$_3$(1:2)).

Table 4. The experimental conditions of the composites preparation and the assessment of the magnetization (yes – magnetic sample, no – sample without magnetic properties)

Sample	Support	Base	Procedure	$FeSO_4 \cdot 7H_2O$ (g)	$FeCl_3 \cdot 6H_2O$ (g)	$Fe^{2+}:Fe^{3+}$ ratio	Magnetization
SEP-M(1)NaOH(1:2)	SEP	NaOH	1	2.31	4.51	1:2	yes
SEP-M(2)NaOH(1:2)			2				
SEP-M(1)NH$_3$(1:2)		NH$_3$	1				
SEP-M(2)NH$_3$(1:2)			2				
SEP-M(1)NaOH(1:2)*		NaOH (1.5 M)					
SEP-M(1)NaOH(1:2)^{more}		NaOH	1	3.46	6.77		
SEP-M(1)NaOH(1:2)^{less}				1.15	2.25		
SEP-M(2)NH$_3$(1:1.5)		NH$_3$	2	2.78	4.06	1:1.5	
ASEP-M(1)NaOH(1:2)	ASEP	NaOH	1	2.31	4.51	1:2	no
ASEP-M(2)NaOH(1:2)			2				
ASEP-M(1)NH$_3$(1:2)		NH$_3$	1				
ASEP-M(2)NH$_3$(1:2)			2				
ASEP-M(2)NH$_3$(1:1.5)				2.78	4.06	1:1.5	
NZ-M(1)NaOH(1:2)	NZ	NaOH	1	2.31	4.51	1:2	yes
NZ-M(2)NH$_3$(1:2)		NH$_3$	2				
NZ-M(2)NH$_3$(1:1.5)				2.78	4.06	1:1.5	

In the Procedure 2, NaOH or NH_3 was added in the suspension of the support with Fe^{2+} and Fe^{3+} and the co-precipitation could take place before the interaction of OH^- ions with the functional groups of the support. When NH_3 was used, the magnetic composites with both SEP and ASEP were obtained, whereas the magnetic properties were not achieved when NaOH, as a strong base, was applied for the co-precipitation in the presence of ASEP (sample ASEP-M(2)NaOH(1:2)).

The magnetic composites based on NZ as a support were prepared intentionally with NaOH by Procedure 1 and with NH_3 by Procedure 2.

Hereinafter, the properties of the samples with magnetic properties (MNCs) were analyzed in comparison to the properties of SEP/ASEP/NZ and Fe_3O_4.

8.2. XRD analysis

The XRD patterns of the magnetite composites together with the patterns of the pure components are shown in Figs. 20-22. The patterns of SEP and ASEP (Figs. 19 and 20, respectively) show that sepiolite (JCPDS card no. 13-0595) is the only phase in the samples. According to the previous research, the crystallinity of ASEP is lower due to acid-activation [20]. The XRD pattern of the NZ sample (Fig. 22) revealed clinoptilolite (C) as the dominant phase with lower contents of quartz (Q) and feldspar (F).

The presence of the peaks characteristic for SEP and ASEP are obvious in the patterns of the SEP/ASEP-based magnetic composites (Figs. 20 and 21, respectively), indicating that the SEP and ASEP structures were preserved. The intensities of the peaks for SEP and ASEP in XRD patterns of the composites are lower than for pure compounds, due to the lower quantity of SEP or ASEP in the composites because of magnetite presence. The sizes of the sepiolite crystalite in the MNCs were approximately the same as in SEP (11.0 nm)/ASEP (8.1 nm), indicating that the crystallinity of SEP and ASEP did not decrease during the composites preparation. The values of the sepiolite crystallite sizes were calculated by using the Sheerer equation (Eq. 26), according to the width of the peak at $2\theta \sim 7.2^o$.
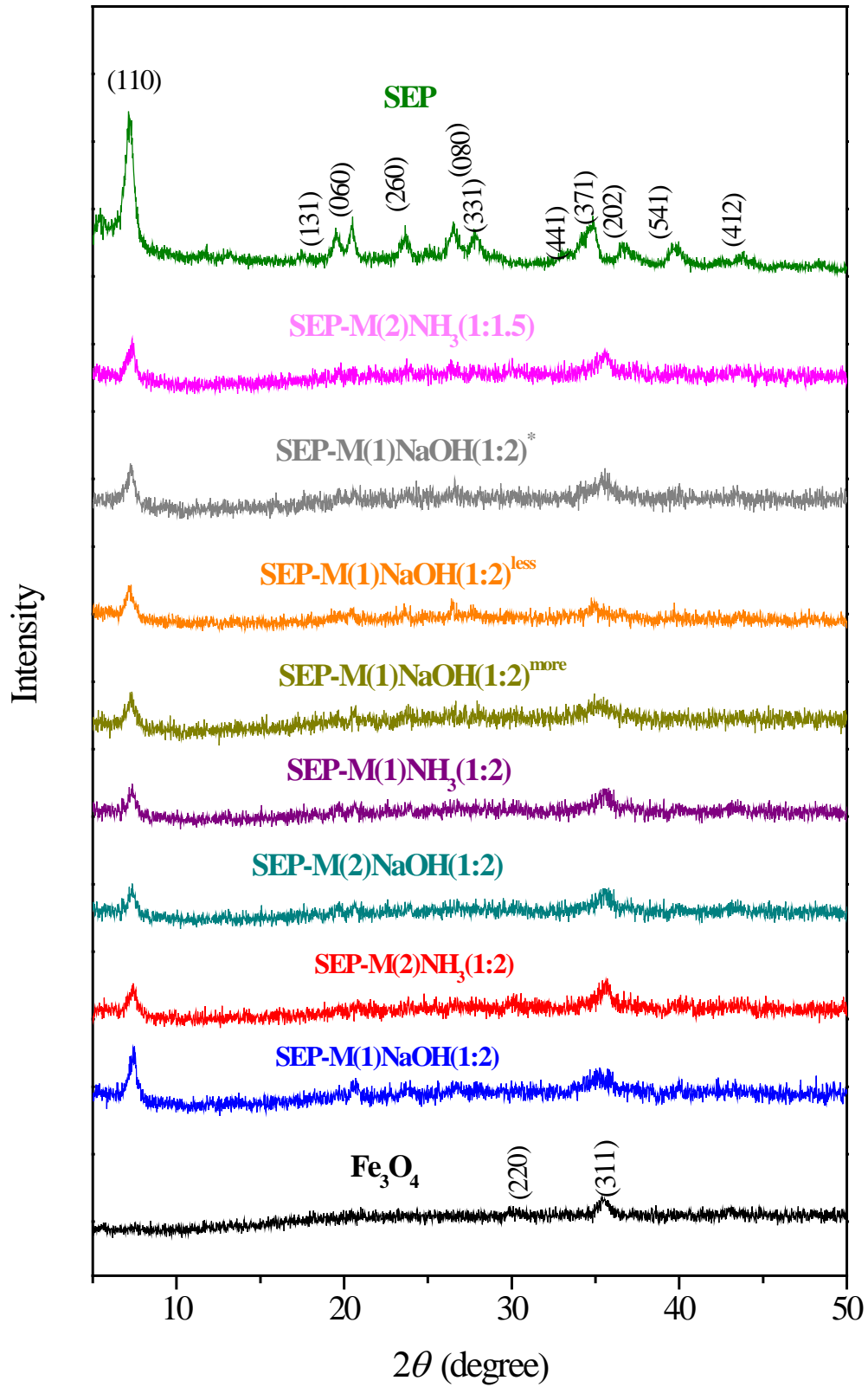
Fig. 20. XRD patterns of the Fe$_3$O$_4$, SEP and the SEP-based MNCs.
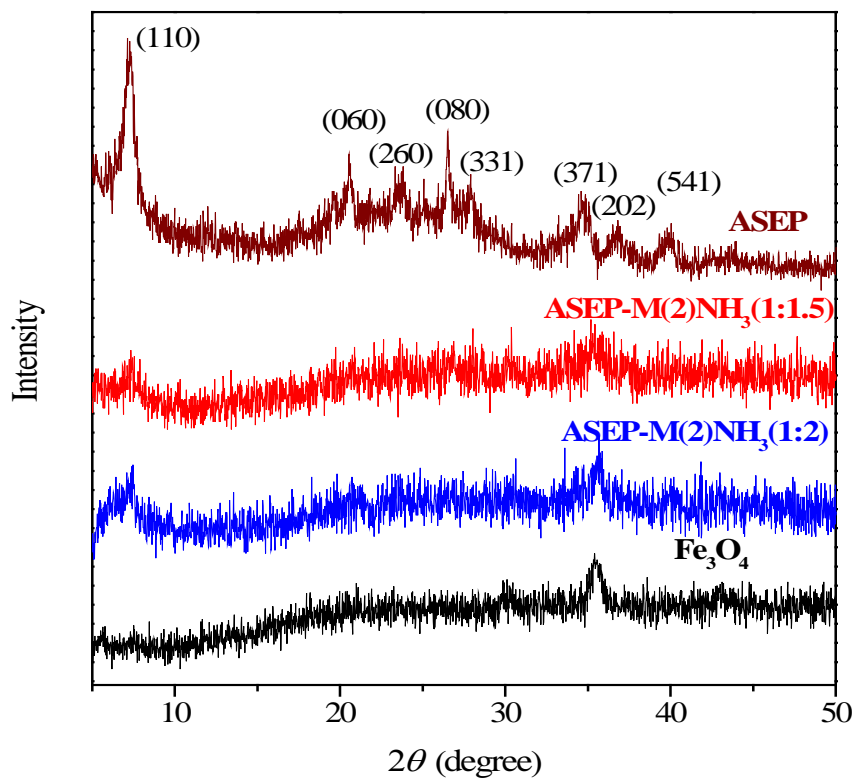
Fig. 21. XRD patterns of the Fe_3O_4, ASEP and the ASEP-based MNCs.
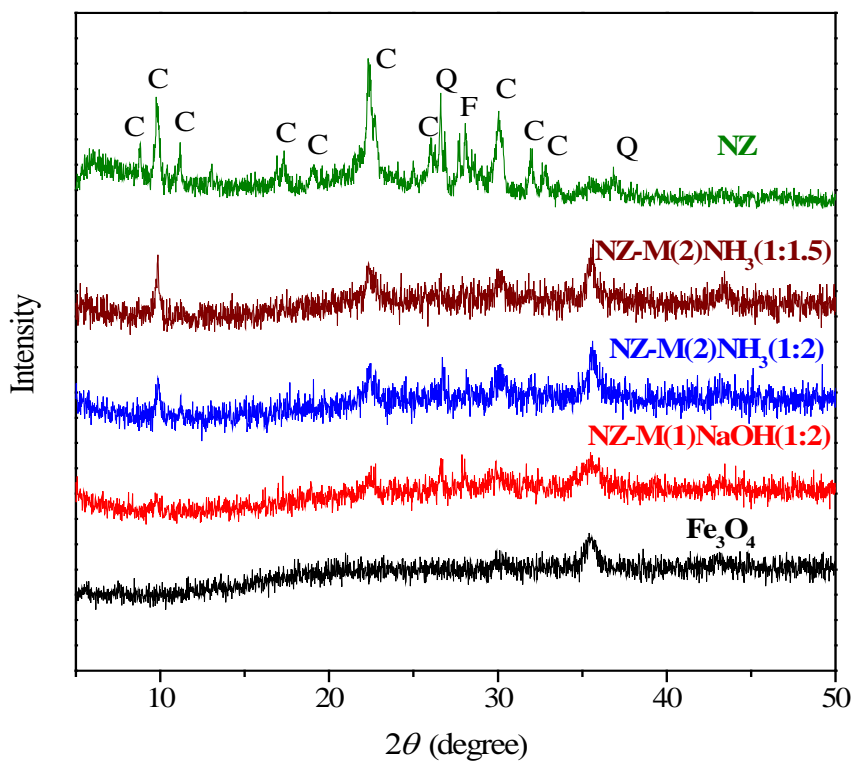
Fig. 22. XRD patterns of the Fe_3O_4, NZ and the NZ-based MNCs.

The main diffraction peak of Fe_3O_4 (JCPDS card no. 65-3107) is observed at 2θ of ~ 35.5°, and it was used for calculation of the size of crystallite in the pure magnetite (10.2 nm). This peak is visible in the XRD patterns of the SEP/ASEP-based magnetic composites, but it partially overlapped with the sepiolite peak at 2θ ~ 35°. Therefore, the size of magnetite crystallites in MNCs could not be precisely calculated according to the XRD analysis. However, taking into account that intensity and width of the peak in the patterns of the MNCs are similar as in the pattern of pure magnetite (Figs 20 and 21), it can be stated that the Fe_3O_4 crystallites in MNCs are of similar sizes as in the pure magnetite. Differences are visible in the case of samples with lower and higher content of magnetite (SEP-M(1)NaOH(1:2)^{less} and SEP-M(1)NaOH(1:2)^{more}). The most intensive magnetite peak is hardly noticeable in the pattern of the SEP-M(1)NaOH(1:2)^{less} sample, probably because of the low quantity of magnetite in the sample. On the other hand, in the case of the sample with higher content of magnetite, SEP-M(1)NaOH(1:2)^{more}, wide peak can indicate the presence of small crystallites as a result of the formation of high number of nuclei at high concentration of Fe^{2+} and Fe^{3+}. In addition, it seems that size of magnetite crystallites in the sample ASEP-M(2)NH$_3$(1:1.5) is lower than in the sample ASEP-M(2)NH$_3$(1:2).

The XRD patterns of the zeolite-based MNCs obtained with NH$_3$ at different Fe^{2+} and Fe^{3+} ratios are very similar (Fig. 22). The intensities of the peaks of both clinoptillolite and magnetite in the pattern of sample NZ-M(1)NaOH(1:2) are lower and peaks are wider than in the patterns of samples NZ-M(2)NH$_3$(1:2) and NZ-M(2)NH$_3$(1:1.5). Lower intensities of the clinoptilolite peaks can be explained by the reaction of the clinoptilolite with NaOH, i.e. alkali leaching which can destroy the crystal structure of clinoptilolite. As in the SEP/ASEP composites, the size of magnetite crystallites in the zeolite-based MNCs could not be determined due to overlapping of the zeolite peak with the magnetite peak. According to the peak intensities and width, it can be supposed that size of crystallites of magnetite in the sample NZ-M(1)NaOH(1:2) is smaller than in samples NZ-M(2)NH$_3$(1:2) and NZ-M(2)NH$_3$(1:1.5).

8.3. FTIR analysis

The FTIR spectra of the MNCs are shown in Figs. 23-25 together with the spectra of pure components, SEP/NZ/ASEP and Fe_3O_4.
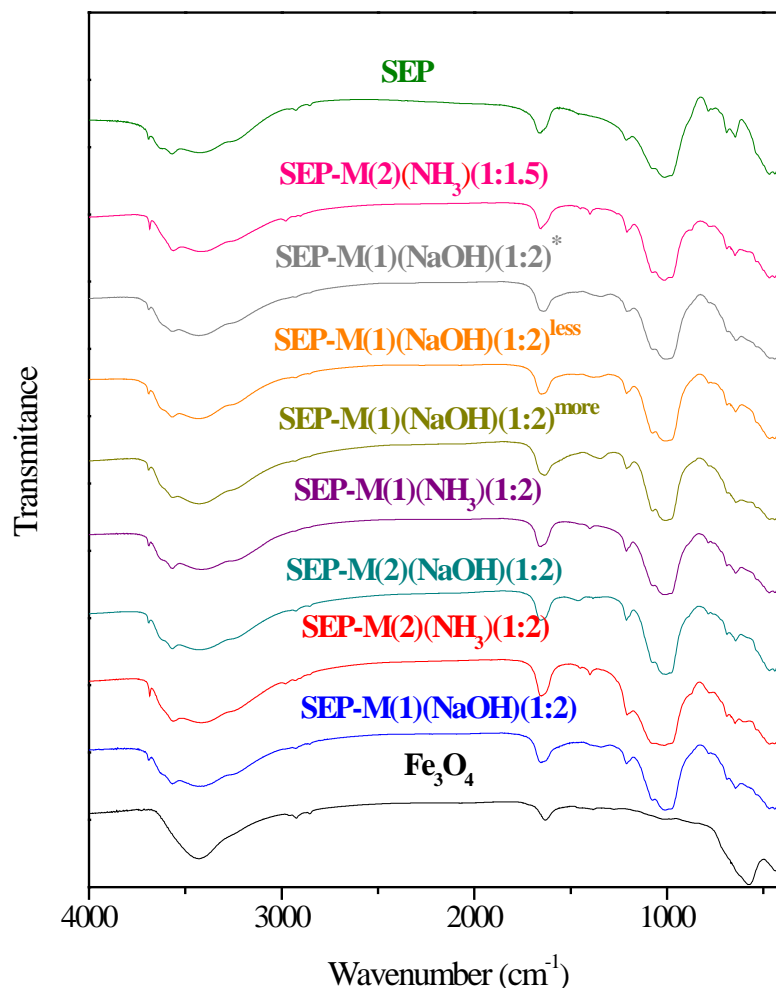
Fig. 23. FTIR patterns of the Fe_3O_4, SEP and the SEP-based MNCs.

The sharp peak in the spectrum of Fe_3O_4 at 593 cm^{-1} can be ascribed to vibrations of Fe–O bonds [146-148], while peaks at 3434 cm^{-1} and 1634 cm^{-1} could correspond to the stretching and bending vibrations of the hydroxyl groups from adsorbed water, respectively [146,149]. The spectra of SEP and ASEP have also a peak at 3434 cm^{-1}, which corresponds to vibration of hydroxyl groups from adsorbed and zeolitic water from the sepiolite [20]. In addition, the band corresponding to the stretching vibrations of the hydroxyl groups attached to the octahedral Mg^{2+} ion in the structure of sepiolite is positioned at 3690 cm^{-1}, while the band at 3565 cm^{-1} originates

from coordinated water in the sepiolite structure. The peak at 1634 cm^{-1} in the spectra of SEP and ASEP corresponds to the vibration of adsorbed, zeolitic and coordinated water. The bands in the 1250–400 cm^{-1} range are characteristic of silicate structure of sepiolite: bands assigned to Si–O–Si vibration, centered at 1016 and 460 cm^{-1}; bands at 1215, 1076 and 980 cm^{-1} due to Si–O bonds; band at 437 cm^{-1} originating from Si–O–Mg bonds and bands at 690 and 637 cm^{-1} corresponding to the Mg–OH bond vibrations.
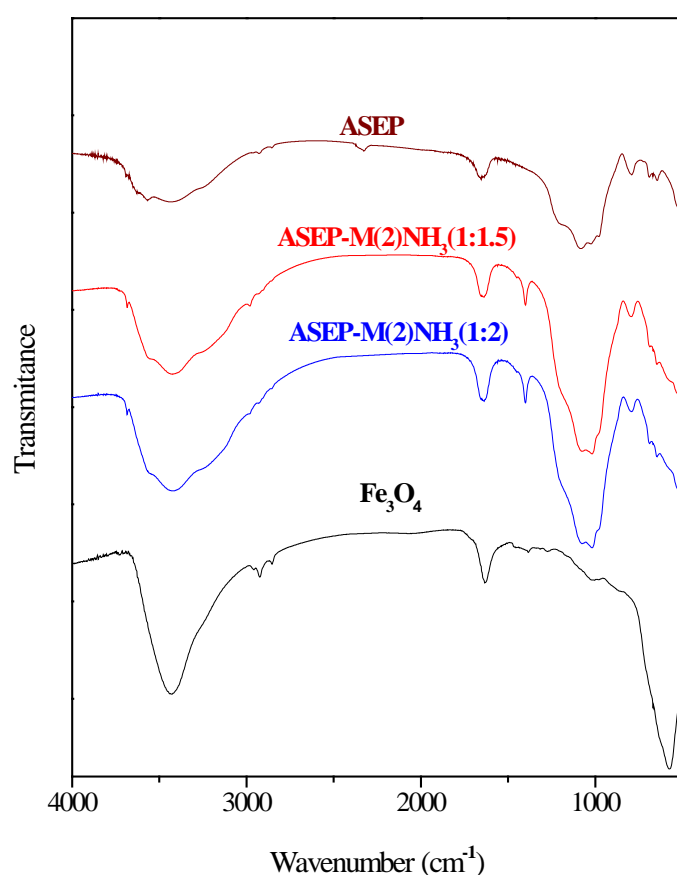
Fig. 24. FTIR patterns of the Fe$_3$O$_4$, ASEP and the ASEP-based MNCs.

In the FTIR spectra of NZ and zeolite-based MNCs, the main band characteristic for the zeolite structure is at about 1060 cm^{-1}, which is attributed to asymmetric O-(Si,Al)-O stretching vibration. This band is sensitive to the content of framework Si and Al [150]. The same position of the band in the spectra of the composites obtained with NH$_3$ as in the spectra of NZ (~ 1062 cm^{-1}) indicates insignificant removal of framework Si and Al during the composite preparation. On the other hand, the shifting of the band position in the spectrum of the sample NZ-

M(1)NaOH(1:2) to lower wave numbers (~ 1054 cm^{-1}) indicate different content of framework Si and Al in comparison to NZ, probably as a result of alkali leaching, as it was assumed according to XRD analysis.
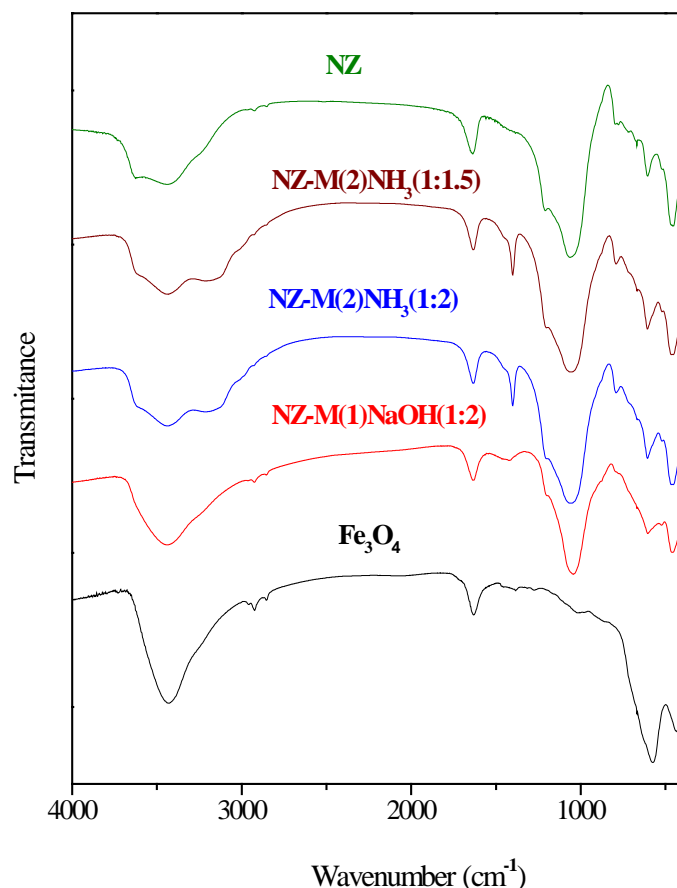
Fig. 25. FTIR patterns of the Fe$_3$O$_4$, NZ and the NZ-based MNCs.

The bands at 460 cm^{-1}, 604 cm^{-1}, 791 cm^{-1} and 1210 cm^{-1}, corresponding to the vibration of the (Si,Al)O$_4$ groups and bonds inside these groups, are at the same positions for all zeolite-based MNCs, indicating unchanged basic zeolite framework. In the spectrum of sample NZ-M(1)NaOH(1:2), the intensity of the band at 604 cm^{-1} is lower and the width is higher than in the spectra of samples obtained with NH$_3$, indicating some differences in the structure of these samples. As in the case of SEP-based composites, due to the presence of the characteristic zeolite bands, the typical magnetite peak at 593 cm^{-1} can not be clearly identified in the spectra of the MNCs.

The bands corresponding to the stretching and bending vibrations of the hydroxyl groups from adsorbed/zeolitic water are positioned at $\sim$ 3430 and 1640 cm^{-1}, respectively, for the composites and pure compounds. The band (shoulder) at

3620 cm^{-1}, corresponds to the bridging OH groups in –Al–OH–Si–, which is attributed to the hydrogen atoms on different oxygen atoms in the framework, is not visible in the spectrum of NZ-M(1)NaOH(1:2). The disappearance of this band for the sample NZ-M(1)NaOH(1:2) indicates that these specific O–H bonds do not vibrate or do not exist because of the changes caused during the formation of the new system. However, the band is visible in the spectrum of samples obtained with NH$_3$, indicating lower degree of the interaction of the zeolite surface with NH$_3$ than with NaOH. Namely, during the composite synthesis, due to strong basic condition, the surface functional groups lose their hydrogen ions and become negatively. The basic conditions were stronger when NaOH was used, so the removal of hydrogen ions was more intensive. In addition, in the spectra of composites obtained by using NH$_3$, wide band at ~ 3300 - ~3050 cm^{-1} is visible, while this band is not appeared in the spectrum of the sample NZ-M(1)NaOH(1:2). This band can be assigned to the polymeric hydrogen bonds [150], indicating higher content of OH groups in the samples obtained with NH$_3$.

Similar as for SEP/ASEP-based composites, there are differences in the spectra of the composites obtained with NH$_3$ and NaOH in the region around 1400 cm^{-1}: the band is sharper and more intensive in the spectra of the MNCs obtained with NH$_3$.

The FTIR spectra of the MNCs (Figs. 23- 25) showed that there are some differences between samples obtained by using NH$_3$ and NaOH and confirmed that the synthesized magnetic composites maintained the basic structure of sepiolite/zeolite.

8.4. Specific surface area and pore size distribution analysis

The nitrogen adsorption/desorption isotherms and mesopore size distribution (PSD) curves of the MNCs and pure compounds are shown in figs 26-28, while the textural properties of the samples are given in Table 5.

a)

b)

c)

d)

e)

f)

g)

h)
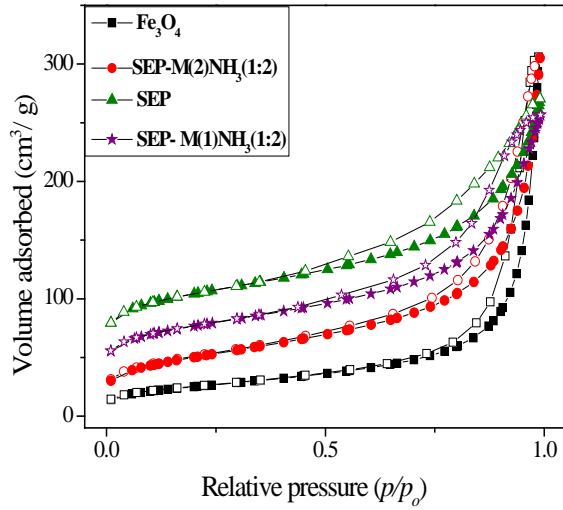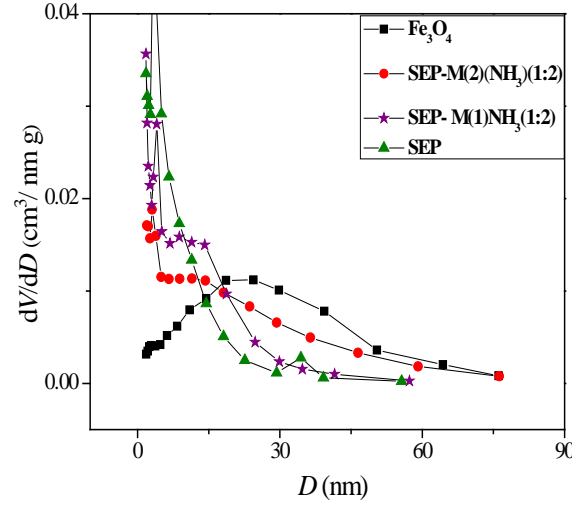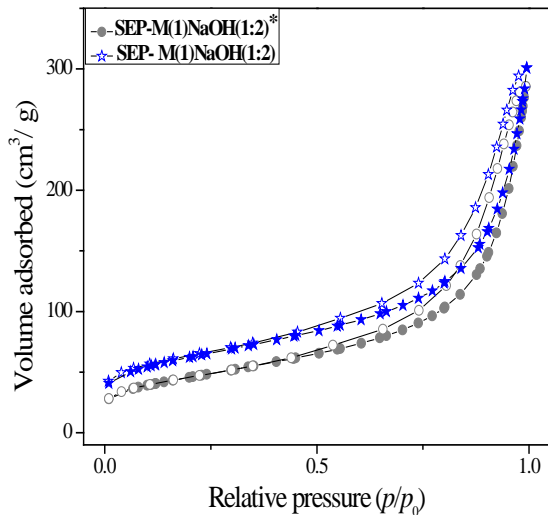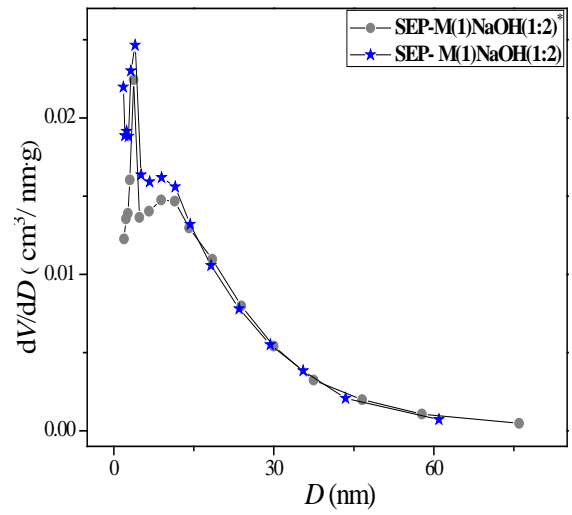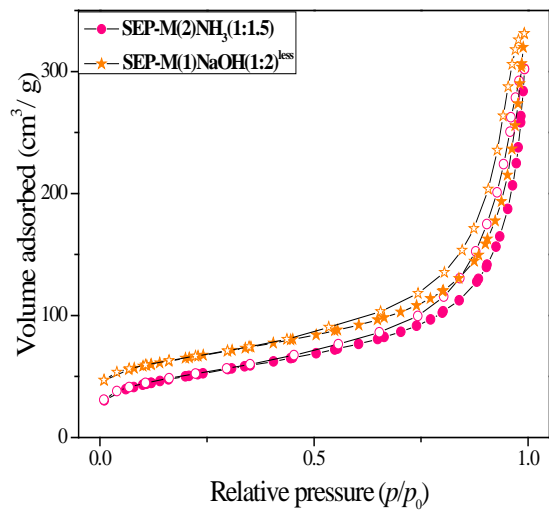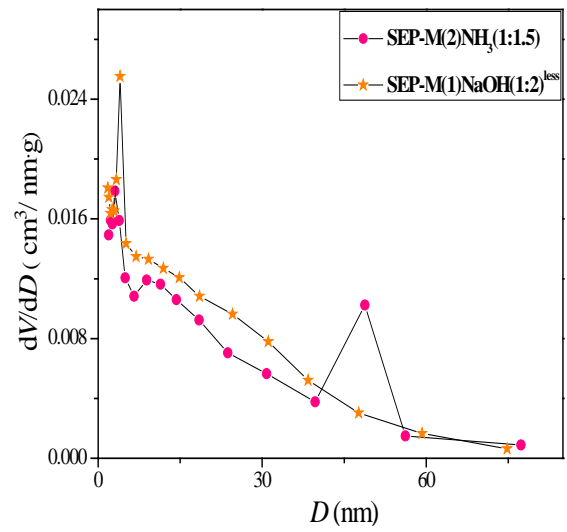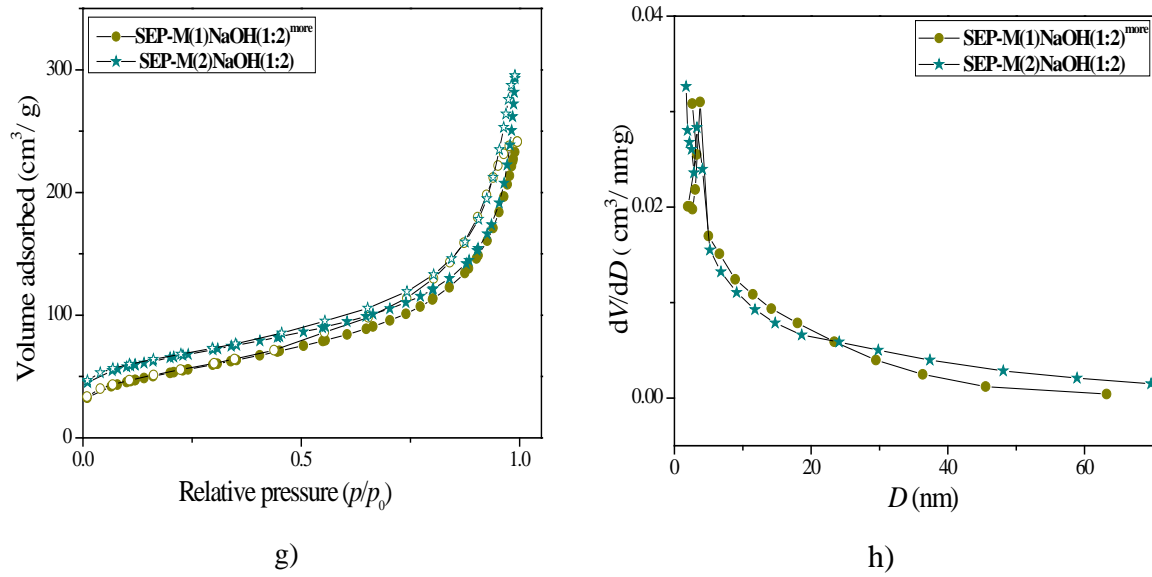
Fig. 26. N$_2$ adsorption–desorption isotherms and pore size distributions of the Fe$_3$O$_4$, SEP and the SEP-based MNCs.

a)

b)
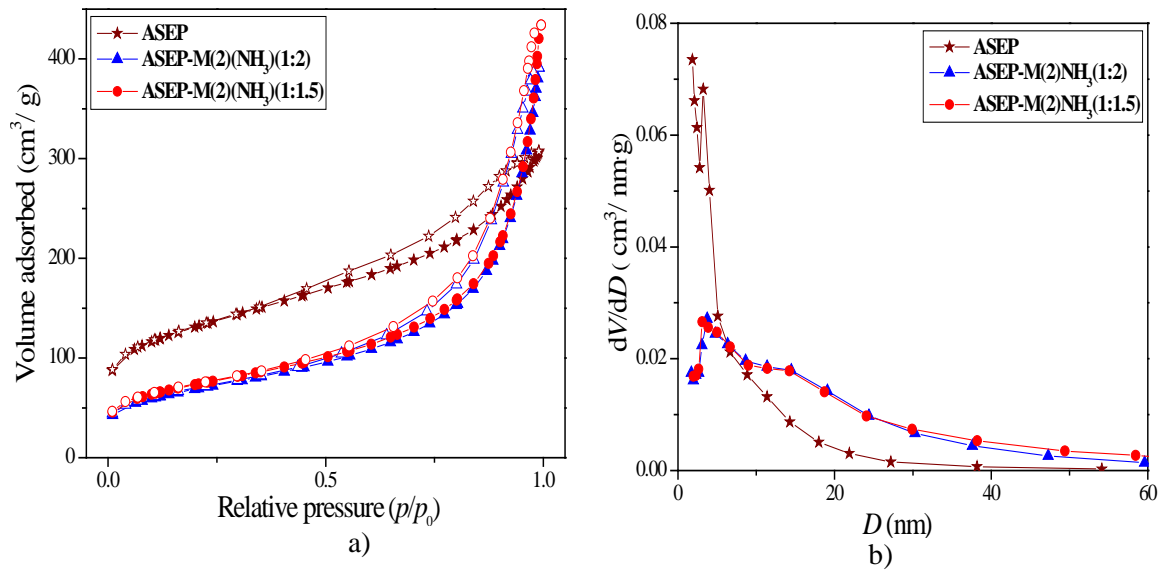
Fig. 27. N$_2$ adsorption–desorption isotherms and pore size distributions of the ASEP and ASEP-based MNCs.
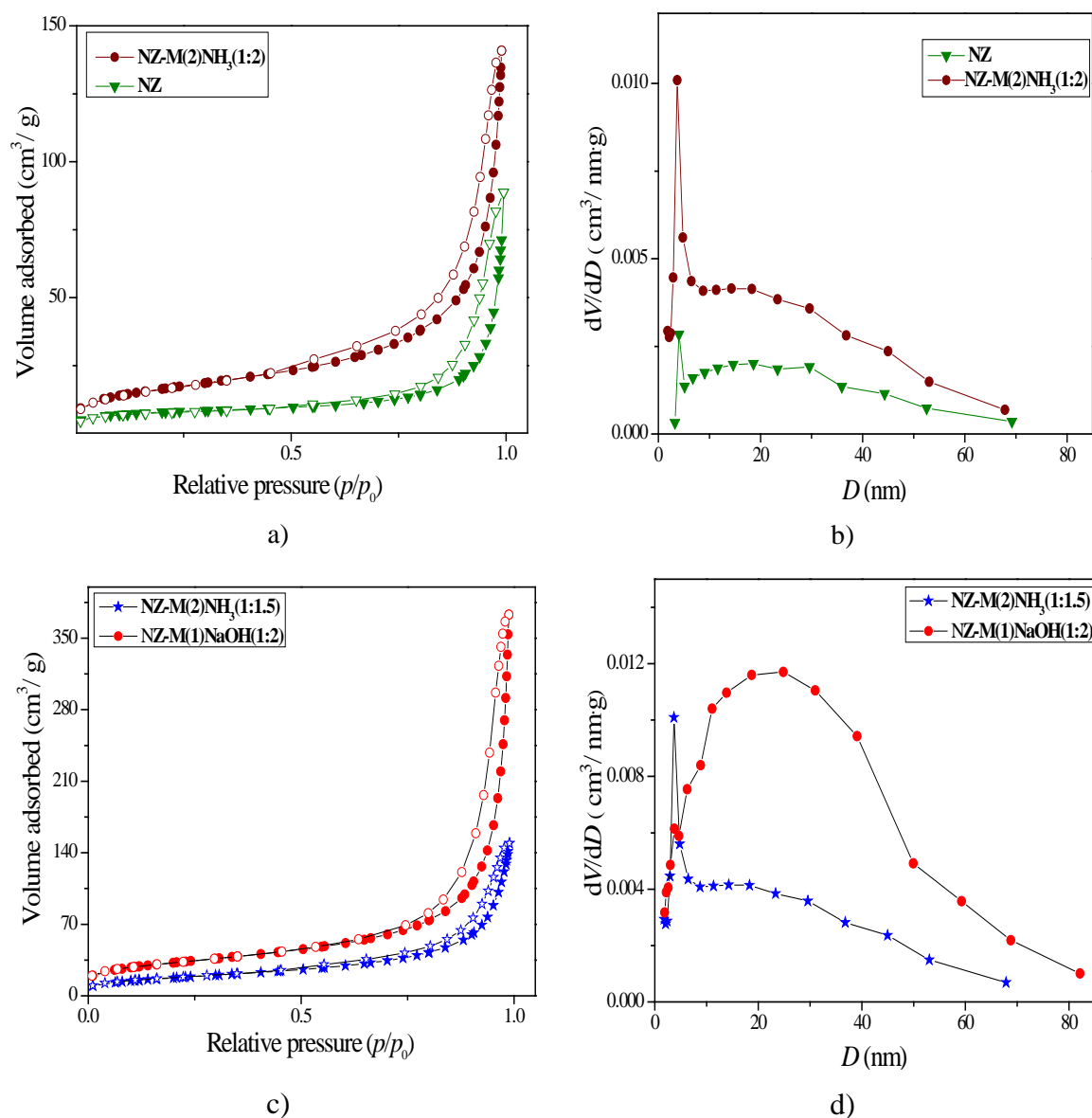
Fig. 28. N_2 adsorption–desorption isotherms and pore size distributions of the NZ and NZ-based MNCs.

The specific surface area of SEP sample is high (Table 5) owing to structural microporosity, *i.e.* the presence of channels in the structure, and inter-fibre micro- and mesoporosity [34]. The specific surface area of ASEP is even higher (Table 5) due to acid activation [20]. The PSD curves of SEP and ASEP (Figs. 26b and 27b) show primary peak at $D_{max} = 3.2$ nm, which corresponds to the main pore population in the samples, but larger mesopores are also present, and the mean pore diameter, D_{mean}, is larger than D_{max} (Table 5).

Table 5. The textural properties of the Fe$_3$O$_4$, SEP, ASEP and the magnetic composites

Sample	S_{BET} (m^2/g)	V_{micro} (cm^3/g)	V_{meso} (cm^3/g)	D_{max} (nm)	D_{mean} (nm)
SEP	359.9	0.139	0.343	3.2	6.7
ASEP	461.6	0.161	0.368	3.2	4.8
NZ	26.7	0.0037	0.092	4.0	18.0
Fe$_3$O$_4$	89.0	0.027	0.463	21.6	18.8
SEP-M(1)NaOH(1:2)	212.6	0.074	0.442	4.1	8.9
SEP-M(1)NH$_3$(1:2)	250.9	0.098	0.379	4.1	7.3
SEP-M(1)NaOH(1:2)*	160.6	0.051	0.427	3.8	10.2
SEP-M(1)NaOH(1:2)^{more}	182.6	0.059	0.354	3.7	7.9
SEP-M(1)NaOH(1:2)^{less}	215.1	0.081	0.498	4.0	10.6
SEP-M(2)NaOH(1:2)	219.7	0.079	0.439	3.4	8.6
SEP-M(2)NH$_3$(1:2)	174.5	0.057	0.443	3.0	11.2
SEP-M(2)NH$_3$(1:1.5)	173.1	0.058	0.432	3.12	11.2
ASEP-M(2)NH$_3$(1:2)	238.0	0.079	0.585	3.8	9.7
ASEP-M(2)NH$_3$(1:1.5)	251.2	0.085	0.636	3.1	10.8
NZ-M(1)NaOH(1M)	112.8	0.0016	0.561	24.7	18.9
NZ-M(2)NH$_3$(1:2)	63.4	0.019	0.220	3.70	12.4
NZ-M(2)NH$_3$(1:1.5)	57.9	0.018	0.206	3.70	13.3

S_{BET} - specific surface area, V_{micro} - micro pore volume, V_{meso} - meso pore volume, D_{max} - maximum pore diameter, and D_{mean} - mean pore diameter.

The specific surface area of zeolite is much lower than of sepiolite and it is close to the values published for natural clinoptilolite [151]. The dominant pores are of 4.0 nm size, but the value of the mean pore diameter (Table 5) indicates the presence of larger pores in the sample. The results indicate that SEP and ASEP are micro/mesoporous materials, while zeolite contains dominantly mesopores. The pure magnetite contains dominantly mesopores, which are pores among magnetite particles

[151,152], while a very low volume of micropores (Table 5) indicates that the particles are almost nonporous. The broad pore size distribution of magnetite (Fig. 26b) shows the presence of pores of different sizes, probably because of the presence of particles of different sizes and because of different degree of the particles aggregation.

The results (Table 5) show that the values of the specific surface areas of the SEP/ASEP-based composites are between the values for pure compounds, Fe_3O_4 and SEP/ASEP. The mesopore volume of the MNCs is higher, while the micropore volume is lower than of SEP/ASEP (Table 5), which can be a consequence of a partial closing of sepiolite structural micropores during the modification and formation of new mesopores between magnetite particles in the composites. However, such results can be explained also by the fact that the composites contain some quantity of the compound with high S_{BET} (sepiolite) and some quantity of compound with low S_{BET} (magnetite). By comparing SEP-M(2)NH$_3$(1:2) and ASEP-M(2)NH$_3$(1:2), obtained by the same procedure and the same base, it is obvious that composite with higher S_{BET} and micro- and mesopore volume was obtained by using the support with higher S_{BET}, V_{micro} and V_{meso}.

With the exception of samples SEP-M(1)NaOH(1:2)[*] and SEP-M(1)NaOH(1:2)[more], the specific surface area, volume of mesopores and volume of micropores of the SEP-based MNCs obtained with NaOH are very similar, despite the different procedures of synthesis. It is obvious that higher quantity of iron salts and higher concentration of NaOH caused lower S_{BET}, V_{micro} and V_{meso}, probably because of higher magnetite content and aggregation, as well as higher closing of sepiolite micropores. In the case of MNCs obtained with NH$_3$, the specific surface area of the sample obtained by first procedure is higher due to higher volume of micropores, while mesopores volume is lower than of the sample obtained by the second procedure (Table 5). The ratio Fe^{2+}/Fe^{3+} had almost no influence on the textural properties of the composites, especially in the case of SEP-based MNCs; the only difference is the appearance of the maximum at PSD curve of SEP-M(2)NH$_3$(1:1.5) sample at 48.8 nm, indicating higher content of larger pores, probably between the bundles of fibers of sepiolite. In the case of ASEP-based MNCs, small differences can be a result of the different content of magnetite in the samples because of the different Fe^{2+}/Fe^{3+} ratio.

77

Similarly as for SEP-based MNCs, the ratio Fe^{2+}/Fe^{3+} had no significant influence on the properties of the zeolite-based MNCs, obtained with NH_3: there is small difference in mesopore volume and mean pore size, which caused small differences in S_{BET}. In comparison to pure zeolite, all zeolite-based MNCs have larger specific surface area and mesopore volume. Obviously, deposition of magnetite particles on the zeolite surface provided higher specific surface area owing to the presence of small particles.

The shape of PSD curve for zeolite-based MNCs, obtained with NH_3 is similar as of NZ (Fig. 28 b and d), but the pore volume is significantly higher. On the other hand, PSD curve of the sample NZ-M(1)NaOH(1:2) is similar to the curve of magnetite and the specific surface area is higher than of other zeolite-based MNCs and higher than of pure magnetite. In addition, the mesopore volume is higher than of zeolite and magnetite. Such results can be explained by the good distribution of the magnetite particle on the zeolite surface and also by the increase of the zeolite specific surface area during the composite preparation due to some alkali leaching, as it was supposed according to the XRD analysis.

8.5. SEM and TEM analysis

Electronic microscopy analyses were used to reveal morphological characteristics of the pure compounds and the composites. The representative scanning electron micrographs (SEM) of SEP, ASEP and Fe_3O_4 and transmission electron micrograph (TEM) of Fe_3O_4 are presented in Fig. 29.

The particles of SEP and ASEP (Fig. 29 a and b) have a needle-like morphology, but these particles form bundles-like aggregates by the surface interaction between the individual needle-type particles [34]. It seems that ASEP contains slightly shorter and disintegrated particles in comparison to SEP, as a consequence of acid activation, but the acid treatment did not cause de-aggregation, *i.e.* formation of smaller aggregates.

a) (SEP)

b) (ASEP)
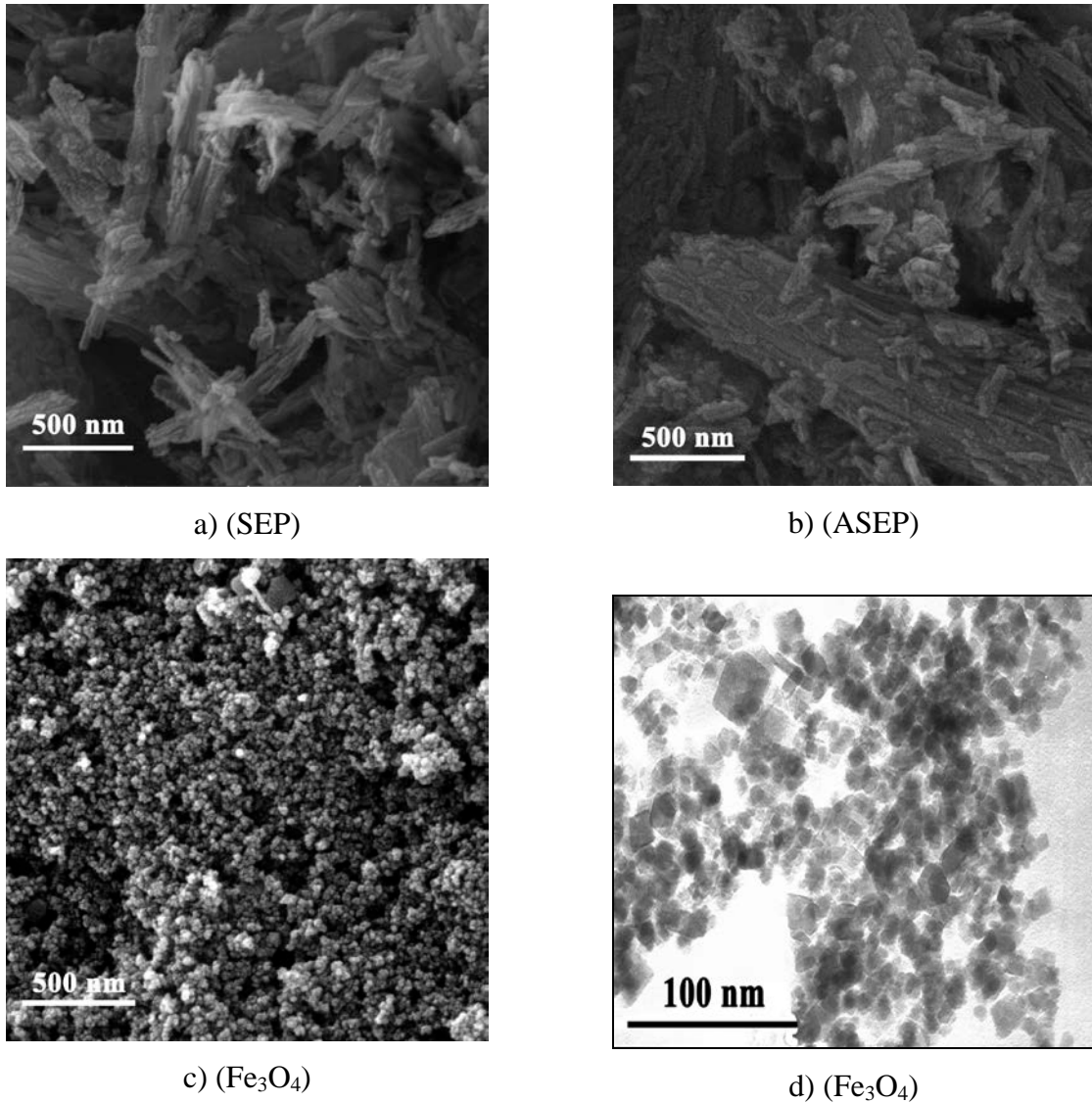
c) (Fe$_3$O$_4$)

d) (Fe$_3$O$_4$)

Fig. 29. SEM micrographs of: a) SEP, b) ASEP and c) Fe$_3$O$_4$; and d) TEM micrograph of Fe$_3$O$_4$

Fig. 29c shows that pure magnetite consists of nearly spherical particles ~20-30 nm in size, which are highly aggregated. Such type of magnetite powders is usually obtained by nucleation and growth from solution through rapid agglomeration of nanometric particles [21,22]. The TEM micrograph of the magnetite (Fig. 29d) shows faceted primary particles, with sizes of about 10 nm. Actually, these primary particles are the magnetite crystallites.

SEM micrographs of the SEP-based composites are shown in Figure 30, while the micrographs of ASEP-based composites in Figure 31. In addition, TEM micrographs of some SEP-based composites are presented in figure 32, and of ASEP-based composite in figure 33.
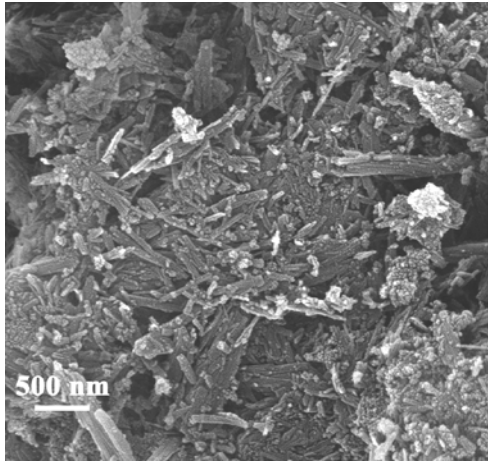
a) (SEP-M(1)NaOH(1:2))
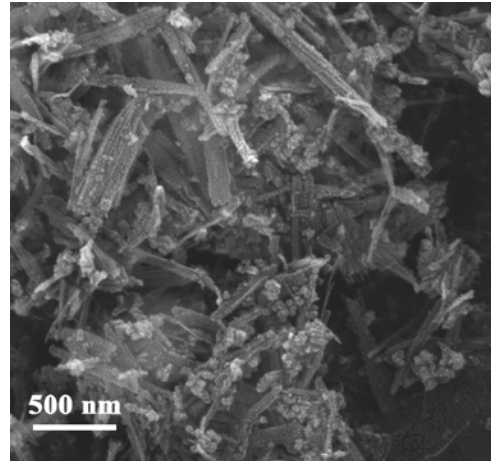
b) (SEP-M(2)NaOH(1:2))
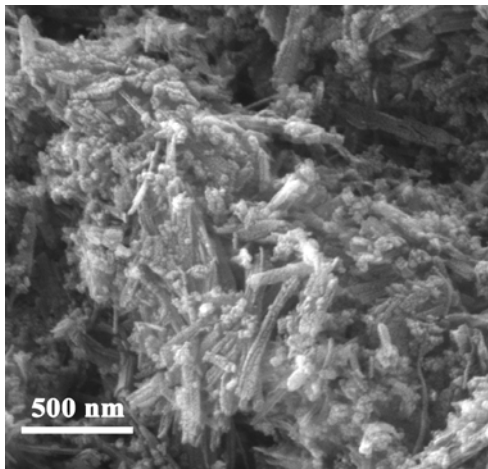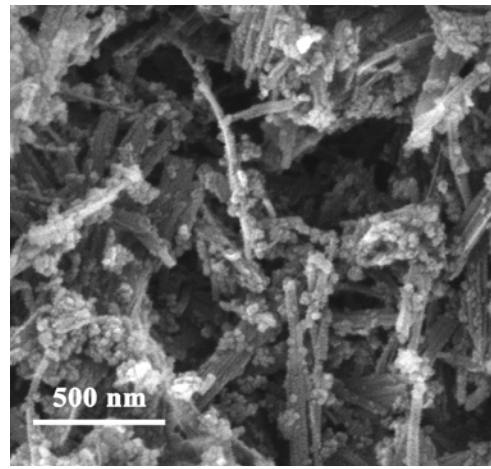
c) (SEP-M(1)NH$_3$(1:2))
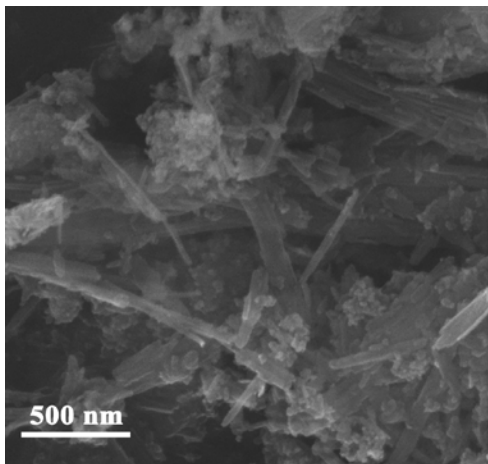
d) (SEP-M(2)NH$_3$(1:2))
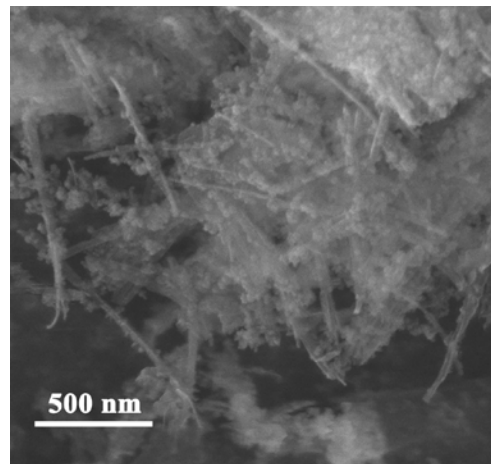
e) (SEP-M(1)NaOH (1:2)*)
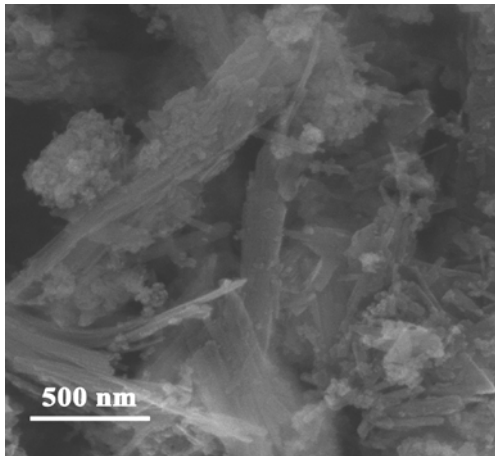
f) (SEP-M(2)NH$_3$(1:1.5))
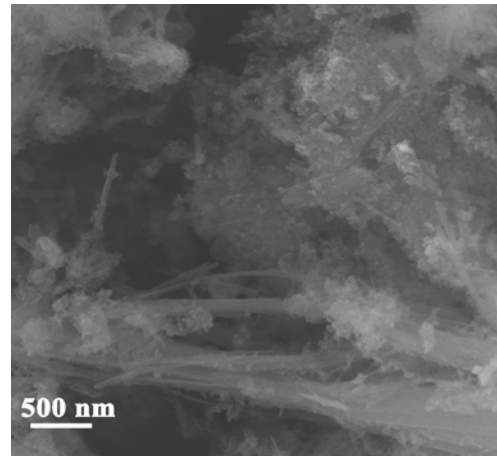
g) (SEP-M(1)NaOH(1:2) ^{more})   h) (SEP-M(1)NaOH(1:2)^{less})

Fig. 30. Scanning electron micrographs (SEM) of the composites: a) SEP-M(1)NaOH(1:2), b) SEP-M(2)NaOH(1:2), c) SEP-M(1)NH$_3$(1:2), d) SEP-M(2)NH$_3$(1:2), (e) SEP-M(1)NaOH (1:2)*, (f) SEP-M(2)NH$_3$(1:1.5), (g) SEP-M(1)NaOH(1:2) ^{more} and (h) SEP-M(1)NaOH(1:2)^{less}.
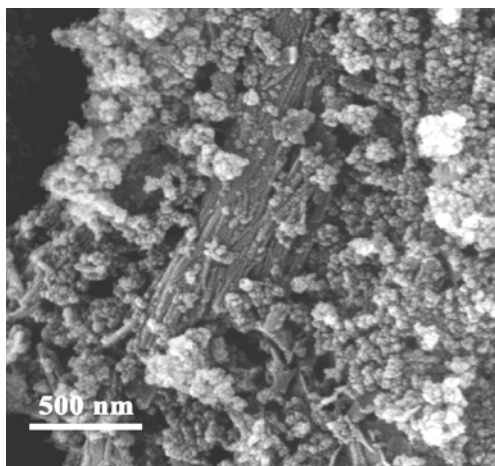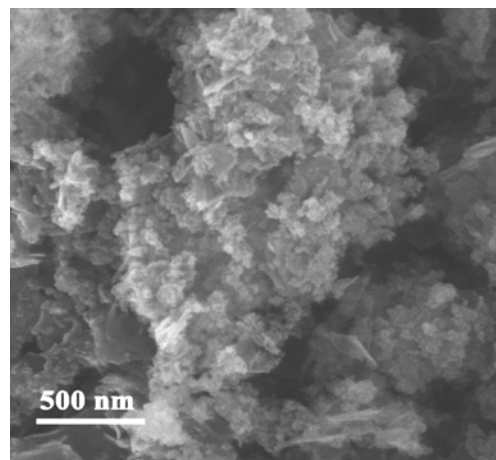
a (ASEP-M(2)NH$_3$(1:2))   b (ASEP-M(2)NH$_3$(1:1.5))

Fig. 31. Scanning electron micrographs (SEM) of the ASEP-based composites: a) ASEP-M(2)NH$_3$(1:2) and b) ASEP-M(2)NH$_3$(1:1.5).

a)   (SEP-M(1)NaOH(1:2))

b) (SEP-M(2)NaOH(1:2))

c) (SEP-M(1)NH$_3$(1:2))
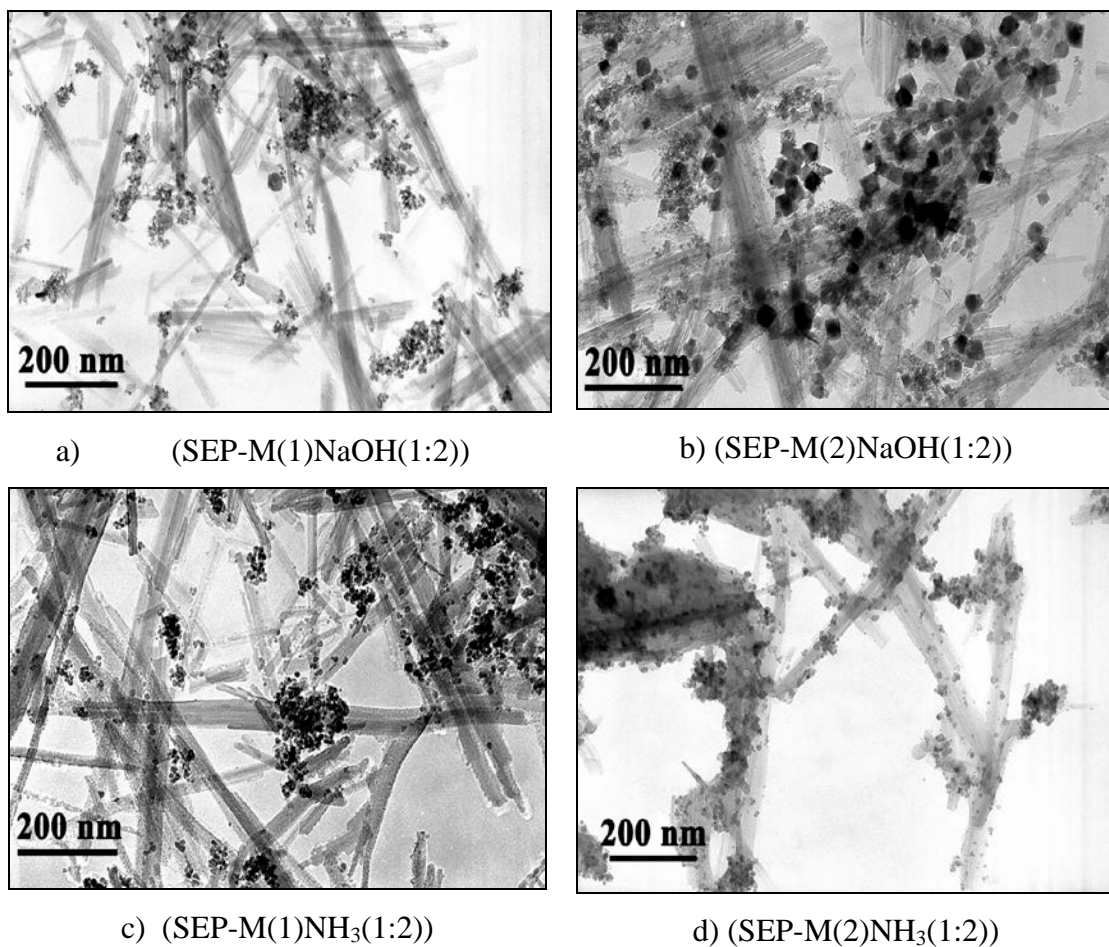
d) (SEP-M(2)NH$_3$(1:2))

Fig. 32. Transmission electron micrographs (TEM) of the composites: a) SEP-M(1)NaOH(1:2), b) SEP-M(2)NaOH(1:2), c) SEP-M(1)NH$_3$(1:2), d) SEP-M(2)NH$_3$(1:2).
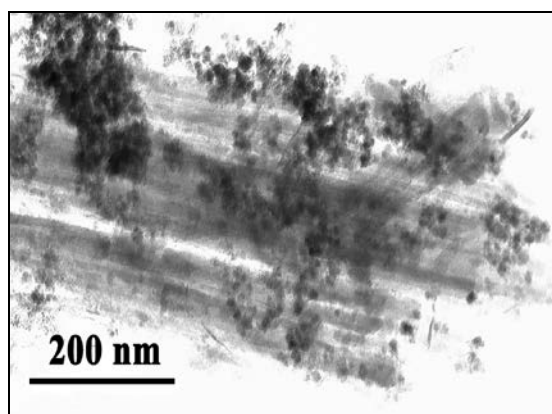
Fig. 33. Transmission electron micrographs (TEM) of the composite ASEP-M(2)NH$_3$(1:2).

The SEM micrograph of the SEP-M(1)NaOH(1:2) composite (Fig 30 a) shows both fine and aggregated magnetite particles distributed throughout the sepiolite matrix. Similar situation is observed in the case of the sample SEP-M(1)NH$_3$(1:2) (Fig. 30 c), that seems to have the magnetite particles better dispersed. In the TEM micrographs of the composites (Figs. 32 a and c), the isolated fibers and tiny bundles of the sepiolite fibers are clearly visible. Also, the magnetite particles of ~ 10 nm in size and fine aggregates attached to the sepiolite fibers/bundles, can be observed. Despite the fact that the magnetite particles are not distributed on the surface of the sepiolite fibers/bundles entirely as separated particles, the presence of sepiolite provided formation of fine aggregates, *i.e.* decreasing of magnetite agglomeration in comparison to pure magnetite. In addition, the primary magnetite particles/crystallites are spherical, not faceted as in pure magnetite (Fig. 29 d). The morphology of the samples SEP-M(1)NaOH(1:2)* (Fig. 30 e), SEP-M(1)NaOH(1:2)[more] (Fig. 30 g) and SEP-M(1)NaOH(1:2)[less] (Fig. 30 h) are similar as morphology of the sample SEP-M(1)NaOH(1:2). Regardless of the different content of magnetite in samples SEP-M(1)NaOH(1:2)[more] and SEP-M(1)NaOH(1:2)[less], significant differences in morphology were not observed (Figs. 30 g and h).

According to SEM micrographs of the samples SEP-M(2)NaOH(1:2), SEP-M(2)NH$_3$(1:2) and SEP-M(2)NH$_3$(1:1.5) (Figs. 30 b, d and f), it is obvious that the magnetite particles are better dispersed in these composites than the samples obtained by the Procedure 1 (Figs. 30 a, c, e, g and h). Best dispersibility was achieved in the SEP-M(2)NH$_3$(1:2) and SEP-M(2)NH$_3$(1:1.5) samples (Figs. 30 d and f), where the sepiolite fibers and fine bundles are uniformly decorated with the spherical particles and very fine aggregates of magnetite particles. The ratio Fe^{2+}/Fe^{3+} did not have influence on the morphology of the composite (Figs. 30 d and f).

The TEM analysis confirmed that spherical magnetite nanoparticles (~ 10 nm in size) and small aggregates were anchored on the surface of sepiolite fibers/bundles with high density in the SEP-M(2)NH$_3$(1:2) sample (Fig. 32 d). In the case of the SEP-M(2)NaOH(1:2) sample, both the aggregates of very fine particles, smaller than 10 nm in size, and the individual, larger faceted magnetite crystalite, sizes of ~ 30 nm, are present.

The ASEP-M(2)NH$_3$(1:2) and ASEP-M(2)NH$_3$(1:1.5) composites contain large sepiolite bundles, larger than in the composites with SEP, and the magnetite aggregates larger than in the MNCs with SEP (Figs. 31 and 33). Obviously, stronger

interfibers bonds exist in ASEP than in SEP, which reduced disaggregation of the acid-activation of sepiolite and prevented good dispersibility of the magnetite particles.

SEM micrographs of the natural zeolite and the obtained composites are shown in Fig. 34. A tabular morphology of the zeolite is seen in Fig. 34a. In the case of the zeolite-based composites, the individual magnetite particles, as well as aggregates, are attached to the surface of the zeolite particles (Figs. 34 b, c and d). It is obvious that the magnetite particles are better dispersed in NZ-M(2)NH$_3$(1:2) and NZ-M(2)NH$_3$(1:1.5) (Figs. 34 c and d) than in composite NZ-M(1)NaOH(1:2) (Fig. 34 b), similar as in the case of SEP-based composite.

a) (NZ)

b) (NZ-M(1)NaOH(1:2))

c) (NZ-M(2)NH$_3$(1:2))
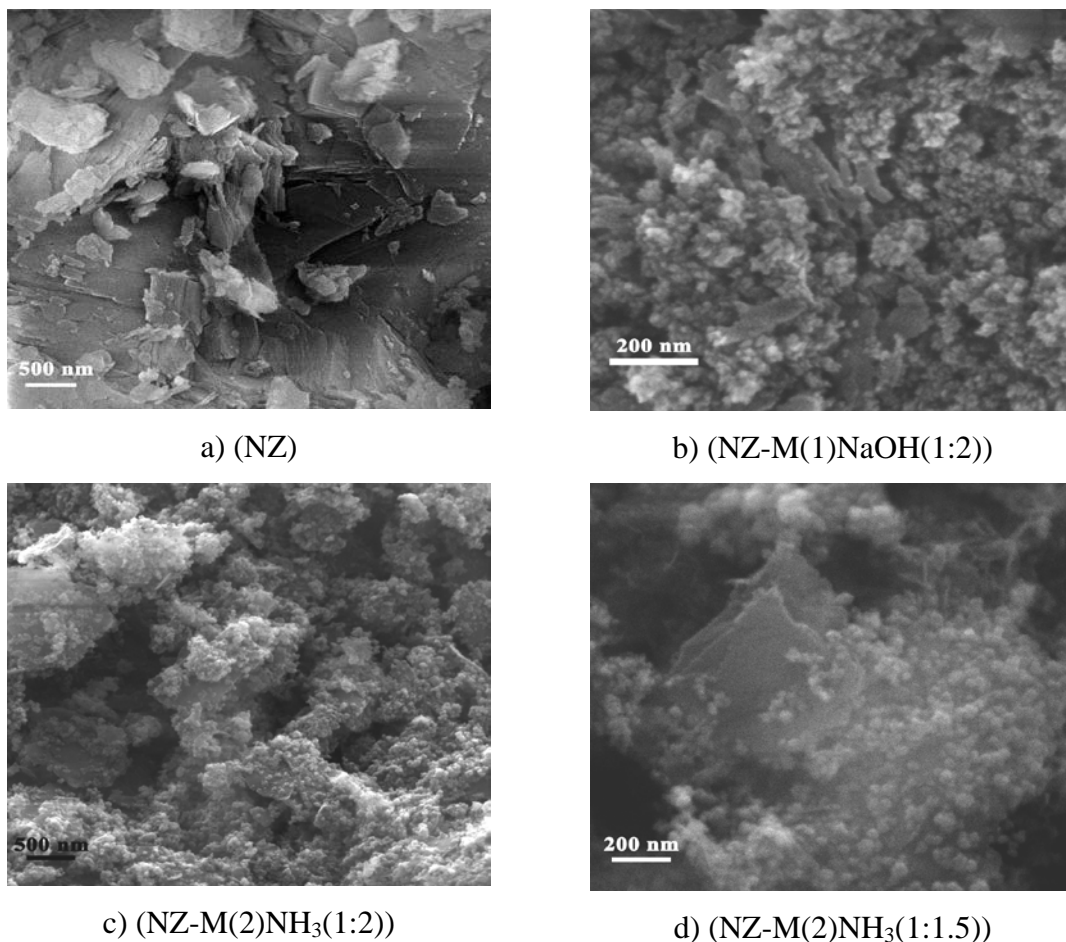
d) (NZ-M(2)NH$_3$(1:1.5))

Fig. 34. Scanning electron micrographs (SEM) of: a) NZ, b) NZ-M(1)NaOH(1:2), c) NZ-M(2)NH$_3$(1:2) and d) NZ-M(2)NH$_3$(1:1.5).

The SEM and TEM analysis showed that the dispersibility of the magnetite particles depends on the type of the supported material (natural or acid-activated

sepiolite or zeolite), the type of base (NaOH or NH$_3$) and the sequence of reagents mixing (Procedure 1 or Procedure 2), while the ratio Fe^{2+}/Fe^{3+} did not have a significant influence on the dispersibility of the magnetite particles in MNCs. The best dispersibility was achieved by the Procedure 2, with ammonia as a precipitating agent and with the natural sepiolite or natural zeolite as the support media.

8.6. Differential-thermal/thermo gravimetric analyses (DTA/TGA)

Differential-thermal and thermo gravimetric analyses were applied to investigate a thermal behavior of the composites. The SEP-based composites obtained at Fe^{2+}/Fe^{3+} = 2 , by both bases and both procedures (SEP-M(1)NaOH(1:2), SEP-M(1)NH$_3$(1:2), SEP-M(2)NaOH(1:2) and SEP-M(2)NH$_3$(1:2)) were chosen to investigate the influence of the type of base used for co-precipitation and the reagent mixing order on the thermal behavior. The results are presented in Fig. 35.

DTA patterns showed the presence of the peaks characteristic for both parent materials: the exothermal peaks in the region 200-350 ℃, indicating magnetite oxidation [153], and the exothermal peak at ~ 800 ℃, indicating the phase transformation of sepiolite to enstatite (MgSiO$_3$) and SiO$_2$ [20]. In addition, endothermal peak at about 100 ℃ indicates the removal of physically adsorbed water and zeolitic water from sepiolite channels.

The TGA curves showed the weight loss in the whole temperature range because of the removal of different types of water from sepiolite: adsorbed, zeolitic, bound and constitutional water. The lost of constitutional water of sepiolite, dehydroxilation, takes place at temperatures just below its temperatures of transformation to enstatite (in the region from 730-780 ℃) [20]. On the other hand, the samples weight should be increased in the region from 200-350 ℃ due to magnetite oxidation [153]. Apparently, the weight loss due to water removal is higher than the weight increase due to the magnetite oxidation, so the samples weight was continually decreasing.

Two exothermal peaks at ~ 200 ℃ and ~ 310 ℃, indicating the magnetite oxidation, are visible on the DTA curves of the SEP-M(1)NH$_3$(1:2) and SEP-M(2)NH$_3$(1:2) samples, while just one peak for the magnetite oxidation appeared on the DTA curves of the samples SEP-M(1)NaOH(1:2) and SEP-M(2)NaOH(1:2).
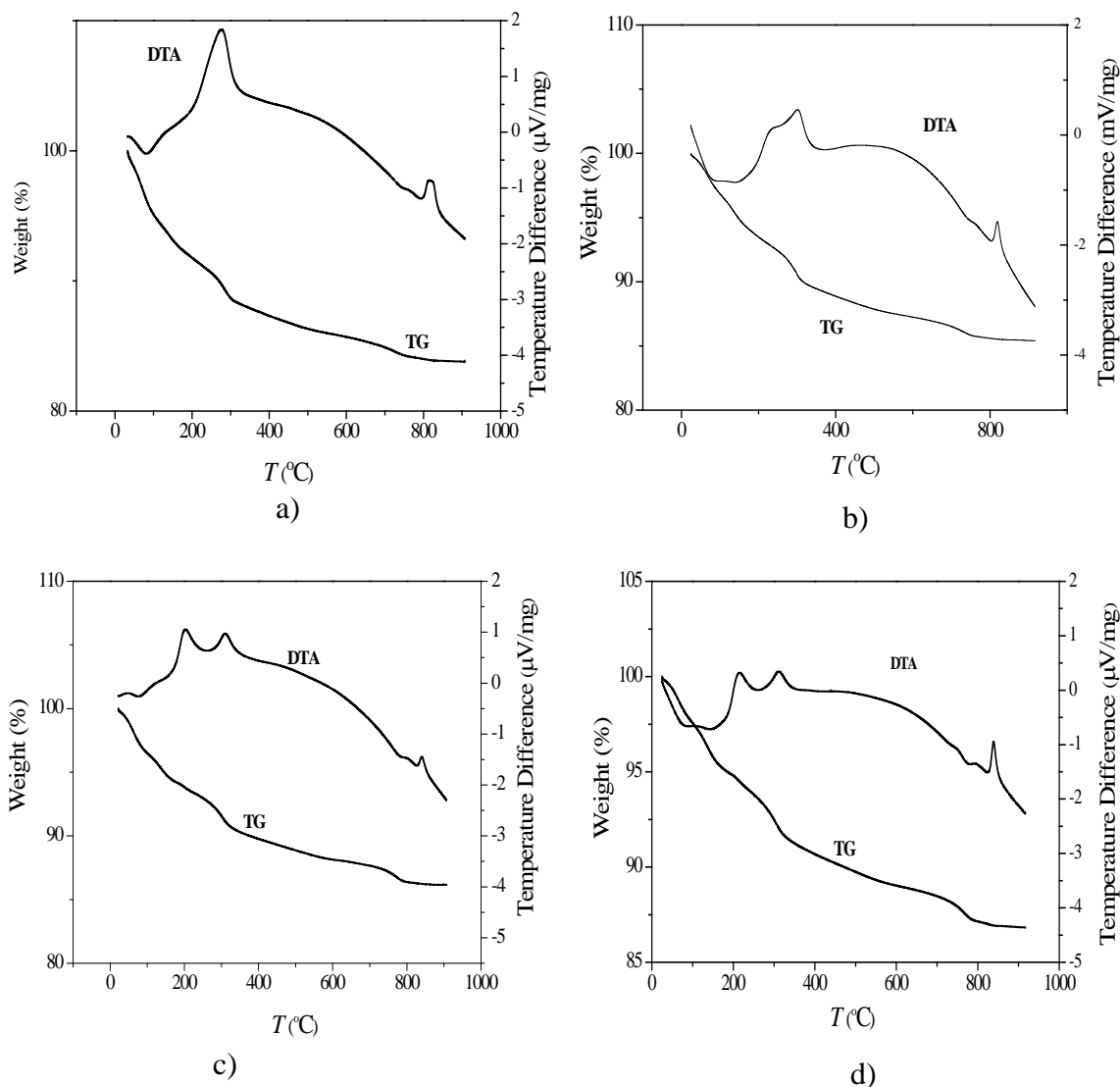
Fig 35. The DTA patterns of the samples: a) SEP-M(1)NaOH(1:2), b) SEP-M(2)NaOH(1:2), c) SEP-M(1)NH$_3$(1:2) and d) SEP-M(2)NH$_3$(1:2).

According to the literature [153], the oxidation of the magnetite occurs first on the surface of the particles, resulting in the formation of a protective film of Fe$_2$O$_3$ around the particles (the first peak on the DTA curve) and then, at higher temperatures, the remaining magnetite is oxidized by diffusion of oxygen through the Fe$_2$O$_3$ layer into the magnetite structure (the second peak on the DTA curve).

The presence of just one peak on the DTA curves of the samples SEP-M(1)NaOH(1:2) and SEP-M(2)NaOH(1:2) indicates a one-step oxidation process or the overlapping of the peaks for the surface and the bulk oxidation. The overlapping is clearly visible for the sample SEP-M(2)NaOH(1:2). Such one-step oxidation process

can be explained by the presence of very small particles, where the surface oxidation is dominant. However, the SEM and TEM analyses showed the presence of particles of similar sizes in these samples as in the samples obtained by using NH_3. Therefore, it can be supposed that the SEP-M(1)NaOH(1:2) and SEP-M(2)NaOH(1:2) samples contain both larger and very small particles, which cannot be seen clearly by SEM and TEM. In addition, the area of the peak originated from the magnetite oxidation in the SEP-M(1)NaOH(1:2) and SEP-M(2)NaOH(1:2) samples is larger than the sum area of the peaks originated from the magnetite oxidation in the SEP-M(1)NH_3(1:2) and SEP-M(2)NH_3(1:2) samples. It is an indication of a higher content of the magnetite in the SEP-M(1)NaOH(1:2) and SEP-M(2)NaOH(1:2) samples, obtained with a strong base, than in the SEP-M(1)NH_3(1:2) and SEP-M(2)NH_3(1:2) samples, obtained by using a weak base. Having in mind that all samples were prepared at the same Fe^{2+}/Fe^{3+}/SEP ratio, lower quantity of magnetite in the samples SEP-M(1)NH_3(1:2) and SEP-M(2)NH_3(1:2) can be explained by higher quantity of iron(III)-oxihydroxide due to the oxidation during the synthesis or due to some precipitation of $Fe(OH)_3$ instead of co-precipitation owing to lower quantity of OH^- ions when weak base was used.

8.7. Magnetic properties

In addition to qualitative assessment of the magnetization, the detailed investigation of the magnetic properties was performed for some SEP/ASEP based composites synthesized by Procedure 2 in order to investigate the influence of the support type (SEP or ASEP) and the ratio Fe^{2+}/Fe^{3+} on the magnetic properties of the composites. The temperature dependence of the magnetization was recorded for these samples (SEP-M(2)NH_3(1:2), ASEP-M(2)NH_3(1:2), SEP-M(2)NH_3(1:1.5) and ASEP-M(2)NH_3(1:1.5)) in two modes: the ZFC (measurement was performed after the sample cooling from room temperature to 5 K in the zero field), and the FC mode (measurement was performed after cooling to 5 K in the field of 100 Oe) [154]. As it can be seen in the Fig. 36, all the samples showed similar behavior.
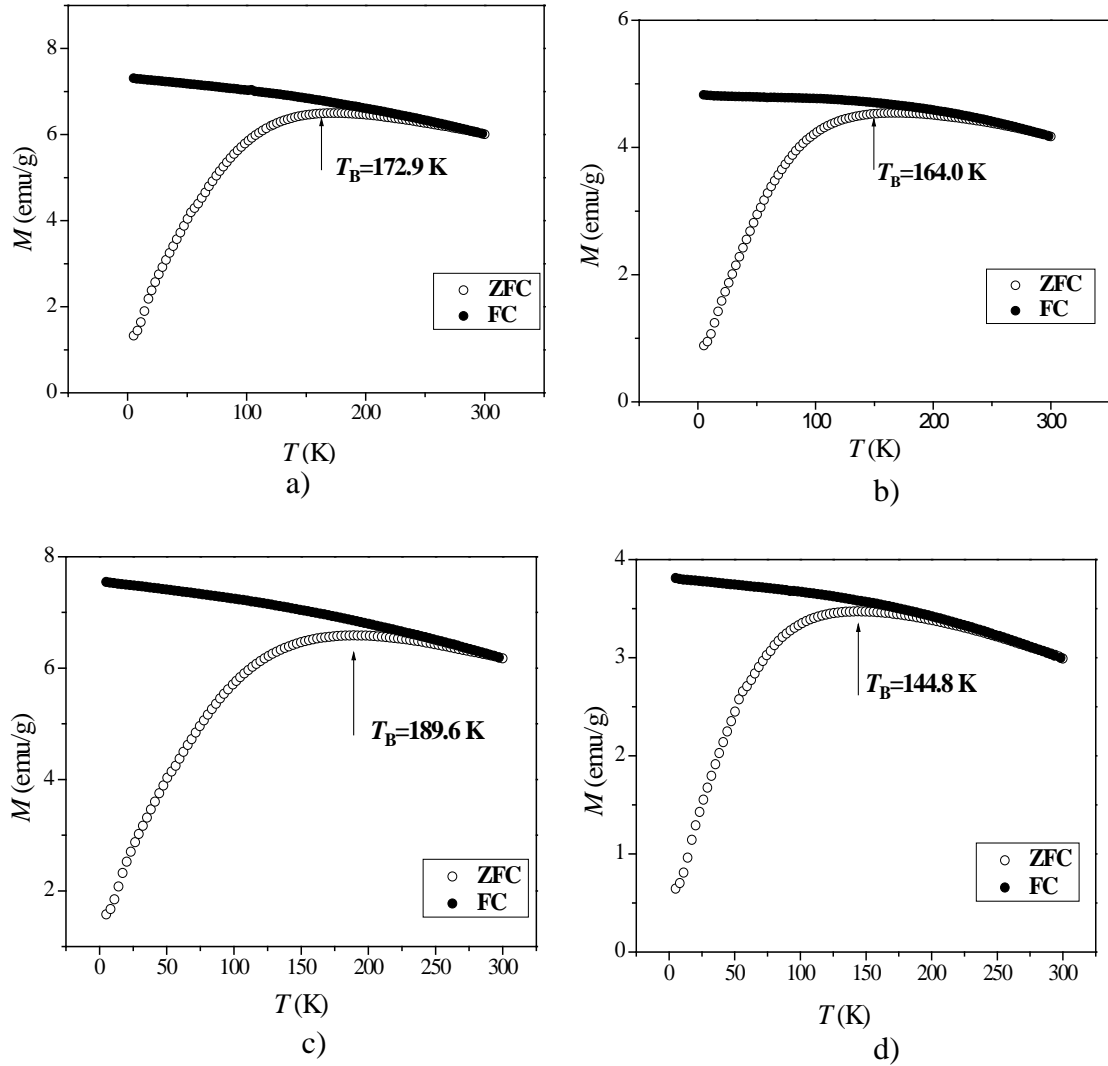
Fig. 36. Temperature dependence of the magnetization recorded in $H = 100$ Oe for the samples: a) SEP-M(2)NH$_3$(1:2), b) ASEP-M(2)NH$_3$(1:2), c) SEP-M(2)NH$_3$(1:1.5) and d) ASEP-M(2)NH$_3$(1:1.5).

The large difference between ZFC and FC magnetization branches below certain blocking temperature, T_B, speaks in favor of the existence of a strong magnetic anisotropy, and the maximums at T_B can be attributed to the blocking process of single domain magnetic nanoparticles. Below this temperature the magnetic moment inside the particle is blocked in a certain direction, while above T_B it oscillates i.e. the particles are in superparamagnetic state [155,156]. It can be seen that the blocking temperature of the samples lie in relatively narrow range from 140 K to 190 K. From this it can concluded, that in all the samples, the size distribution of magnetic nanoparticles, i.e. nanocrystals should be similar, but lower T_B values for the ASEP-

based composites indicates somewhat smaller crystals than in the SEP-based MNCs [156]. By comparing these T_B values with the literature data [157] it can be expected that the size of the magnetite crystals in these samples is well below 50 nm. Above this size, the so-called Verwey transition [157] appears which is not detected in these measurements. Also, an almost flat FC branch at low temperatures indicates the existence of some interactions between the magnetic nanoparticles.

Further insight in the properties of the magnetic composites can be obtained from $M(H)$, i.e. from hysteresis measurements. The dependence of magnetization of the samples on magnetic field strength was determined at constant temperature below blocking temperature (at 5 K). In addition to already mentioned samples, $M(H)$ dependence was determined for the sample SEP-M(1)NaOH(1:2), to compare the magnetization of the samples synthesized with SEP by both procedures. For this sample, the measurements were performed at 5 K and well above blocking temperature, at $T = 300$ K. The hysteresis curves are depicted in Fig. 37.

It can be seen that at 5 K the SEP-M(2)NH$_3$(1:2) and SEP-M(2)NH$_3$(1:1.5) samples exhibits higher magnetization than the ASEP-M(2)NH$_3$(1:2) and ASEP-M(2)NH$_3$(1:1.5). Taking into account the T_B values, it can be supposed that the lower magnetization of the ASEP-based composites is a result of the lower magnetite crystallites. Regardless of different Fe^{2+}/Fe^{3+} ratio, the magnetization of the samples SEP-M(2)NH$_3$(1:2) and SEP-M(2)NH$_3$(1:1.5) is the same. On the other hand, magnetization of the ASEP-M(2)NH$_3$(1:1.5) is lower than of ASEP-M(2)NH$_3$(1:2), indicating lower content of magnetite or smaller crystallites. According to the T_B values, it can be supposed that lower magnetization of ASEP-M(2)NH$_3$(1:1.5) is a result of smaller magnetite crystallites than in sample ASEP-M(2)NH$_3$(1:2).
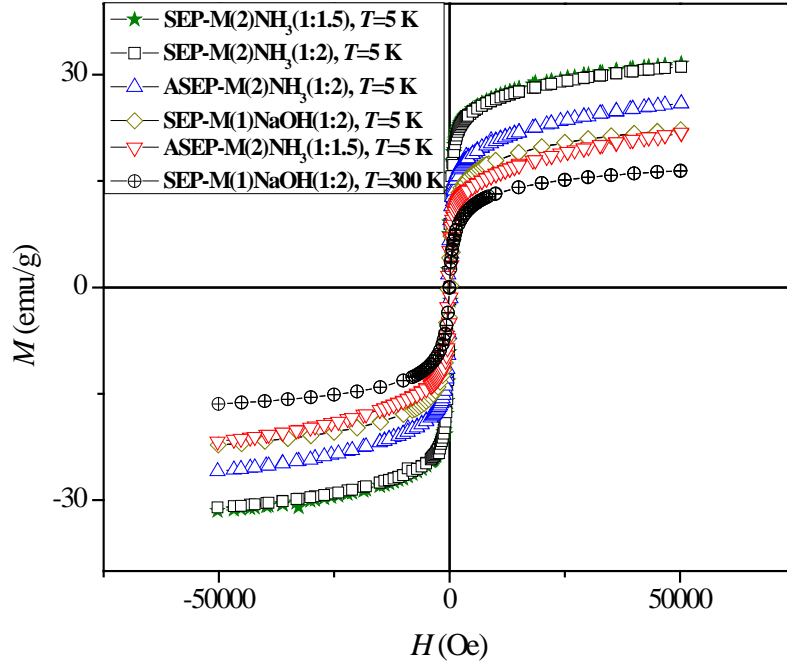
Fig. 37. Magnetic field dependence of magnetization.

The magnetization of the sample SEP-M(1)NaOH(1:2) is lower than of SEP-M(2)NH$_3$(1:2) and SEP-M(2)NH$_3$(1:1.5) (Fig. 37), which is in an agreement with the qualitative assessment of the magnetization, where it was found that all MNCs obtained with NaOH had lower magnetization in comparison to the MNCs obtained with NH$_3$. In addition, magnetization at 300 K is lower than at 5 K, as it can be seen for the SEP-M(1)NaOH(1:2) sample (Fig. 37). Such behavior was expected, because the degree of the orientation of the magnetic moments decreases with increasing temperature.

In the Fig. 38, the $M(H)$ dependence is given for the sample SEP-M(1)NaOH(1:2) at 5 and 300 K, for low H values. From the dependence at 5 K, the remanent magnetization M_R of 4.1 emu/g and coercivity H_C of 288 Oe can be found (Table 6). At 300 K (~ room temperature), the sample shows superparamagnetic behavior where both, the remanence magnetization M_R and the coercivity H_C, are zero (Fig. 38), ensuring that the composite does not retain magnetization when the magnetic field is removed. The values of the parameters M_R and H_C for other samples at 5 K are also given in Table 6.
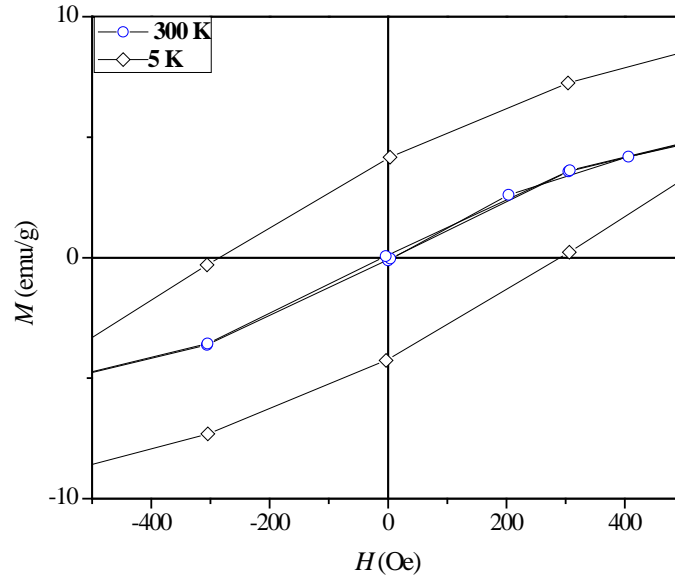
Fig. 38. The $M(H)$ dependence for SEP-M(1)NaOH(1:2) sample at 5 and 300 K, for low H values.

Table 6. The values of the parameters M_R and H_C at 5 K for some SEP/ASEP based composites

Sample	M_R (emu/g)	H_C (Oe)
SEP-M(2)NH$_3$(1:2)	8.9	256
SEP-M(2)NH$_3$(1:1.5)	9.1	246
ASEP-M(2)NH$_3$(1:2)	6.5	261
ASEP-M(2)NH$_3$(1:1.5)	5.2	283

The M_R and H_C values given in Table 6 are close to the values for sample SEP-M(1)NaOH(1:2), which is an indication that the size distribution of the magnetic nanocrystals are similar in all samples. However, it can be seen that for samples SEP-M(2)NH$_3$(1:2) and SEP-M(2)NH$_3$(1:1.5), the values of M_R are higher and the values of H_C lower than for SEP-M(1)NaOH(1:2) and the ASEP-based composites, indicating larger magnetite crystallites. These results and conclusions are in an agreement with the previous results and conclusions made based on T_B values and $M(H)$ dependences.

Further information on the size and size distribution of the magnetic nanoparticles can be extracted from $M(H)$ measurements in superparamagnetic region (at 300 K for sample SEP-M(1)NaOH(1:2)). Assuming that all particles have the same

magnetic moment, μ, the $M(H)$ dependence (Fig. 37) can be described by the Langevin function (Eq. 2) [89,158]. Fitting this equation to the experimental data, the average magnetite crystallites diameter of 7.6 nm was obtained (Eq. 3) for the sample SEP-M(1)NaOH(1:2), which is in agreement with the results of XRD analysis. It can be assumed that the magnetite crystals are little larger because the magnetic measurements detect only particle core which is magnetically ordered while its shell is often disordered and in most cases magnetically ''dead''.

8. 8. Determination of the point of zero charge (PZC)

An important parameter characterizing solids used as adsorbents is the point of zero charge (PZC), which represents the solution pH value at which the net surface charge of the solid equals zero [20]. The surface is positively charged at pH<PZC due to the protonization of the surface functional groups and negatively charged at pH>PZC as a results of the deprotonation. The PZC values of the Fe_3O_4, SEP, NZ, ASEP and the composites, obtained as the pH value of the plateau at the pH_f *vs.* pH_i dependence, are shown in Table 7. The results of the PZC determination for some samples are illustrated in Fig. 39.

The position of the plateau in all cases was at the same pH value for KNO_3 solutions of different concentrations, which indicates that KNO_3 was indifferent electrolyte, i.e. pH value of the plateau was PZC.

The PZC of the synthesized magnetite was 4.8 ± 0.1, which is lower than PZC of most of commercial Fe_3O_4, but lies within the reported range of values for magnetite [3,91,159]. For example, the PZC of magnetite nanospheres was 2.11 [3], while the PZC of one commercial magnetite was 8.2 [159]. The PZC values of all magnetic composites, except for NZ-M(1)NaOH(1:2), were between the values for pure compounds, but closer to the PZC of SEP/ASEP/NZ due to their higher quantity in the composites.
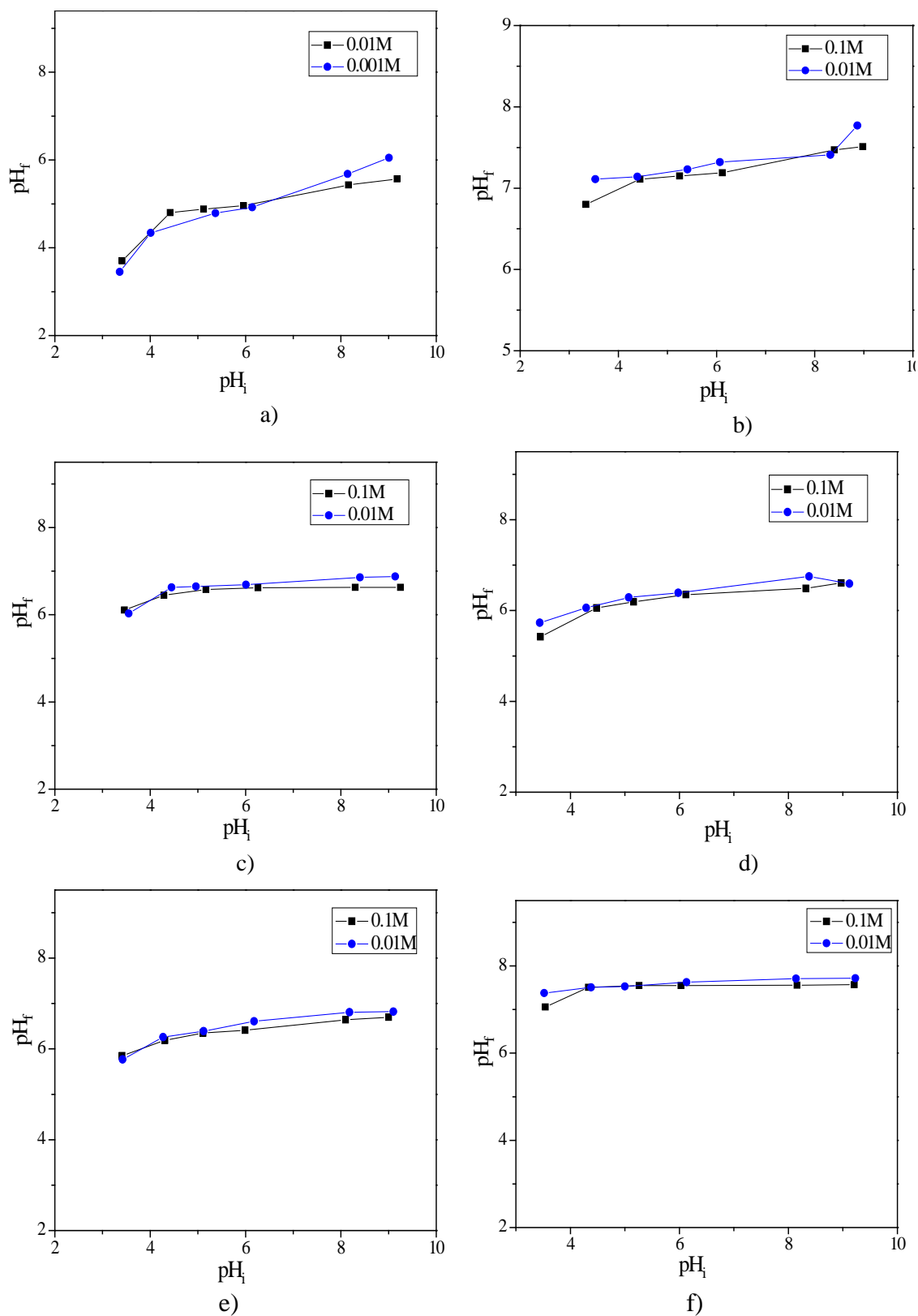
Fig. 39. Determination of the PZC of the samples: a) Fe_3O_4, b) SEP-M(1)NaOH(1:2), c) SEP-M(2)NH$_3$(1:2), d) NZ-M(2)NH$_3$(1:2), e) ASEP-M(2)NH$_3$(1:2), f) SEP-M(1)NaOH(1:2)^{more}, in KNO$_3$ solutions of different concentrations.

The magnetic composites that were synthesized by using NaOH have higher PZC than that synthesized by using ammonia. Generally, lower PZC indicates higher acidity of the surface functional groups and vice versa. Thus, higher values of PZC of the samples obtained by using NaOH can be explained by some leaching of acid compounds from the sepiolite/zeolite structure when NaOH used for co-precipitation. Namely, sepiolite and zeolite contain interconected SiO_4 tetrahedra, which can partially react with NaOH as a strong base. In that way, the samples obtained by using NaOH contain less acid groups and higher PZC values than the samples obtained by using NH_3. The leaching is especially pronounced in the case of the zeolite-based composite (sample NZ-M(1)NaOH(1:2)), as it was concluded according to XRD and FTIR analyses, so the PZC of this sample is the highest.

Table 7. PZC of the Fe_3O_4, SEP, NZ, ASEP and the magnetic composites.

Sample	PZC
SEP [20]	7.4 ± 0.1
ASEP [20]	6.9 ± 0.1
NZ [19]	7.5 ± 0.1
Fe_3O_4	4.8 ± 0.1
SEP-M(1)NaOH(1:2)	7.2 ± 0.1
SEP-M(2)NaOH(1:2)	7.3 ± 0.1
SEP-M(1)NH$_3$(1:2)	6.6 ± 0.1
SEP-M(1)NaOH(1:2)^{more}	7.4 ± 0.1
SEP-M(1)NaOH(1:2)^{less}	7.4 ± 0.1
SEP-M(1)NaOH(1:2)*	7.3 ± 0.1
SEP-M(2)NH$_3$(1:2)	6.6 ± 0.1
SEP-M(2)NH$_3$(1:1.5)	6.7 ± 0.1
NZ-M(2)NH$_3$(1:2)	6.4 ± 0.1
NZ-M(2)NH$_3$(1:1.5)	6.3± 0.1
NZ-M(1)NaOH(1:2)	8.3 ± 0.1
ASEP-M(2)NH$_3$(1:2)	6.5 ± 0.1
ASEP-M(2)NH$_3$(1:1.5)	6.4 ± 0.1

The PZC of the ASEP-M(2)NH$_3$(1:2) and ASEP-M(2)NH$_3$(1:1.5) samples is slightly lower than for the SEP-based samples obtained with ammonia, because the acid-activated sepiolite, *i.e.* sepiolite with more acid groups than SEP, was used for the synthesis.

8.9. Adsorption studies and isotherms modeling

The adsorption experiments were performed to compare the adsorption capacities of the synthesized magnetic nanocomposites (MNCs) for Cd^{2+}, Cr(VI), phosphate, Basic Yellow 28 and C.I. Reactive Orange 16.

<u>8. 9.1. Adsorption of Cd^{2+} ions</u>

The adsorption isotherms were determined for the MNCs and the pure compounds at the initial pH = 7.0 ± 0.1 [160] and the obtained results are presented in Figs. 40 - 42. The Langmuir, Freundlich and Sips isotherms constants are summarized in Table 8. In the figures, the Sips model fit curves, as the best fit, are presented with the experimental data.
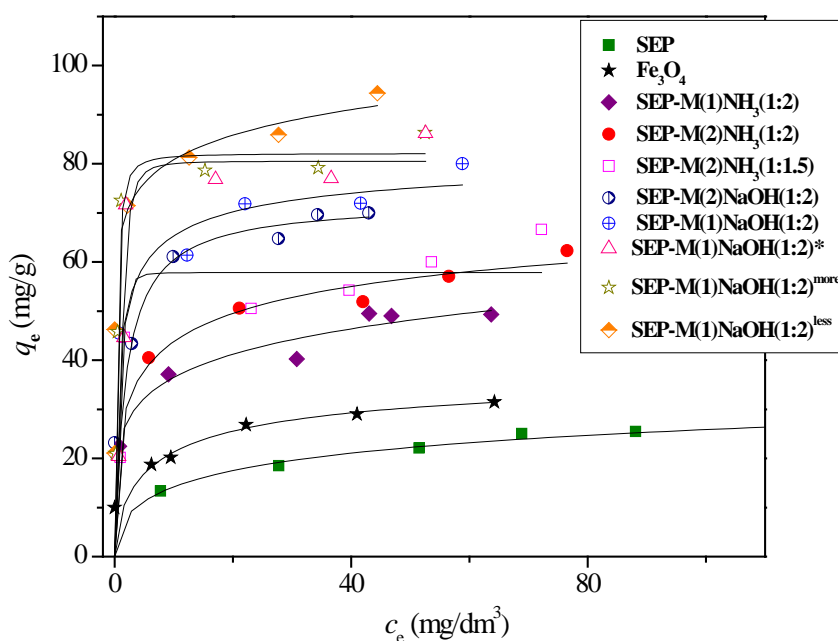
Fig. 40. Adsorption isotherms for Cd^{2+} onto the pure compounds and the SEP-based composites (adsorbent dosage = 0.02 g/20 cm^3, pH$_i$ = 7.0 ± 0.1).
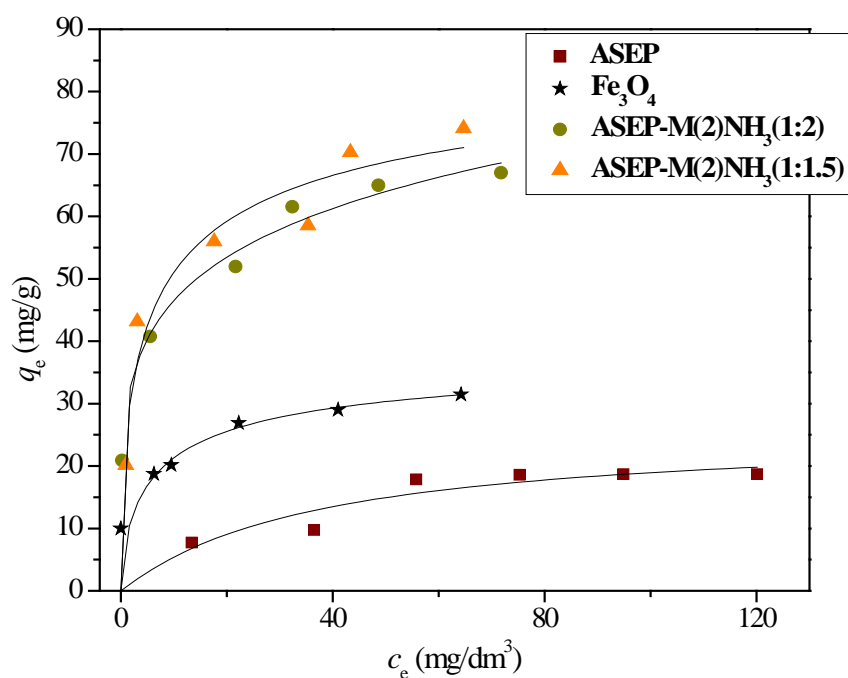
Fig. 41. Adsorption isotherms for Cd^{2+} onto the pure compounds and the ASEP-based composites (adsorbent dosage = 0.02 g/20 cm^3, pH$_i$ = 7.0 ± 0.1).
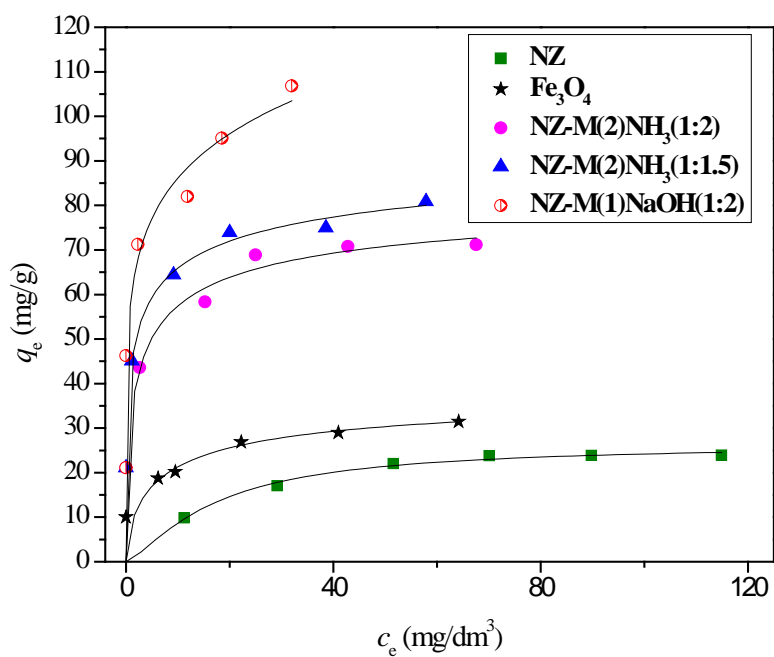
Fig. 42. Adsorption isotherms for Cd^{2+} onto the pure compounds and the NZ-based composites (adsorbent dosage = 0.02 g/20 cm^3, pH$_i$ = 7.0 ± 0.1).

Table 8. Langmuir, Freundlich and Sips isotherms constants and coefficient of correlation (R^2) for the adsorption of Cd^{2+} onto the Fe_3O_4, SEP, ASEP, NZ and the magnetic composites at $pH_i = 7.0 \pm 0.1$

Sample	Adsorption model									
	Langmuir			Freundlich			Sips			
	q_m (mg/g)	K_L (dm^3/mg)	R^2	$k_{f\,(mg^{(1-1/n)}dm^{3/n}/g)}$	$1/n$	R^2	q_m (mg/g)	K_a (dm^3/mg)^{ns}	n_S	R^2
SEP	27.71	0.099	0.984	8.083	0.254	0.994	29.05	0.156	0.457	0.995
SEP-M(1)NaOH(1:2)	73.07	7.93	0.975	39.30	0.176	0.968	76.06	1.01	0.539	0.982
SEP-M(1)NaOH(1:2)^{more}	83.39	0.274	0.977	51.02	0.140	0.878	82.10	4.240	1.450	0.988
SEP-M(1)NaOH(1:2)^{less}	89.80	1.73	0.851	66.04	0.087	0.856	88.93	0.185	0.107	0.856
SEP-M(1)NaOH(1:2)*	84.50	0.895	0.916	43.40	0.177	0.846	80.05	0.704	2.360	0.958
SEP-M(2)NaOH(1:2)	72.12	0.528	0.932	39.08	0.160	0.926	75.52	0.542	0.966	0.932
SEP-M(1)NH$_3$ (1:2)	47.00	1.04	0.955	24.08	0.177	0.986	56.12	0.117	0.211	0.986
SEP-M(2)NH$_3$(1:2)	56.54	0.758	0.964	26.64	0.193	0.988	64.40	0.431	0.398	0.993
SEP-M(2)NH$_3$(1:1.5)	59.96	0.918	0.927	30.20	0.174	0.926	57.78	0.700	3.190	0.956
ASEP	25.99	0.027	0.994	2.752	0.420	0.931	25.49	0.025	1.030	0.944
ASEP-M(2)NH$_3$(1:2)	65.71	0.372	0.936	29.01	0.202	0.995	68.06	0.068	0.225	0.995
ASEP-M(2)NH$_3$(1:1.5)	69.80	0.437	0.965	27.40	0.240	0.967	71.45	0.363	0.530	0.971
NZ	29.40	0.048	0.993	5.40	0.331	0.966	26.40	0.021	1.351	0.996
NZ-M(1)NaOH(1:2)	101.30	0.898	0.861	59.50	0.159	0.874	105.6	0.035	0.167	0.874
NZ-M(2)NH$_3$(1:2)	72.10	0.530	0.940	39.05	0.153	0.940	86.40	0.066	0.514	0.944
NZ-M(2)NH$_3$(1:1.5)	77.20	1.09	0.948	45.96	0.142	0.953	89.04	0.741	0.391	0.956
Fe$_3$O$_4$	33.51	0.181	0.926	12.64	0.224	0.924	39.41	0.265	0.647	0.946

Metal cations adsorb from aqueous solutions on amphoteric oxide materials mainly via formation of outer-sphere complexes (electrostatic bonding) or inner-sphere complexes, where the adsorbing ion forms a direct coordinate covalent bond with surface functional groups (specific adsorption) [115]. Besides specific adsorption, the main mechanisms of Cd^{2+} adsorption onto sepiolite is ion-exchange with the structural Mg^{2+} ions [20], while in the case of zeolite, Cd^{2+} ions form both other-sphere complexes (ion-exchange with exchangeable ions in the zeolite channels) and inner-sphere complexes with (Si,Al)-OH groups at the surface [19,80]. The adsorption of cations on amphoteric oxide materials is affected by the solution pH, because the pH influences both degree of protonation or deprotonation of functional groups at the adsorbent surface and the metal chemistry (e.g. speciation and precipitation). The adsorption capacity generally increases with the increase of initial pH because the number of H^+ ions that compete with the cations for the adsorption sites decreases. In addition, at higher pH values, Cd^{2+} can precipitate as $Cd(OH)_2$, which increases the removal efficiency. According to the value of the solubility product constant of $Cd(OH)_2$ and Cd^{2+} concentration used in the experiments, the $Cd(OH)_2$ precipitation can starts at pH > 8.5. In order to avoid precipitation in the experiments, because the precipitation is not mechanism of Cd^{2+} removal by the adsorbent, the experiments were done at the pH lower than 8.5. On the other hand, in order to exclude the influence of protonization or deprotonization of the surface functional groups, the adsorption was investigated at the initial pH 7, which is very close to pH_{pzc} of the composites. In that way, the electrostatic bonding can be minimized and Cd^{2+} can form dominantly the inner-sphere complexes.

According to the adsorption isotherms (Figs. 40-42), it is obvious that the capacities of all the MNCs are higher than of the pure compounds. In addition, the capacity of magnetite is higher than of SEP, ASEP and NZ. The capacity of ASEP is lower than of SEP due to the removal of the structural magnesium during acid activation, as it was shown previously [20].

The higher capacity of MNCs than of the pure compounds can be explained by lower aggregation of the compounds in the composites than of the pure SEP/NZ/ASEP and magnetite and, in that way, the higher accessibility of the surface to the ions. It was shown [161] that adsorption capacity of magnetite for Cd^{2+} is highly dependent on the specific surface area, i.e. on the size and aggregation of magnetite particles. For example, the adsorption capacity of magnetite with $S_p = 351.9$

m^2/g is much higher (~ 224 mg/g) than of magnetite synthesized in this work (S_p ~ 89 m^2/g, adsorption capacity ~ 33.5 mg/g), owing to higher S_p.

The influence of the type of basis used for co-precipitation: The adsorption capacities of all SEP-M,NH$_3$ composites are lower than of the SEP-M,NaOH samples (Fig. 40), regardless of better dispersibility of the magnetite particles and higher magnetization. As already stated, the magnetization depends on the quantity of magnetite and the size of magnetite crystallite [21,22]. According to the TEM and magnetic measurements, the magnetite crystallites in the composites have similar sizes, although the magnetic measurements showed slightly larger crystallites in the SEP-M,NH$_3$ than in SEP-M,NaOH samples. On the other hand, it was shown by the thermal analysis that the quantity of the magnetite is lower in the SEP-M(1)NH$_3$(1:2) and SEP-M(2)NH$_3$(1:2) than in the SEP-M(1)NaOH(1:2) and SEP-M(2)NaOH(1:2) composites. Having in mind lower content of magnetite, the higher magnetization of the SEP-M,NH$_3$ composites can be explained by higher content of crystalline magnetite, while the SEP-M,NaOH composites probably contain larger quantity of amorphous, disordered magnetite, which is magnetically ''dead''. It can be supposed that the amorphous magnetite was formed as very fine particles or as a layer at the sepiolite surface when the strong base was used, providing high number of nuclei for the magnetite formation due to the high OH$^-$ concentration. In that way, the adsorption capacity of the SEP-M,NaOH composites is higher and the magnetization is lower, but high enough for the magnetic separation.

The influence of the type of the procedure: The SEP-M(1)NaOH(1:2) and SEP-M(2)NaOH(1:2) composites have similar adsorption capacities. Regardless of slightly different morphology, these composites have similar properties: textural characteristics, magnetization, point of zero charge and phase composition; therefore, the adsorption capacities are similar. Accordingly, in the case of sepiolite, the sequence of reagents mixing (procedure 1 or 2) does not have a large influence on the properties and adsorption capacity of the composites obtained by using NaOH for co-precipitation. Obviously, both procedures provide similar conditions for the magnetite nucleation and growth when NaOH was used. On the other hand, when the composites were prepared by using ammonia, the Procedure 2 provided better dispersibility of the magnetite particles and higher adsorption capacity, probably due to higher volume of mesopores, despite the fact that the specific surface area of this sample is lower than of the SEP-M(1)NH$_3$(1:2) sample.

The influence of the iron content: In the case of the composites obtained by first procedure with NaOH, adsorption capacity increased when the concentration of NaOH and quantity of iron salts increased (samples SEP-M(1)NaOH(1:2)* and SEP-M(1)NaOH(1:2)^{more}, respectively). Higher quantity of iron salts provided higher content of magnetite in the composites and higher capacity. On the other hand, it can be supposed that higher concentration of NaOH provided more centers for the magnetite nucleation and formation of smaller crystallites or amorphous magnetite. In that way, adsorption capacity is higher, regardless of lower specific surface area (Table 5) in comparison to other samples obtained by first procedure, by using NaOH.

Surprisingly, the adsorption capacity of the sample SEP-M(1)NaOH(1:2)^{less} is even higher than of sample SEP-M(1)NaOH(1:2)^{more}, despite the fact that the iron salt content in the synthesis was three times lower. It can be supposed that in such conditions, the magnetite dispersibility was much better than in the composite with higher content of iron salts, which provides the highest adsorption capacity. Probably, besides fine particles, thin layer of magnetite is formed, which cannot be seen in SEM micrographs.

The influence of the type of sepiolite and Fe^{2+}/Fe^{3+} ratio: Regardless of worse dispersion of the magnetite particles in the ASEP-M(2)NH3(1:2) and ASEP-M(2)NH3(1:1.5) in comparison to the SEP-M(2)NH3(1:2) and SEP-M(2)NH3(1:1.5), the volume of mesopores is higher and the adsorption capacities are higher than of the SEP-based MNCs (Figs 40 and 41). In both cases, the Fe^{2+}/Fe^{3+} ratio did not have significant influence on the adsorption capacity. This is understandable for the SEP-based MNCs, having in mind the same textural and magnetic properties. On the other hand, the magnetization of the sample ASEP-M(2)NH3(1:1.5) was lower, the mesopore volume was higher and the adsorption capacity was slightly higher, which can indicate lower magnetite crystallites.

The influence of samples aging during storage: The adsorption capacity of the SEP-M(1)NaOH(1:2) was checked after storage for 3 month (Fig. 43). The capacity was lower than of freshly synthesized sample (new quantity of the sample SEP-M(1)NaOH(1:2) was synthesized and the adsorption isotherm was determined immediately after the synthesis, sample SEP-M(1)NaOH(1:2)fresh in Fig. 43).and it was similar to the capacity of the composite SEP/iron(III) oxihydroxide (approximately 41 mg/g) [162], which was synthesized previously [66] by the precipitation of Fe^{3+} with NaOH, at the same SEP/Fe ratio as in the MNCs. As it can

be seen, the adsorption capacity of the sample SEP-M(1)NaOH(1:2)fresh is the same as of the sample presented in Fig. 40. Having in mind that the sample had magnetization after storage, it was supposed that just surface of the magnetite particles was oxidized and surface groups Fe^{2+}-OH were transformed to Fe^{3+}-OH, which have lower affinity for Cd^{2+} ions.

These results suggests that the magnetite has higher affinity to Cd^{2+} ions than iron(III)-oxihydroxide compounds, which can be formed by magnetite oxidation in air during storage. Therefore, magnetite adsorbents should be storage in the protected atmosphere in order to prevent oxidation and retain high adsorption capacity for Cd^{2+} ions.
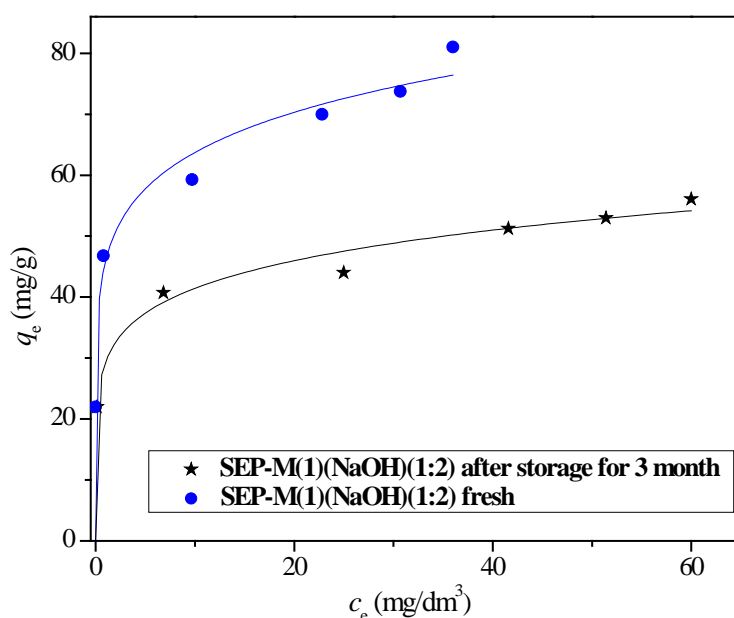
Fig. 43. Adsorption isotherms for Cd^{2+} onto fresh SEP-based MNC and the composite after storage for 3 months.

Adsorption of NZ-based composites: Similar as for SEP-based composites, adsorption capacity of the sample Z-M(1)NaOH(1:2) is significantly higher than of samples Z-M(2)NH$_3$(1:2) and Z-M(2)NH$_3$(1:1.5) (Fig. 42), although the dispersibility of the magnetite is higher in the samples obtained with NH$_3$ (Fig. 34). Bearing in mind the results of XRD analysis, higher adsorption capacity of the sample Z-M(1)NaOH(1:2) can be explained by the presence of smaller crystallites or amorphous magnetite in comparison to samples Z-M(2)NH$_3$(1:2) and Z-

M(2)NH$_3$(1:1.5). In addition, higher surface area and higher volume of mesopores contributes to higher adsorption capacity.

Comparison of adsorption capacity of zeolite/magnetite and zeolite oxihydroxides composites: In Fig. 44, the adsorption isotherm for the sample Z-M(1)NaOH(1:2) is compared with the adsorption isotherm for the sample Fe(III)-zeolite [112], synthesized in highly basic conditions starting from FeCl$_3$ [19], at the same ratio Fe/zeolite as in the sample Z-M(1)NaOH(1:2). The sample Fe(III)-zeolite contains amorphous iron(III) oxihydroxides, the specific surface area is 175 m^2/g and the point of zero charge is 9.3 [19]. As in the case of sepiolite/magnetite and sepiolite/Fe(III) oxihydroxide composites, the adsorption capacity of the zeolite/magnetite composite is higher than of sample zeolite/Fe(III) oxihydroxides, indicating higher affinity of magnetite to Cd^{2+} ions than of Fe(III) species.
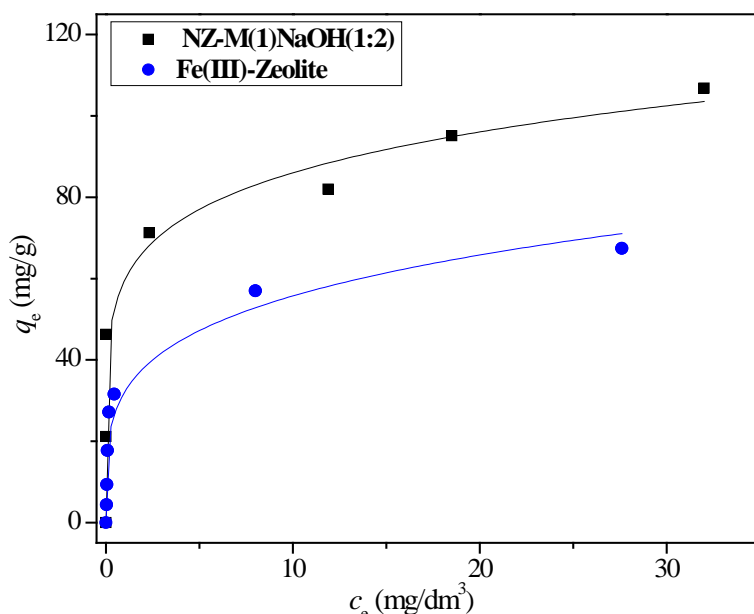
Fig. 44. Adsorption isotherms for Cd^{2+} ions of the sample NZ-M(1)NaOH(1:2) and sample zeolite/ Fe(III) oxihydroxides.

Adsorption isotherms modeling: As shown in Table 8, coefficients of correlation (R^2) suggest that the Sips model is the best model to explain the adsorption behavior of Cd^{2+} on all the samples, except for ASEP and ASEP-M(2)NH$_3$(1:1.5), but also both Langmuir and Freundlich models fit the results well. It is understandable, having in mind that the Sips model is a combination of Langmuir and Freundlich models. At low adsorbate concentrations, *i.e.* when the adsorbate content is much

lower than the adsorbent capacity, the Sips model is reduced to Freundlich model, while at high concentrations, when the adsorbate content is higher than the adsorbent capacity, the model predicts a monolayer adsorption capacity, characteristic of the Langmuir isotherm [162-164]. Further, the Langmuir model assumes adsorption at specific sites of the same energy, without any interactions between adsorbed species (formation of chemical bonds) [119], while the Freundlich model describes adsorption (possibly multilayer in nature) on a heterogeneous surface consisting of non-identical and energetically non-uniform sites [120]. The bonds between adsorbate and adsorbent can be chemical (if active sites of adsorbent are strong enough) or physical, but the bonds between adsorbate layers are always physical.

According to the adsorption isotherm modeling, bearing in mind that different functional groups are present at the surface of the composites (M-OH, Fe^{2+}-OH, Fe^{3+}-OH), it can be concluded that Cd^{2+} is chemisorbed on a heterogeneous surface of the composites, as well as on SEP and Fe_3O_4 (formation of inner-sphere complexes), at energetically non-uniform sites until monolayer was formed. The Langmuir model fitted better the results of Cd^{2+} adsorption on ASEP because this material contains dominantly Si-OH surface functional groups of the same energy.

8.9.2. Adsorption of Cr(VI) ions

The adsorption isotherms were determined for the MNCs and the pure magnetite at the initial pH = 2.0 ± 0.1 and the obtained results are presented in Figs. 45-47. The adsorption isotherms constants are summarized in Table 10.
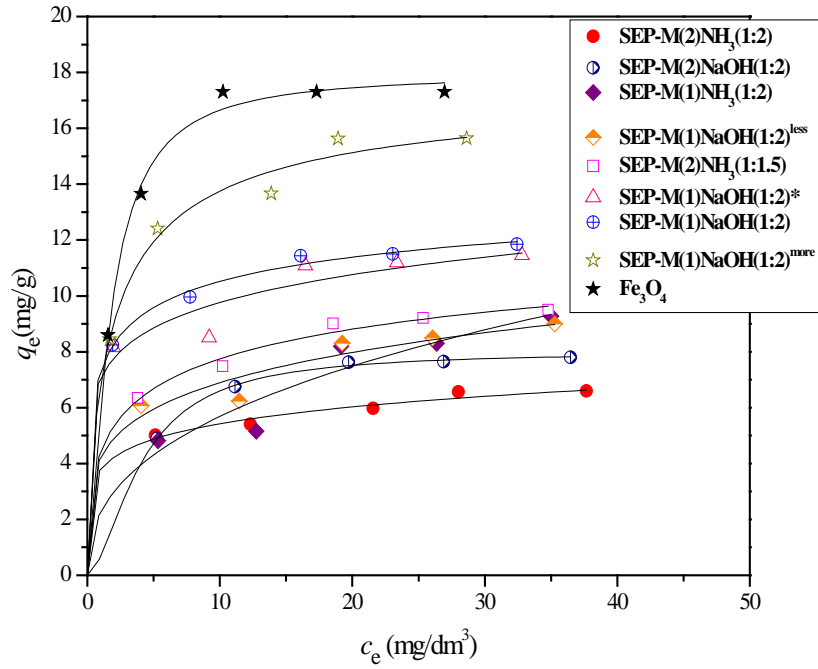
Fig. 45. Adsorption isotherms for Cr(VI) onto Fe_3O_4 and the SEP-based composites (adsorbent dosage = 0.02 g/20 cm^3, pH = 2.0 ± 0.1).
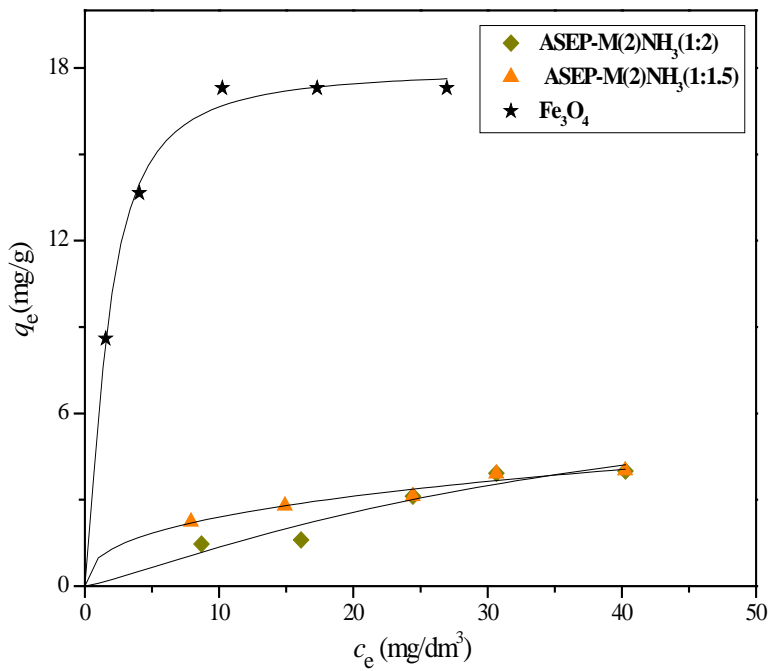
Fig. 46. Adsorption isotherms for Cr(VI) onto Fe_3O_4 and the ASEP-based composites (adsorbent dosage = 0.02 g/20 cm^3, pH = 2.0 ± 0.1).
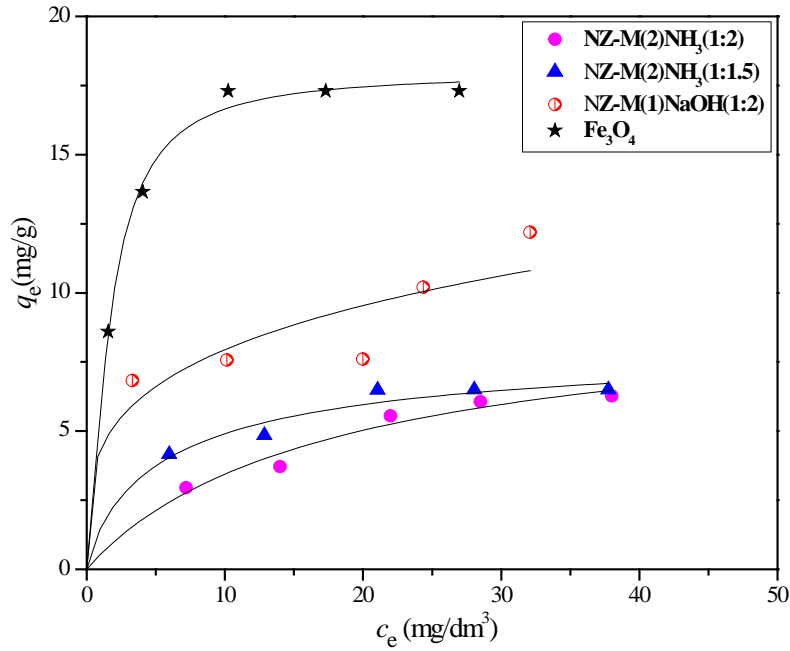
Fig. 47. Adsorption isotherms for Cr(VI) onto Fe_3O_4 and the NZ-based composites (adsorbent dosage = 0.02 g/20 cm^3, pH = 2.0 ± 0.1).

According to the literature [165] the retention of Cr(VI) on natural and acid-activated sepiolites, as well as zeolite was negligible, even at low initial pH values. The surface of sepiolite and zeolite is negatively charged in aquatic solutions in a wide range of pH values, while Cr(VI) is present as anions, CrO_4^{2-}, $HCrO_4^-$ or $Cr_2O_7^{2-}$, depending on its concentration and solution pH: $HCrO_4^-$ is the main species at low concentrations and pH range of 2–4, whereas CrO_4^{2-} becomes dominant species at pH $\geq$ 7, and $Cr_2O_7^{2-}$ and $HCr_2O_7^-$ exist only in solutions of high concentration and lower pH values. Therefore, the adsorption of Cr(VI) anions on negatively charged surface is very low. In addition, previous studies [2,7,133] have shown that the adsorption capacity of magnetite and magnetite-composites drastically decreased when pH increased from pH_i = 2, due to increase of negative charge of the surface with the pH increase.

Table 10. Langmuir, Freundlich and Sips isotherms constants and coefficients of correlation (R^2) for the adsorption of Cr(VI) onto the Fe_3O_4 and the magnetic composites at $pH_i = 2.0 \pm 0.1$

Sample	Adsorption model									
	Langmuir			Freundlich			Sips			
	q_m (mg/g)	K_L (dm^3/mg)	R^2	$k_{f\,(mg^{(1-1/n)}\,dm^{3/n}/g)}$	$1/n$	R^2	q_m (mg/g)	Ka (dm^3/mg)^{ns}	n_S	R^2
Fe_3O_4	17.82	0.579	0.993	9.503	0.206	0.958	17.96	0.481	1.419	0.997
SEP-M(1)NaOH(1:2)	11.91	1.087	0.994	7.668	0.131	0.997	12.43	0.827	0.359	0.998
SEP-M(1)NaOH(1:2)^{more}	16.31	0.608	0.992	8.209	0.203	0.987	17.79	0.621	0.738	0.994
SEP-M(1)NaOH(1:2)^{less}	9.26	0.364	0.963	4.237	0.211	0.981	9.83	0.022	0.219	0.981
SEP-M(1)NaOH(1:2)*	11.23	1.110	0.960	1.705	0.141	0.980	11.56	0.039	0.148	0.980
SEP-M(2)NaOH(1:2)	8.84	0.257	0.996	3.755	0.217	0.983	8.00	0.091	1.711	0.999
SEP-M(1)NH$_3$ (1:2)	9.67	0.098	0.952	2.278	0.397	0.965	9.89	0.007	0.407	0.964
SEP-M(2)NH$_3$(1:2)	6.79	0.473	0.989	3.816	0.152	0.996	6.95	0.074	0.170	0.996
SEP-M(2)NH$_3$(1:1.5)	9.85	0.403	0.992	4.930	0.191	0.996	9.54	0.401	0.401	0.996
ASEP-M(2)NH$_3$(1:2)	5.34	0.0131	0.955	0.252	0.767	0.952	5.23	0.012	1.205	0.956
ASEP-M(2)NH$_3$(1:1.5)	5.06	0.088	0.982	1.005	0.377	0.988	5.42	0.014	0.396	0.988
NZ-M(1)NaOH(1:2)	9.43	0.057	0.984	1.158	0.479	0.980	9.76	0.059	0.963	0.984
NZ-M(2)NH$_3$(1:2)	6.76	0.057	0.984	1.158	0.479	0.980	6.98	0.059	0.963	0.984
NZ-M(2)NH$_3$(1:1.5)	6.54	0.182	0.983	2.640	0.262	0.980	6.73	0.220	0.818	0.984

The influence of initial pH value on the adsorption capacity for the sample MSEP-M(1)NaOH(1:2) (Fig. 48) also showed that adsorption capacity significantly decreases at $pH_i > 2$. These are the reasons why the Cr(VI) adsorption isotherms were determined for initial $pH_i = 2$.
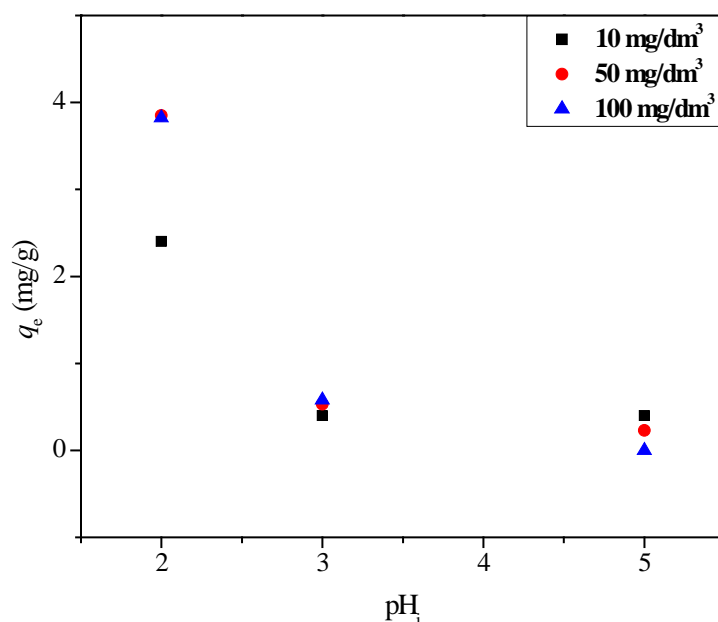
Fig. 48. The influence of pH_i on the Cr(VI) adsorption onto sample SEP-M(1)NaOH(1:2) at the initial concentrations 10, 50 and 100 mg/dm^3.

According to the literature [167], besides formation of inner- and outer-sphere complexes, possible mechanism of Cr(VI) adsorption onto magnetite and magnetite composites is the reduction of Cr(VI) by magnetite to Cr(III) and the precipitation of Cr^{3+} ions as $Cr(OH)_3$ or Cr_2O_3 on the surface of the adsorbent. Bearing in mind that the adsorption capacity is very low at $pH_i > 2$, it can be supposed that the main mechanism of chromate adsorption on magnetite and magnetite composites is the electrostatic interactions of chromate anions and protonated surface functional groups, *i.e.* formation of outer-sphere complexes.

According to the adsorption isotherm (Figs. 45-47), the adsorption capacity of the pure magnetite for Cr(VI) is about 17.5 mg/g, which is comparable with the literature data [3, 133]. Adsorption capacities of all MNCs are lower than of the pure magnetite, unlike the capacity for Cd^{2+} ions, where the capacities of MNCs were higher

than of the pure magnetite and the support. The highest capacity for chromates has the SEP-based composite with the highest content of magnetite (SEP-M(1)NaOH(1:2)^{more}). Obviously, the content of magnetite is the factor that determines the adsorption capacity because the capacity of the support is negligible. Having in mind that the adsorption capacity of the sample SEP-M(1)NaOH(1:2)^{more} is slightly lower than of pure magnetite, while the theoretical content of magnetite in the sample is 36.5 mas.%, it can be concluded that the presence of sepiolite as a support improved the adsorption properties of the magnetite, as it was the case with the Cd^{2+} adsorption. On the other hand, adsorption capacity was not increased as much as in the case of Cd^{2+}. It can be explained by different adsorption mechanisms: inner-sphere complexes are formed in the case of Cd^{2+} ions, which are exchanged with H^+ ions from surface functional groups, while chromate ions formed outer-sphere complexes. Outer-sphere complexes are formed when H^+ ions protonate the surface functional groups and contra ions (e.g. NO_3^- ions from HNO_3 used for pH adjustment) are concentrated around the particle and exchanged with chromate ions.

Therefore, it can be supposed that the protonization degree is the decisive factor for the chromate adsorption. Generally, basic groups are protonated better and the chromate ions are adsorbed more than on adsorbent with acidic groups. Accordingly, it can be expected that MNCs with lower PZC values have lower adsorption capacities for chromates. Indeed, ASEP-based composites and the SEP/NZ-based composites obtained with NH_3 have lower PZC and lower adsorption capacities than composites obtained with NaOH.

However, despite the similar PZC values and the same ratio SEP/($Fe^{2+}+Fe^{3+}$), the adsorption capacities of the SEP-based MNCs obtained by using NaOH (SEP-M(1)NaOH(1:2), SEP-M(2)NaOH(1:2) and SEP-M(1)NaOH(1:2)*) are different. Higher adsorption capacity was achieved by the first procedure. The adsorption capacities of these samples for Cd^{2+} were similar, although the samples obtained by first procedure had slightly higher capacities. Obviously, the synthesis by first procedure with NaOH provided best adsorption properties for both cations and anions.

As shown in Table 10, coefficients of correlation (R^2) suggest that the Sips model is the best model to explain the adsorption behavior of Cr(VI) on all the samples, but also both Langmuir and Freundlich models fit the results well.

8.9.3. Comparison of Cd^{2+} and Cr(VI) adsorption onto the composites and other magnetic adsorbents

A comparison between the adsorption capacity of the samples prepared in this study and other magnetic adsorbents reported in the literature, for the adsorption of Cd^{2+} and Cr(VI), are listed in Tables 11 and 12, respectively.

Table 11. A comparison between the adsorption capacity of the samples prepared in this study and magnetic adsorbents reported in the literature for the adsorption of Cd^{2+}

Adsorbent	Optimal pH	Adsorption capacity (mg/g)
Magnetite/acid-activated sepiolite composite [26]	6.5	14.2
α-ketoglutaric acid modified magnetic chitosan [168]	6	201.2
Shellac-coated iron oxide [168]	8	18.8
Magnetic hydroxyapatite nanoparticles [169]	5	220.7
Magnetic graphene oxide nanocomposite [170]	6	91.3
Magnetic mesoporous carbon [171]	7	288.7
Polyacrylic acid modified magnetic mesoporous carbon [171]	7	406.6
Magnetic Fe_3O_4-MnO_2 [172]	6	169.9
Polyethylenimine grafted magnetic adsorbent [168]	6.5	105.3
Maghemite-magnetite[173]	9	2.7
Magnetite [this study]	7	31.5
Magnetic sepiolite composites [this study]	7	49.3-94.4
Magnetic acid-activated sepiolite composite [this study]	7	67.0-74.1
Magnetic zeolites [this study]	7	71.2-106.8

Table 12. A comparison between the adsorption capacity of the samples prepared in this study and magnetic adsorbents reported in the literature for the adsorption of Cr(VI)

Adsorbent	Optimal pH	Adsorption capacity (mg/g)
Magnetite nanoparticle [2]	2.5	20.2
Magnetite nanoparticles [133]	2	20.2
Diatomite-supported/magnetite nanoparticles [2]	2.5	13.7
Magnetite/reduced graphene oxide nanocomposites [171]	-	33.9
Montmorillonite-supported magnetite nanoparticles [7]	2.5	13.9
Magnetite- maghemite [174]	2	2.4
Magnetic natural zeolite-polypyrrole [175]	2	344.9
Zero-valent iron (nZVI)–Fe_3O_4 nanocomposites [176]	3	100
	8	29
Magnetic multi-wall carbon nanotubes [177]	5	14.3
Magnetic activated carbon composites [177]	5	2.8
Nano crystalline iron oxide/hydroxide [178]	-	11.2
Magnetic chitosan composites [179]	3.0−5.0	21.0
Magnetite [this study]	2	17.3
Magnetic sepiolite composites [this study]	2	6.6-15.6
Magnetic acid-activated sepiolite composite [this study]	2	4.0
Magnetic zeolites [this study]	2	6.3-12.2

It can be seen that adsorption capacities for Cd^{2+} differ significantly depending on the support type and type of support modification. The composites synthesized in this work have significantly higher capacity than composite synthesized previously with

acid-activated sepiolite as a support [26]. It is worth to point out that the capacities of SEP/ASEP/NZ composites are similar to the capacity of the composite based on an expensive support (graphene oxide) [171]. On the other hand, the capacities of magnetic adsorbents for Cr(VI) are relatively similar, with some exceptions, and generally lower than 40 mg/g. The capacity of the sample SEP-M(1)NaOH(1:2)^{more} is comparable to the capacity of similar composites (for example montmorillonite-supported magnetite nanoparticles [7] and some composites obtained with an expensive support (for example multi-wall carbon nanotubes [177]).

8.9.4. Adsorption of cationic and anionic dye and phosphate

The adsorption capacities of the composites were checked for some more cationic and anionic pollutants: anionic dye C.I. Reactive Orange 16 at $pH_i = 5 \pm 0.1$, cationic dye Basic Yellow 28 at $pH_i = 5 \pm 0.1$ and phosphate anions at $pH_i = 4 \pm 0.1$. The results obtained for one initial concentration are presented in Table 13.

The results show that the adsorption capacities of the composites for anions (phosphates and C.I. Reactive Orange 16) are very low.

Adsorption capacities of SEP, ASEP and NZ for phosphates at $pH_i = 4 \pm 0.1$ are practically equal to zero. The capacity of pure Fe_3O_4 is relatively low, but comparable with the literature data for magnetite obtained by co-precipitation method [180]. According to the literature data [180,181], the main mechanism of phosphates adsorption onto magnetite is the formation of inner-sphere complexes. The MNC's capacities are lower than capacity of Fe_3O_4, whereas the SEP- and NZ-based composites obtained with NH_3 had the highest capacities. These samples have higher magnetization in comparison to samples obtained by using NaOH and ASEP-based composites. Obviously, the phosphate adsorption is higher when magnetization is higher.

Adsorption capacities of the SEP, ASEP and NZ for anionic dye C.I. Reactive Orange 16 are not equal to zero, as for phosphate. It can be supposed that large dye anions can interact by Van der Waals forces with the mineral's surface. Due to positive charge, regardless of lower specific surface area, the adsorption capacity of the pure

Fe$_3$O$_4$ is slightly higher than of the supports. All MNCs had lower capacity than Fe$_3$O$_4$, but the dependence of capacity on the composite properties could not be determined.

Table 13. Adsorption capacity of MCNs and pure compounds for Basic Yellow 28 (pH$_i$ = 5 ± 0.1; c_i = 147 mg/dm^3, adsorbent dosage = 0.02 g/100 cm^3), C.I. Reactive Orange 16 (pH$_i$ = 5 ± 0.1; c_i = 72 mg/dm^3, adsorbent dosage = 0.02 g/20 cm^3) and phosphate (pH$_i$ = 4 ± 0.1; c_i = 16 mg/dm^3, adsorbent dosage = 0.02 g/20 cm^3).

Sample	q_e (mg/g)		
	Basic Yellow 28	C.I. Reactive Orange 16	Phosphates
SEP	93.6	2.10	~ 0
SEP-M(1)NaOH(1:2)	92.4	2.05	1.1
SEP-M(1)NaOH(1:2)*	85.7	2.92	0.92
SEP-M(1)NaOH(1:2)^{more}	92.8	1.69	1.5
SEP-M(1)NaOH(1:2)^{less}	95.1	3.04	0.68
SEP-M(2)NH$_3$(1:2)	89.1	1.04	2.1
SEP-M(2)NH$_3$(1:1.5)	90.8	2.10	2.4
NZ	34.7	1.75	~ 0
Z-M(1)NaOH(1:2)	-	2.57	1.4
Z-M(2)NH$_3$(1:2)	33.4	1.11	1.9
Z-M(2)NH$_3$(1:1.5)	33.3	1.83	2.3
ASEP	48.3	1.03	~ 0
ASEP-M(2)NH$_3$(1:2)	71.2	1.47	0.50
ASEP-M(2)NH$_3$(1:1.5)	71.1	0.75	0.68
Fe$_3$O$_4$	4.12	3.48	3.4

Adsorption capacity of all supports and the composites are much higher for cationic dye Basic Yellow 28 than for the anionic dye, similarly as in the case of Cd^{2+} and Cr(VI) adsorption, regardless of different pH$_i$. Owing to higher capacity of SEP in comparison to ASEP and NZ, SEP-based samples had higher capacity than ASEP- and

NZ-based composites. Despite the fact that adsorption capacity of Fe_3O_4 is much lower than of SEP, ASEP and NZ, it seems that the capacities of the MNCs are not lower than of the support. In the case of ASEP-MNCs, the capacities are even higher. De-aggregation during the composite preparation can be the reason for such results, as in the case of Cd^{2+} adsorption.

Obviously, pure sepiolite is effective adsorbent for cationic dye Basic Yellow 28, but the presence of magnetite is desirable to provide magnetic separation after the adsorption. In order to check whether the presence of magnetite decreases the adsorption capacity of sepiolite for the cationic dye, adsorption isotherms were determined for pure sepiolite and the composite with the lowest content of magnetite, SEP-M(1)NaOH(1:2)^{less} (Fig. 49). It can be seen that the presence of magnetite caused just small decrease of the adsorption capacity of sepiolite, which indicate that the composite can be used for efficient removal of Basic Yellow 28 from water and can be easily separated from water by magnetic separation.
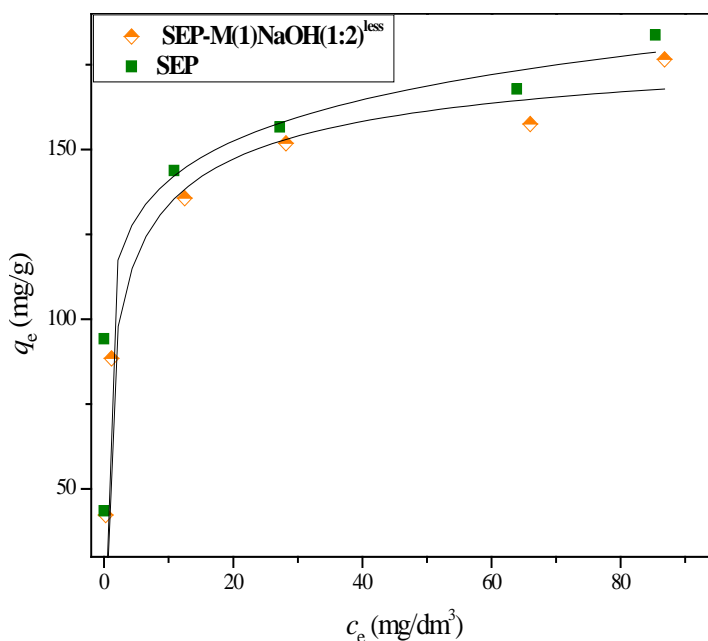
Fig. 49. Adsorption isotherms for Basic Yellow 28 onto SEP-M(1)NaOH(1:2)^{less} and sepiolite (adsorbent dosage = 0.02 g/100 cm^3, pH = 5.0 ± 0.1).

8.9.5. Effect of contact time and temperature on Cd^{2+} and Cr(VI) adsorption

The effect of contact time and temperature on the adsorption of Cd^{2+} ions were investigated for SEP-based composites, one prepared with NaOH and one prepared with NH_3 (SEP-M(2)NaOH(1:2) and SEP-M(1)NH_3(1:2)), while for Cr(VI) adsorption, sample with the highest adsorption capacity was chosen (SEP-M(1)NaOH(1:2)^{more}).

8.9.5.1. Adsorption kinetics

The dependences of adsorbed quantity of Cd^{2+} or Cr(VI) on adsorption time are presented in Figs. 50 and 51, respectively.

The adsorption equilibrium time was 60 min for Cd^{2+} ions for both adsorbents, while for Cr(VI) the time for equilibrium reaching was longer – 480 min. In addition, it can be seen that the adsorption capacity of the sample SEP-M(2)NaOH(1:2) is higher than of SEP-M(1)NH_3(1:2) sample, as it was shown according to adsorption isotherms (Fig. 40).

The time needed for reaching equilibrium was significantly longer for chromium than for Cd^{2+} adsorption. It can be explained by different mechanism of adsorption: Cd^{2+} ions form stronger bonds with the adsorbent surface, inner-sphere complexes, and the ions were captured strongly, practically without desorption. On the other hand, chromium ions form outer-sphere complexes, where the ions are concentrated near the charged surface and these bonds are weaker than bonds in inner-sphere complexes. Therefore, the equilibrium is established slowly.
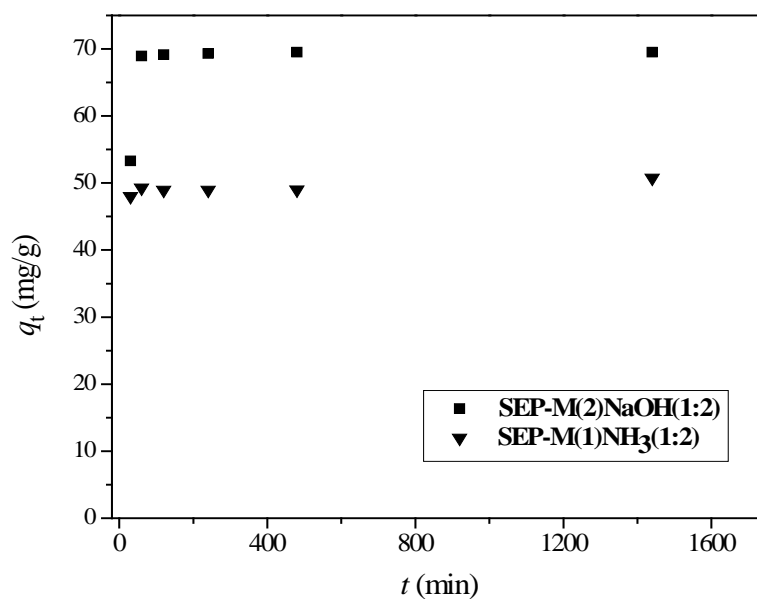
Fig. 50. The effects of adsorption time on the adsorbed quantity of Cd^{2+} at $pH_i = 7.0$ ±0.1 onto SEP-M(2)NaOH(1:2) and SEP-M(1)NH$_3$(1:2) (Cd^{2+} concentration was 100 mg/dm^3).
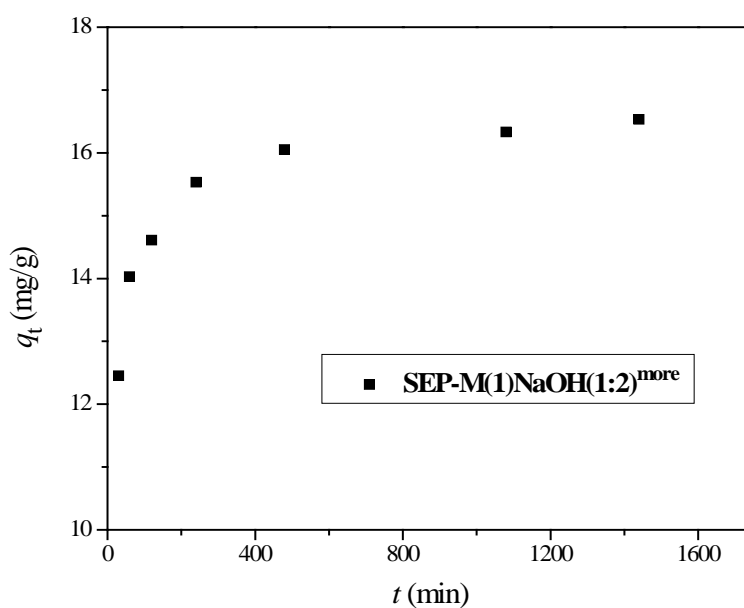
Fig. 51. The effects of adsorption time on the adsorbed quantity of Cr(VI) at $pH_i = 2.0$ ±0.1 onto SEP-M(1)NaOH(1:2)^{more} (Cr(VI) concentration was 40 mg/dm^3).

In order to evaluate the adsorption kinetics of Cd^{2+} and Cr(VI) on the composites, the conventional kinetic models, pseudo-first and pseudo-second order models, were applied to test the experimental data. The adsorption kinetics constants, obtained by linear fitting and correlation coefficients (R^2) are summarized in Table 14.

The correlation coefficients suggest that the adsorption kinetic data was fitted much better by the pseudo-second order rate equation than by the pseudo-first order equation. The R^2 values for the pseudo-first order model are much lower than 1, while for pseudo-second model are close to 1. Moreover, the equilibrium adsorption capacities (q_e) obtained by the pseudo-second model were close to the experimental ones ($q_{e,exp}$), further confirming the feasibility of this model for both Cd^{2+} and Cr(VI).

According to the pseudo-first order model, the adsorption rate is proportional to the number of free sites, while in the case of the pseudo-second order kinetic model, the rate of adsorption is proportional to the square of the number of unoccupied sites. Obviously, the number of free sites is strongly important for the adsorption kinetics, therefore the pseudo-second order model is more suitable than pseudo-first order model.

Analysis of the literature data for different adsorbents and different cations and anions as adsorbates showed that the pseudo-second order model fitted the results of adsorption kinetics much better than the pseudo-first order model in almost all cases. According to a suitability of the model for the kinetic results fitting, the authors usually concluded that "the rate-limiting step may be a chemical adsorption involving valency forces through sharing or exchanging of electrons between adsorbent and adsorbate". But, the pseudo-second-order is pseudo-model, because it includes all steps of adsorption, such as external film (boundary layer) diffusion, internal particle diffusion and adsorption. The overall rate of adsorption is controlled by the slowest step. Of the three mentioned steps, the adsorption step is assumed rapid and thus the slowest step would be either film diffusion or pore diffusion. Therefore, it cannot be stated that chemisorption is the rate-limiting step according to an appropriateness of the pseudo-second order model for the adsorption kinetic data.

Table 14. The kinetic parameters and correlation coefficients for the adsorption of Cd^{2+} and Cr(VI) onto the magnetic composites.

Adsorbent/Adsorbate	Pseudo-first order model			Pseudo-second order model		
	k_1 (min^{-1})	q_e (mg/g)	R^2	q_e (mg/g)	k_2 (g/mg·min)	R^2
SEP-M(2)NaOH(1:2)/Cd^{2+}	0	2.06	0.335	71.43	0.350	0.999
SEP-M(1)NH$_3$(1:2)/Cd^{2+}	8.615	1.47	0.390	50.50	0	0.999
SEP-M(1)NaOH(1:2)^{more}/ Cr(VI)	$2.30·10^{-3}$	1.53	0.858	16.66	0.074	0.999

8.9.5.2. Effect of temperature on adsorption of Cd^{2+} and Cr(VI) and thermodynamic analysis

The effect of temperature on the adsorption of Cd^{2+} onto SEP-M(1)NH$_3$(1:2) and SEP-M(2)NaOH)(1:2) and Cr(VI) onto SEP-M(1)NaOH(1:2)^{more} was studied in the temperature range from 25 ^{o}C to 60 ^{o}C (Figs. 52-54).

The adsorption capacity of both SEP-M(1)NH$_3$(1:2) and SEP-M(2)NaOH(1:2) for Cd^{2+} ions (Figs. 52 and 53, respectively) increased with increasing temperature, indicating that the adsorption process is endothermic in nature.
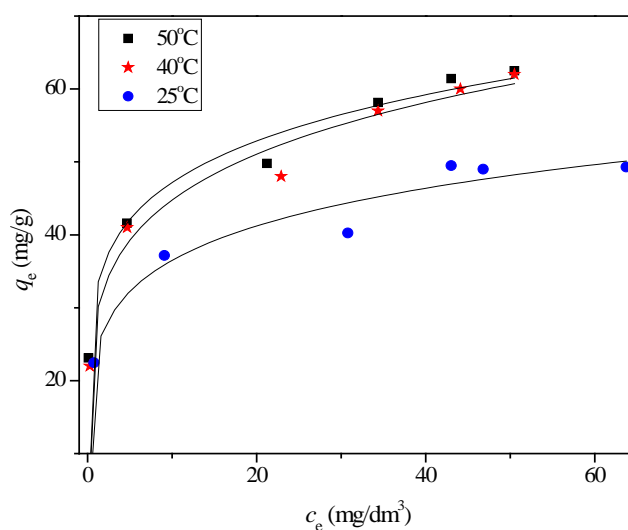
Fig. 52. The effect of temperature on the adsorption of Cd^{2+} onto SEP-M(1)NH$_3$(1:2).
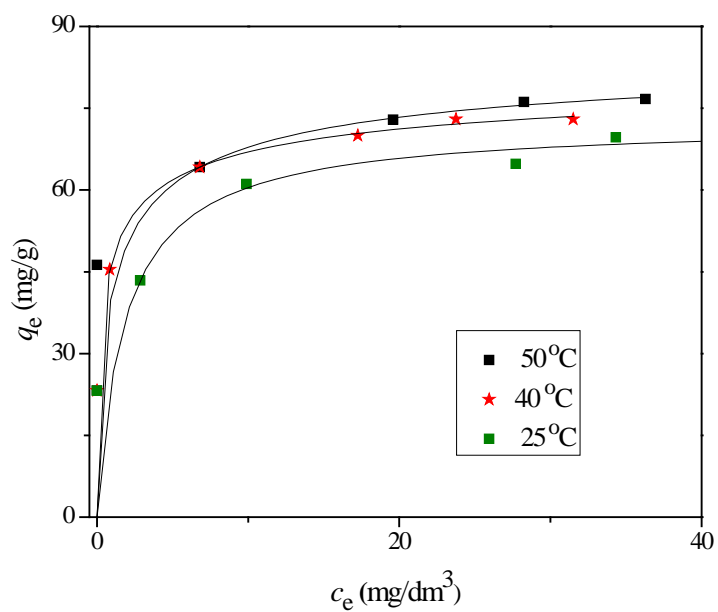
Fig. 53. The effect of temperature on the adsorption of Cd^{2+} onto SEP-M(2)NaOH)(1:2).
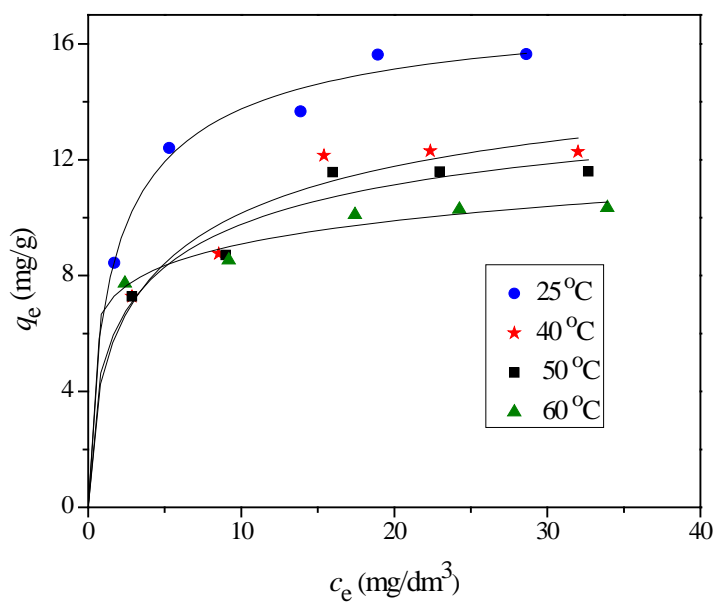
Fig. 54. The effect of temperature on the adsorption of Cr(VI) onto SEP-M(1)NaOH(1:2)[more].

It is well known that Cd^{2+} ions in aqua solutions are well hydrated. In order to form inner-sphere complexes, the ions have to be denuded of their hydration sheath [80]. That process is an endothermic. On the other hand, the adsorption is exothermic process. Obviously, the enthalpy of the dehydration process exceeds the enthalpy of adsorption by a considerable extent, so the overall process is endothermic. With increasing temperature, dehydration process is more efficient and ion adsorption increased.

Temperature had higher influence on Cd^{2+} adsorption of onto SEP-M(1)NH$_3$(1:2) than onto SEP-M(2)NaOH(1:2). It can indicate that enthalpy of adsorption for sample SEP-M(1)NH$_3$(1:2) is lower than for sample SEP-M(2)NaOH(1:2) and the overall enthalpy change of the adsorption process (dehydration + adsorption) is lower for sample SEP-M(2)NaOH(1:2) and the increase of the adsorption capacity with the temperature is lower.

Adsorption capacities at 50 ℃ are just slightly higher than those at 40 ℃. It can be supposed that the efficiency of the dehydration is similar at these temperatures and therefore enthalpy of dehydration is not changed much.

In the case of Cr(VI) ions adsorption onto SEP-M(2)NaOH(1:2)^{more} (Fig. 54), adsorption capacity decreased with increasing temperature, indicating that the adsorption process is exothermic in nature. The decrease in adsorption capacity may be attributed to a relative increase in the escaping tendency of the Cr(VI) ions from the solid phase to the bulk phase with the increase in solution temperature [167]. Bearing in mind the proposed mechanism of Cr(VI) adsorption at $pH_i = 2 \pm 0.1$, *i.e.* formation of outer-sphere complexes, it can be supposed that endothermic dehydration process was not included in the adsorption process. In other words, it is not necessary to remove the hydrated layer to form outer-sphere complexes. Therefore, the overall effect of the adsorption process is exothermal and increasing of the temperature leads to the decrease of the adsorption capacity.

The adsorption results were fitted by the Langmuir, Freundlich and Sips model and the isotherms constants are shown in Table 15. The coefficients of correlation (R^2) suggest that the Sips model is the best model to explain the adsorption behavior of the samples for Cd^{2+} and Cr(VI) on the investigated temperatures, but also both Langmuir and Freundlich models fit the results well.

Table 13. Langmuir, Freundlich and Sips isotherms constants and coefficient of correlation (R^2) for the adsorption of Cd^{2+} onto SEP-M(1)NH$_3$(1:2) and SEP-M(2)NaOH(1:2), and adsorption of Cr(VI) onto SEP-M(1)NaOH(1:2)[more].

Adsorbate	Adsorbent	T	Langmuir model			Freundlih model			Sips model			
		(^{o}C)	q_m (mg/g)	K_L (dm^3/mg)	R^2	k_f (mg$^{(1-1/n)}$dm$^{3/n}$/g)	$1/n$	R^2	q_m (mg/g)	K_a (dm^3/mg)^{ns}	n_s	R^2
Cd^{2+}	SEP-M(1)NH$_3$(1:2)	25	47.00	1.04	0.955	24.08	0.177	0.986	56.12	0.117	0.211	0.986
		40	55.90	1.77	0.934	28.80	0.190	0.991	61.23	0.029	0.198	0.991
		50	55.4	6.37	0.915	32.20	0.164	0.994	62.21	0.016	0.168	0.994
Cd^{2+}	SEP-M(2)NaOH(1:2)	25	72.12	0.53	0.932	39.08	0.160	0.926	75.52	0.542	0.966	0.932
		40	72.70	1.86	0.938	48.00	0.129	0.938	84.60	1.24	0.481	0.941
		50	80.10	0.58	0.797	52.20	0.109	0.797	87.20	0.982	0.593	0.797
Cr(VI)	SEP-M(1)NaOH(1:2)[more]	25	16.31	0.608	0.992	8.209	0.203	0.987	17.79	0.621	0.738	0.994
		40	13.50	0.34	0.975	5.750	0.235	0.976	13.30	0.370	0.581	0.980
		50	12.50	0.42	0.979	5.910	0.208	0.981	12.20	0.444	0.530	0.983
		60	10.40	1.05	0.986	6.840	0.122	0.994	10.80	0.119	0.143	0.994

Thermodynamic parameters of adsorption, enthalpy (ΔH^o) and entropy (ΔS^o), were calculated from the dependence of $\ln k_a$ on $1/T$, where k_a is thermodynamic equilibrium constant. The equilibrium constant was determined as k_d, by extrapolating the dependence of q_e/c_e on c_e to $c_e = 0$, or the Langmuir constant was used as the equilibrium constant (part 5.6.1.). The good correlation ($R^2 = 0.98$) was obtained only for Cd^{2+} adsorption onto SEP-M(1)NH$_3$(1:2), when k_a was determined from the dependence of q_e/c_e on c_e. The dependences of q_e/c_e on c_e for 25, 40 and 50 °C are presented in Fig. 55, while the dependence of $\ln k_d$ on $1/T$, is shown in Fig. 56. ΔG^o was calculated according to the Eq. 21. The obtained value of ΔH^o, ΔS^o and ΔG^o are presented in Table 16.
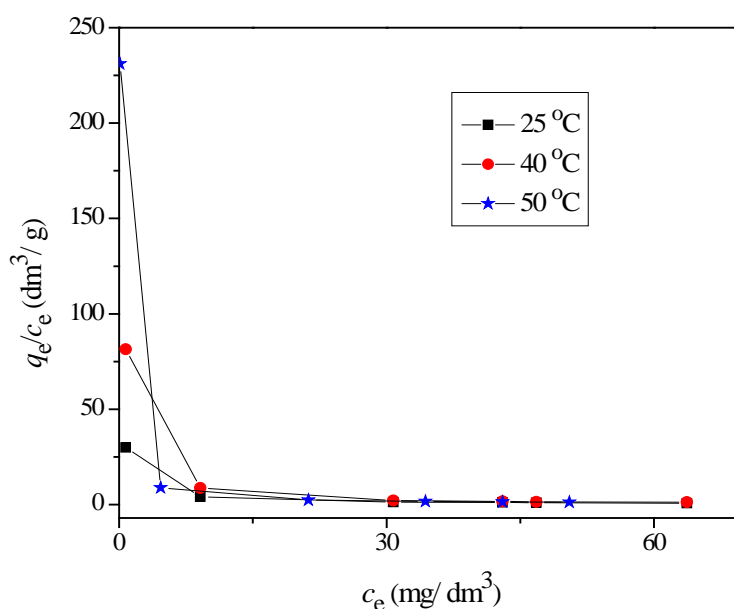
Fig. 55. The dependences of q_e/c_e on c_e for the adsorption of Cd^{2+} onto SEP-M(1)NH$_3$(1:2) at 25, 40 and 50 °C.
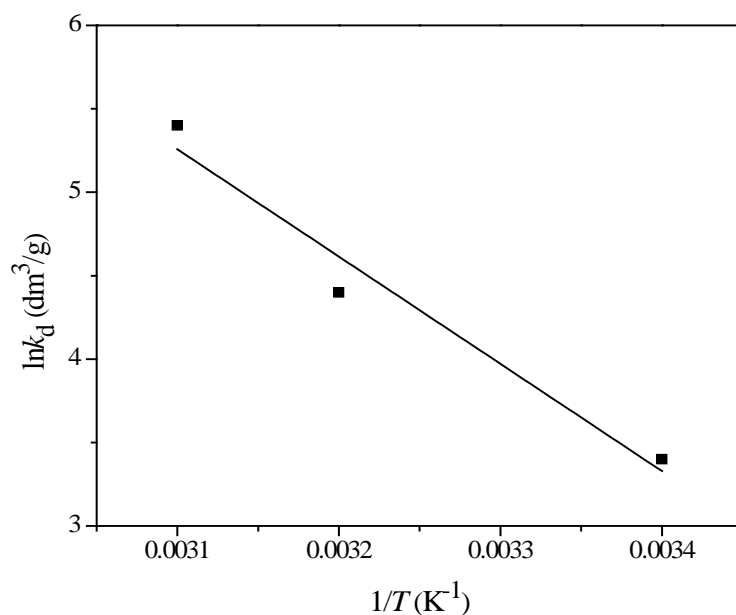
Fig. 56. The dependence of $\ln k_d$ on $1/T$ for the adsorption of Cd^{2+} onto SEP-M(1)NH$_3$(1:2).

Table 16. Thermodynamic parameters for the adsorption of Cd^{2+} onto SEP-M(1)NH$_3$(1:2)

Sample	ΔH^o (kJ/mol)	ΔS^o (kJ/molK)	ΔG^o (kJ/mol) at T (K)		
			298.15	313.15	323.15
SEP-M(1)NH$_3$(1:2)	53.44	0.209	-8.42	-11.45	-14.51

Positive value of ΔH^o indicates that the adsorption process is endothermic, as it was already stated. The negative values of ΔG^o, which increase with the temperatures, show that the process is spontaneous and the spontaneity of the adsorption increases with the temperature.

9. Conclusions

In this dissertation, natural sepiolite (SEP), partially acid-activated sepiolite (ASEP), and natural zeolite (NZ), were used to synthesize the magnetic nano-composites (MNCs) for the removal of Cd^{2+}, Cr(VI), phosphate and dyes (anionic Reactive Orange 16 and cationic Basic Yellow 28) from water. The synthesis conditions were varied in order to obtain magnetic nano-composites with high adsorption capacity and good magnetic properties. The co-precipitation of Fe^{3+} and Fe^{2+} ions by NaOH or NH_3 in the presence of NZ/SEP/ASEP was applied, while the base was added before (procedure 1) or after (procedure 2) adding of Fe^{3+} and Fe^{2+} in the support suspension. In addition, the molar ratio Fe^{2+}/Fe^{3+} and the quantity of iron salts have been varied.

According to the results of the composites characterization and the adsorption experiments, the following conclusions were made:

• Concentration of hydroxyl ions in the suspensions could significantly decrease due to the interactions with the support functional groups, that can cause the precipitation of just $Fe(OH)_3$ instead of the Fe^{3+}/Fe^{2+} co-precipitation and the magnetite formation. Because of the strong interactions of ASEP with hydroxyl ions, it was not possible to synthesize the magnetic composites when NaOH or NH_3 was added to the support suspension before Fe^{3+} and Fe^{2+} adding (procedure 1), but only when NH_3 was added in the suspension of ASEP having Fe^{3+} and Fe^{2+} ions (procedure 2). On the other hand, magnetic composites with SEP and NZ were prepared by both procedures, using both bases.

• Sepiolite/zeolite structures were preserved in the composites, although some alkali leaching occurred when NaOH was used for co-precipitation, that caused lower acidity of the composite's surface, i.e. higher values of point of zero charge (PZC).

• Composites contained individual or aggregated magnetite crystalliites, of about 10 nm size. Dispersibility of the magnetite particles depended on the type of the supported material, the type of base and the sequence of reagents mixing, while the ratio Fe^{2+}/Fe^{3+} did not have a significant influence. The best dispersibility was achieved when NH_3 was added in the SEP or NZ suspension containing Fe^{2+} and Fe^{3+} ions.

• Regardless of higher specific surface area of ASEP in comparison to SEP, magnetite dispersibility in ASEP-based composites was lower than in SEP-based

composite because of stronger bonds between sepiolite fibers. Nevertheless, the specific surface area of ASEP-based MNC was higher than of SEP-based MNC, obtained at the same conditions.

• MNCs obtained by using NH_3 oxidized in two steps during heating, while the oxidation of the composites obtained by using NaOH was one-step process. Lower quantity of magnetite in NH_3-MNCs in comparison to NaOH-MNCs obtained at the same content of Fe^{2+} and Fe^{3+} ions was explained by different quantity of iron(III)-oxide, formed during synthesis.

• Regardless of higher quantity of magnetite, magnetization of NaOH-MNCs was lower than of NH_3-MNCs, which was a result of the higher quantity of amorphous magnetite formed as a layer on the support surface. At room temperature, the samples showed superparamagnetic behavior, which ensures that the composites do not retain magnetization when the magnetic field is removed.

• Adsorption capacities of the composites are much higher for cations than for anions owing to higher affinity of both support and magnetite for cations.

• Adsorption capacities of the MNCs for Cd^{2+} at initial pH = 7 were higher than of pure compounds, as a result of lower aggregation of compounds in the MNCs and, in that way, the higher accessibility of the surface to the ions. Main mechanism of adsorption was the formation of inner-sphere complexes.

• Composites prepared by using NaOH had higher adsorption capacities for Cd^{2+} than composites NH_3-MNCs, while all MNCs had higher capacity than the composites SEP/NZ- iron(III) oxide. The adsorption capacity of the MNCs decreased during storage as a consequence of oxidation.

• Adsorption capacity of magnetite for cationic dye Basic Yellow 28 is low, but the presence of magnetite caused just small decrease of the adsorption capacity of sepiolite, which indicates that the composites can be used for efficient removal of Basic Yellow 28 from water and can be easily separated from water by magnetic separation.

• Adsorption capacity of composites for anions decreases with pH increase; at $pH_i = 2$, chromates adsorb dominantly by formation of outer-sphere complexes with protonated surface. The highest removal efficiency was achieved with the composite having the highest content of magnetite. Content of magnetite is the factor that determines the adsorption capacity because the capacity of the support is negligible.

• Adsorption of all asorbates onto the composites was best fitted with the Sips model, which suggests adsorption on a heterogeneous surface at energetically non-uniform sites until a monolayer was formed.

• Rate of Cd^{2+} adsorption is higher than the rate of chromate adsorption. Pseudo-second order model fitted the adsorption kinetics for both Cd^{2+} and chromates much better than the pseudo-first order model.

• Adsorption capacity of the SEP-based composites for Cd^{2+} ions increased with increasing temperature, indicating endothermic nature of the adsorption, while the adsorption of chromates was exothermic.

In summary, the results of this doctoral dissertation enable the optimization of the synthesis of magnetic composite adsorbents with a high adsorption capacity and high magnetization, providing an efficient treatment of water by the adsorbent and its subsequent removal by magnetic separation.

10. References

[1] W. Wang, Q. Feng, K. Liu, G. Zhang, J. Liu, Y. Huang, A novel magnetic 4A zeolite adsorbent synthesised from kaolinite type pyrite cinder (KTPC), Solid State Sci. 39 (2015) 52-58.

[2] P. Yuan, D. Liu, M. Fan, D. Yang, R. Zhu, F. Ge, J. Zhu, H. He, Removal of hexavalent chromium [Cr(VI)] from aqueous solutions by the diatomite supported/unsupported magnetite nanoparticles, J. Hazard. Mater. 173 (2010) 614-621.

[3] M. Kumari, C.U. Pittman Jr, D. Mohan, Heavy metals [chromium (VI) and lead (II)] removal from water using mesoporous magnetite (Fe_3O_4) nanospheres, J. Colloid Interf. Sci. 442 (2015) 120-132.

[4] S.R. Chowdhury, E.K. Yanful, Kinetics of cadmium(II) uptake by mixed maghemite magnetite nanoparticles, J. Environ. Manage. 129 (2013) 642-651.

[5] X. Yu, X. Tian, S. Wang, Adsorption of Ni, Pd, Pt, Cu, Ag and Au on the Fe_3O_4 (111) surface, Surf. Sci. 628 (2014) 141-147.

[6] K. Song, W. Kim, C-Y. Suh, D. Shin, K-S. Ko, K. Ha, Magnetic iron oxide nanoparticles prepared by electrical wire explosion for arsenic removal, Powder Technol. 246 (2013) 572-574.

[7] P. Yuan, M. Fan, D. Yang, H. He, D. Liu, A. Yuan, J. Zhu, T. Chen, Montmorillonite-supported magnetite nanoparticles for the removal of hexavalent chromium [Cr(VI)] from aqueous solutions, J. Hazard. Mater. 166 (2009) 821-829.

[8] I.W. Nah, K.-Y. Hwang, Y-G. Shul, A simple synthesis of magnetically modified zeolite, Powder Technol. 177 (2007) 99-101.

[9] L.C. Oliveira, D.I. Petkowicz, A. Smaniotto, S.B. Pergher, Magnetic zeolites: a new adsorbent for removal of metallic contaminants from water, Water Res. 38 (2004) 3699-3704.

[10] H. Liu, W. Chen, C. Liu, Y. Liu, C. Dong, Magnetic mesoporous clay adsorbent: Preparation, characterization and adsorption capacity for atrazine, Micropor. Mesopor. Mat. 194 (2014) 72-78.

[11] N. Tian, X. Tian, L. Ma, C. Yang, Y. Wang, Z. Wang, L. Zhang, Well-dispersed magnetic iron oxide nanocrystals on sepiolite nanofibers for arsenic removal, RSC Adv. 5 (2015) 25236-25243.

[12] A. Middea, L.S. Spinelli, F.G. Souza Junior, R. Neumann, O.F.M. Gomes, T.L.A.P. Fernandes, L.C. de Lima,V.M.T.S. Barthem, F/V. Carvalho, Synthesis and characterization of magnetic palygorskite nanoparticles and their application on methylene blue remotion from water, Appl. Surf. Sci. 346 (2015) 232-239.

[13] L. Lian, X. Cao, Y. Wu, D. Sun, D. Lou, A green synthesis of magnetic bentonite material and its application for removal of microcystin-LR in water, Appl. Surf. Sci. 289 (2014) 245-251.

[14] D. Wan, W. Li, G. Wang, K. Chen, L. Lu, Q. Hu, Adsorption and heterogeneous degradation of rhodamine B on the surface of magnetic bentonite material, Appl. Surf. Sci. 349 (2015) 988-996.

[15] J.H. Kwon, L.D. Wilson, R. Sammynaiken, Synthesis and characterization of magnetite and activated carbon binary composites, Synthetic Met. 197 (2014) 8-17.

[16] G.Z. Kyzas, E.A. Deliyanni, N.K. Lazaridis, Magnetic modification of microporous carbon for dye adsorption, J. Colloid Interf. Sci. 430 (2014) 166-173.

[17] C. Cao, L. Xiao, C. Chen, X. Shi, Q. Cao, L. Gao, In situ preparation of magnetic Fe_3O_4/chitosan nanoparticles via a novel reduction–precipitation method and their application in adsorption of reactive azo dye, Powder Technol. 260 (2014) 90-97.

[18] R. Rakhshaee, Decreasing FeO and Fe_3O_4 nano particle size by simultaneous synthesis on a bio-polymeric structure: kinetic study to remove Amaranth from aqueous solution, Powder Technol. 254 (2014) 494-499.

[19] M. Mihajlović, S. Lazarević, I. Janković-Častvan, B. Jokić, Đ. Janaćković, R. Petrović, A comparative study of the removal of lead, cadmium and zinc inons from aqueous solutions by natural and Fe(III)-modified zeolite, Chem. Ind. Chem. Eng. Q. 20 (2014) 283-293.

[20] S. Lazarević, I. Janković-Častvan, D. Jovanović, S. Milonjić, Đ. Janaćković, R. Petrović, Adsorption of Pb^{2+}, Cd^{2+} and Sr^{2+} ions onto natural and acid-activated sepiolites, Appl. Clay Sci. 37 (2007)47-57.

[21] M.C. Mascolo, Y. Pei, T.A. Ring, Room temperature co-precipitation synthesis of magnetite nanoparticles in a large pH window with different bases, Materials, 6 (2013) 5549-5567.

[22] H-C. Roth, S.P. Schwaminger, M. Schindler, F.E. Wagner, S. Berensmeier, Influencing factors in the co-precipitation process of superparamagnetic iron oxide nanoparticles: A model based study, J. Magn. Magn. Mater. 377 (2015) 81-89.

[23] G. Gnanaprakash, S. Mahadevan, T. Jayakumar, P. Kalyanasundaram, J. Philip, B. Raj, Effect of initial pH and temperature of iron salt solutions on formation of magnetite nanoparticles, Mater. Chem. Phys. 103 (2007) 168-175.

[24] G. Nabiyouni, M. Julaee, D. Ghanbari , P. C. Aliabadi, N. Safaie, Room temperature synthesis and magnetic property studies of Fe_3O_4 nanoparticles prepared by a simple precipitation method, J. Ind. Eng. Chem. 21 (2015) 599-603.

[25] S. Upadhyay, K. Parekh, B. Pandey, Influence of crystallite size on the magnetic properties of Fe_3O_4 nanoparticles, J. Alloys Compd. 678 (2016) 478-485.

[26] S. Yu, L. Zhai, S. Zhong, Y. Qiu, L. Cheng, X. Ren, Synthesis and structural characterization of magnetite/sepiolite composite and its sorptive properties for Co(II) and Cd(II), J. Taiwan Inst. Chem. E. 59 (2016) 221-228.

[27] https://www.tititudorancea.net/z/sepiolite.htm.

[28] https://www.ima-europe.eu/sites/ima-europe.eu/files/minerals/Sepiolite_An-WEB2011.pdf.

[29] https://www.sems.qmul.ac.uk/research/honours/doc.php?id=324.

[30] P. Suchorska-Woźniak, O. Rac, M. Fiedot, H. Teterycz, The impact of sepiolite on sensor parameters during the detection of low concentrations of alcohols, Sensors 16 (2016) 1881-1896.

[31] C. Serna, J. L. Ahlrichs, J. M. Serratosa, Folding in sepiolite crystas, Clays Clay Miner. 23 (1975) 452-457.

[32] G. E. Vanscoyoc, C. J. Serna, J. L. Alhrichs, Structural changes in palygorskite during dehydration and dehydroxylation, Am. Mineral. 64 (1979) 215-223.

[33] M.R. Weir, E. Rutinduka, C. Detellier, C.Y. Feng, Q. Wang, T. Matsuur, R. Le Van Mao, Fabrication, characterization and preliminary testing of all-inorganic ultrafiltration membranes composed entirely of a naturally occurring sepiolite clay mineral, J. Membr. Sci. 182 (2001) 41-50.

[34] M. Suárez, E. García-Romero, Variability of the surface properties of sepiolite, Appl. Clay Sci. 67-68 (2012) 72-82.

[35] E. Galan, Properties and applications of palygorskite-sepiolite clays, Clay Miner. 31 (1996) 443-453.

[36] S. Hojati, H. Khademi, Thermal behavior of a natural sepiolite from Northeastern Iran, J. Sci. (Islamic Republic of Iran), 24 (2013)129-134.

[37] https://www.sems.qmul.ac.uk/research/honours/doc.php?id=324.

[38] http://www.britannica.com/science/zeolite.

[39] http://www.nzpam.govt.nz/cms/documents/business/minerals-commodity-reports/zeolite.pdf.

[40] E. Passaglia, R. Sheppard, Crystal structures of natural zeolites, In D.L. Bish & D.W. Ming, (eds). Natural zeolites: occurrence, properties, applications. Rev. Mineral. Geochem. 45 (2001) 69-116.

[41] www.fischer-tropsch.org/DOE/DOE_reports/84016246/de84016246_sec04.pdf

[42] S. Wang, Y. Peng, Natural zeolites as effective adsorbents in water and wastewater treatment, Chem. Eng. J. 156 (2010) 11-24.

[43] R. Xu, J. Chen, W. Pang, Q. Huo, J. Yu, Chemistry of zeolites and related porous materials: synthesis and structure, John Wiley & Sons (Asia) Pte Ltd, Singapore, 2007.

[44] L. Liu, Inorganic and metal-organic framework materials - synthesis and structure characterization, PhD thesis, Stockholm University, Stockholm, 2014.

[45] Handbook of zeolite science and technology, Ed. By S. M. Auerbach, K. A. Carrad, P. K. Dutta, Marcel Dekker, Inc., New-York, Basel, 2003.

[46] http://www.intechopen.com/books/water-treatment/natural-zeolites-in-water-treatment-how-effective-is-their-use.

[47] P. Kowalczyk, M. Sprynskyy, A. P. Terzyk, M. Lebedynets, J. Namiesnik, B. Buszewski, Porous structure of natural and modified clinoptilolites, J. Colloid Interface Sci. 297 (2006) 77-85.

[48] M. Ackley, R.T. Yang, Diffusion in ion-exchanged clinoptilolites, AIChE J. 37 (1991) 1645-1656.

[49] http://www.iza-online.org/natural/Datasheets/Clinoptilolite/clinoptilolite.htm

[50] http://nevada-outback-gems.com/mineral_information/Zeolites_mineral_info.htm.

[51] http://cleanageminerals.com/zeolite.

[52] https://bib.irb.hr/datoteka/433256.2CSSZ-MTrgo_corrected.pdf

[53] J. Perez-Ramırez, G. Mul, F. Kapteijn, J. Moulijn, A. Overweg, A. Domenech, A. Ribera, I. Arends, Physicochemical characterization of isomorphously substituted FeZSM-5 during activation, J. Catal. 207 (2002) 113-126.

[54] http://cool.conservation-us.org/byorg/abbey/an/an20/an20-7/an20702.html.

[55] F. Mumpton, Uses of natural zeolites agriculture and musty, Proceedings of the National Academy of Sciences of the United States, 96 (1999) 3463-3470.

[56] M.E.Davis, Zeolites from a materials chemistry perspective, Chem. Mater. 26 (2014) 239−245

[57] L. G. Hernandez, L. I. Rueda, A. R. Diaz, C. C. Anton, Preparation of amorphous silica by acid dissolution of sepiolite: kinetic and textural study, J. Colloid Interf. Sci. 109 (1986) 150-160.

[58] A. Kilislioglu, G. Aras, Adsorption of uranium from aqueous solution on heat and acid treated sepiolites, Appl. Radiat. Isot. 68 (2010) 2016-2019.

[59] M. Myriam, M. Suarez, J. M. Martin-Pozas, Stractural and textural modification of palygorskite and sepiolite under acid treatment, Clays Clay Miner. 46 (1998) 225-231.

[60] A. Miura, K. Nakazawa, T. Takei, N. Kumada, N. Kinomura, R. Ohki, H. Koshiyama, Acid-, base-, and heat-induced degradation behavior of Chinese sepiolite, Ceram. Int. 38 (2012) 4677-4684.

[61] Z. Yan , D. Ma, J. Zhuang, X. Liu, X. Liu , X. Han, X. Bao, F. Chang, L. Xu, Z. Liu, On the acid-dealumination of USY zeolite: a solid state NMR investigation, J. Mol. Catal. A: Chem. 194 (2003) 153-167.

[62] B. E. Alver, M. Sakizci, Influence of acid treatment on structure of clinoptilolite tuff and its adsorption of methane, Adsorption, 21 (2015) 391-399.

[63] Y. Qiu, S. Yu, L. Cheng, F. Lu, Sorption of radiocobalt on acid-activated sepiolite: effects of pH, ionic strength, foreign ions, humic acid and temperature, J. Radioanal. Nucl. Chem. 295 (2013) 1673-168.

[64] A. Kuleyin, Removal of phenol and 4-chlorophenol by surfactant-modified natural zeolite, J. Hazard. Mater. 144 (2007) 307-315.

[65] M. Doula, A. Dimirkou, Use of an iron-overexchanged clinoptilolite for the removal of Cu^{2+} ions from heavily contaminated drinking water samples, J. Hazard. Mater. 151(2008) 738-745.

[66] S. Lazarević, I. Janković-Častvan, V. Djokić, Ž. Radovanović, Dj. Janaćković, R. Petrović, Iron-modified sepiolite for Ni^{2+} sorption from aqueous solution: an equilibrium, kinetic, and thermodynamic study, J. Chem. Eng. Data. 55 (2010) 5681-5689.

[67] http://www.helcom.fi/stc/files/environment/haz_subs/cadmium.pdf.

[68] E. Eren, B. Eren, Removal of copper ions by modified sepiolite samples, Desalin. Water Treat. 20 (2010) 114-122.

[69] A. Aznar, E. Gutiérrez, P. Díaz, A. Alvarez, G. Poncelet, Silica from sepiolite: Preparation, textural properties, and use as support to catalysts. Microporous Mater. 6 (1996) 105-114.

[70] M. Radojević, V. Jović, D. Karaulić, D. Vitorović, Study of sepiolite from Goleš (Kosovo, Yugoslavia). II. Acid activation. J. Serb. Chem. Soc. 67 (2002) 499-506.

[71] F. Franco, M. Pozo, JA. Cecilia, M. Benítez-Guerrero, E. Pozo, JA. Martín Rubí, Microwave assisted acid treatment of sepiolite: the role of composition and crystallinity. Appl. Clay Sci. 102 (2014)15-27.

[72] http://dx.doi.org/10.1155/2013/789410.

[73] S. Abello, A. Bonilla, J. Perez-Ramırez, Mesoporous ZSM-5 zeolite catalysts prepared by desilication with organic hydroxides and comparison with NaOH leaching, Appl. Catal. A. 364 (2009) 191-198.

[74] B. Chamnankid, C. Ratanatawanate, K. Faungnawakij, Conversion of xylose to levulinic acid over modified acid functions of alkaline-treated zeolite Y in hot-compressed water, Chem. Eng. J. 258 (2014) 341-347.

[75] J. Perez-Ramırez, G. Mul, F. Kapteijn, J.A. Moulijn, A. R. Overweg, A. Domenech, A. Ribera, I. W. Arends, Physicochemical characterization of isomorphously substituted FeZSM-5 during activation, J. Catal. 207 (2002) 113-126.

[76] A. Mockovčiaková, Z. Orolínová, M. Matik, P. Hudec, E. Kmecová, Iron Oxide contribution to the modification of natural zeolite, Acta Montan. Slovaca 11 (2006) 353-357.

[77] E. Eren, H. Gumus, Characterization of the structural properties and Pb(II) adsorption behavior of iron oxide coated sepiolite, Desalination. 273 (2011) 276-284.

[78] S. Lazarević, I. Janković-Častvan, B. Potkonjak, Dj. Janaćković, R. Petrović, Removal of Co^{2+} ions from aqueous solutions using iron-functionalized sepiolite, Chem. Eng. Process. 55 (2012) 40-47.

[79] M. Kragović, A. Daković, Z. Sekulić, M. Trgo, M. Ugrina, J. Perić, G. D. Gatta, Removal of lead from aqueous solutions by using the natural and Fe(III)-modified zeolite, Appl. Surf. Sci. 258 (2012) 3667-3673.

[80] M. T. Mihajlović, S. S. Lazarević, I. M. Janković-Častvan, J. Kovač, B. M. Jokić, Dj. T. Janaćković, R. D. Petrović, Kinetics, thermodynamics, and structural investigations on the removal of Pb^{2+}, Cd^{2+}, and Zn^{2+} from multicomponent solutions onto natural and Fe(III)-modified zeolites, Clean Technol. Envir. 17 (2015) 407-419.

[81] S. Hasany, I. Ahmed, J. Rajan, A. Rehman, Systematic review of the preparation techniques of iron oxide magnetic nanoparticles, Nanosci. Nanotechnol. 6 (2012) 148-158.

[82] http://geology.com/minerals/magnetite.shtml

[83] A. P. C. Teixeira, J. C. Tristão, M. H. Araujo, L. C. A. Oliveira, F. C. C. Moura, J. D. Ardisson, C. C. Amorimd, R. M. Lago, Iron: a versatile element to produce materials for environmental applications, J. Braz. Chem. Soc. 23 (2012) 1579-1593.

[84] https://en.wikipedia.org/wiki/Curie_temperature

[85] http://subato.blogspot.rs/2011/02/superparamagnetic-size-effect-of.html)

[86] https://en.wikipedia.org/wiki/ Superparamagnetism

[87] http://nuweb.neu.edu/dheiman/U600/NMAG.pdf

[88] http://www.science20.com/mei/blog/blocking_temperature

[89] M. Aydın, B. Ünal, B. Esat, A. Baykal, E. Karaoğlu, M.S. Toprak, H. Sözeri, Synthesis, magnetic and electrical characteristics of poly(2-thiophen-3-yl-malonic acid)/Fe_3O_4 nanocomposite, J. Alloy Compd. 514 (2012) 45-53.

[90]http://ferrocell.us/references/Magnetite%20(Fe3O4)_%20Properties%20Synthesis%20and%20Applications.pdf.

[91] M. Kosmulski, Compilation of PZC and IEP of sparingly soluble metal oxides and hydroxides from literature, Adv. Colloid Interfac. 152 (2009) 14-25.

[92] T. Daou, G. Pourroy, S. Bgin-Colin, J. Grenche, C. Ulhaq-Bouillet, P. Legar, P. Bernhardt, C. Leuvrey, G. Rogez, Hydrothermal synthesis of monodisperse magnetite nanoparticles, Chem. Mater. 18 (2006) 4399-4404.

[93] A. P. C. Teixeira, J. C. Tristão, M. H. Araujo, L. C. A. Oliveira, F. C. C. Moura, J. D. Ardisson, C. C. Amorimd, R. M. Lago, Iron: a Versatile Element to Produce Materials for Environmental Applications, J. Braz. Chem. Soc. 23 (2012) 1579-1593.

[94] N. Salem, A. Awwad, A novel approach for synthesis magnetite nanoparticles at ambient temperature, Nanosci. Nanotechnol. 3 (2013) 35-39.

[95] S. Alibeigi, M. Vaezi, Phase transformation of iron oxide nanoparticles by varying the molar ratio of $Fe^{2+}:Fe^{3+}$, Chem. Eng. Technol. 3 (2008) 1591-1596.

[96] R. Valenzuela, M. C. Fuentes, C. Parra, J. Baeza, N. Duran, S.K. Sharma, M. Knobel, J. Freer, Influence of stirring velocity on the synthesis of magnetite nanoparticles (Fe_3O_4) by the co-precipitation method, J. Alloys Compd. 488 (2009) 227-231.

[97] http://cdn.intechopen.com/pdfs-wm/41411.pdf.

[98] A. B. Cobb, The elements cadmium, Marshall Cavendish Benchmark, New York, 2008.

[99] P. A. Balch, Prescription for nutritional healing, 4th ed. Penguin Group, 2006.

[100] http://www.envirn.umaryland.edu/files/cadmium.pdf.

[101] J. Febrianto, A. A. Kosasih, J. Sunarso, Y-H Ju, N. Indraswati, S. Ismadji, Equilibrium and kinetic studies in adsorption of heavy metals using biosorbent: A summary of recent studies, J. Hazard. Mater. 162 (2009) 616-645.

[102] D. Mohan, C. Pittman Jr, Activated carbons and low cost adsorbents for remediation of tri- and hexavalent chromium from water, J. Hazard. Mater. 137 (2006) 762-811.

[103] https://www.createspace.com/4489109.

[104] https://www.osha.gov/OshDoc/data_General.../hexavalent_chromium.pdf.

[105] http://www.hse.gov.uk/pubns/indg346.pdf.

[106] http://www.water-research.net/index.php/phosphate-in-water.

[107] S. Yeoman, T. Stephenson, J. N. Lester, R. Perry, The removal of phosphorus during wastewater treatment: a review, Environ. Pollut. 49 (1988) 183-233.

[108] D. Cho, B. Jeon, C. Chon, F. W. Schwartz, Y. Jeong, H. Song, Magnetic chitosan composite for adsorption of cationic and anionic dyes in aqueous solution, J. Ind. Eng. Chem. 28 (2015) 60-66.

[109] R. Sivashankar, A.B. Sathya, K. Vasantharaj, V. Sivasubramanian, Magnetic composite an environmental super adsorbent for dye sequestration - A review, Environmental Nanotechnology, Monitoring & Management 2 (2014) 36-49.

[110] M. Yusuf, M. Ali Khan, M. Otero, E.C. Abdullah, M. Hosomi, A. Terada, S. Riya, Synthesis of CTAB intercalated graphene and its application for the adsorption of AR265 and AO7 dyes from water, J. Colloid Interface Sci. 493 (2017) 51-61.

[111] L. Martins, J. Rodrigues, O. Adarme, T. Melo, L. Gurgel, L. Gil, Optimization of cellulose and sugarcane bagasse oxidation: Application for adsorptive removal of crystal violet and auramine-O from aqueous solution, J. Colloid Interface Sci. 494 (2017) 223-241.

[112] A. Ahribesh, S. Lazarević, B. Potkonjak, A. Bjelajac, D. Janaćković, R. Petrović, Sorption of cadmium ions from saline waters onto Fe(III)-zeolite, Hem. Ind. 69 (2015) 253-260.

[113] https//www.library.iyte.edu.tr/tezler/master/kimya/T000622.pdf

[114] A.A.Ahribesh, The sorption of cadmium ions from sea water and differ aquatic solutions on modified zeolite, Master thesis, Faculty of technology and Metallurgy, University of Belgrade, Belgrade, 2012.

[115] Y-F. Zhou, R. J. Haynes, Sorption of Heavy Metals by Inorganic and organic components of solid wastes: significance to use of wastes as low-cost adsorbents and immobilizing agents, Environ. Sci. Technol. 40 (2010) 909-977.

[116] S. Malamisa, E. Katsou, A review on zinc and nickel adsorption on natural and modified zeolite, bentonite and vermiculite: Examination of process parameters, kinetics and isotherms, J. Hazard. Mater. 252-253 (2013) 428-461.

[117] J. Coca-Prados, G. Gutierrez-CerVelló, Water purification and management, Springer, 2009.

[118] M. H. El-Naas, M. A. Alhaija, Modeling of adsorption processes, In: Mathematical Modelling, Ed. Christopher R. Brennan, Nova Publishers, Inc. 2011.

[119] I. Langmuir, The adsorption of gases on plane surface of glass, mica and platinum, J. Am. Chem. Soc. 40 (1918) 1361-1403.

[120] H. Freundlich, Concerning adsorption in solutions, Zeitschrift für Physikalische Chemie. 57 (1906) 385-470.

[121] P. Figueira, C. Lopes, A. Daniel-da-Silva, E. Pereira, A. Duarte, T. Trindade, Removal of mercury (II) by dithiocarbamate surface functionalized magnetite particles: Application to synthetic and natural spiked waters, Water Res. 45 (2011) 5773-5784.

[122] K.Y. Foo, B.H. Hameed, Review, insights into the modeling of adsorption isotherm systems, Chem. Eng. J. 156 (2010) 2-10.

[123] S. L. Gayatri, M. Ahmaruzzaman, Adsorption technique for the removal of phenolic compounds from wastewater using low-cost natural adsorbents, Phys. Sci. Tech. 5 (2010) 156-166.

[124] H. Qiu, L. LV, B. Pan B, Q. Zhang, W. Zhang, Q. Zhang, Critical review in adsorption kinetic models, J. Zhejiang Univ. Sci. A. 10 (2009) 716-724.

[125] S. Lagergren, Zur tfeoric der sogenannten adsorption gelöster stoff, Kungliga Svenska Vetenskapsa Kademiens Handlinga, 24 (1898) 1-39.

[126] Y. S. Ho, G. McKay, Pseudo-second order model for sorption processes, Process Biochem. 34 (1999) 451-465.

[127] R. Hudson, Hazardous materials in the soild and atmosphere, Nova science publishers, INC, 2006.

[128] W. J. Weber, J. C. Morris, Kinetics of adsorption on carbon from solution, J. Sanit. Eng. Div. Am. Soc. Civil Eng. 89 (1963) 31-60.

[129] S. Malamis, E. Katsou, A review on zinc and nickel adsorption on natural and modified zeolite, bentonite and vermiculite: Examination of process parameters, kinetics and isotherms, J. Hazard. Mater. 252– 253 (2013) 428-461.

[130] J. Toth, Adsorption theory, modeling and analysis, Marcel Dekker, Hungary 2002.

[131] Y. Liu, Is the free energy change of adsorption correctly calculated? J. Chem. Eng. Data. 54 (2009) 1981-1985.

[132] A. A. Khan, R.P. Singh, Adsorption thermodynamics of carbofuran on Sn (IV) arsenosilicate in H^+, Na^+ and Ca^{2+} forms, Colloid Surface, 24 (1987) 33-42.

[133] S. Rajput, C. U. Pittman Jr, D. Mohan, Magnetic magnetite (Fe_3O_4) nanoparticle synthesis and applications for lead (Pb^{2+}) and chromium (Cr^{6+}) removal from water, J. Colloid Interf. Sci. 468 (2016) 334-346.

[134] T. Wang, X. Jin, Z. Chen, M. Megharaj, R. Naidu, Simultaneous removal of Pb(II) and Cr(III) by magnetite nanoparticles using various synthesis conditions, J. Ind. Eng. Chem. 20 (2014) 3543-3549.

[135] S -Y. Yoon, C -G. Lee, J -A. Park, J -H. Kim, S -B. Kim, S -H. Lee, J -W. Choi, Kinetic, equilibrium and thermodynamic studies for phosphate adsorption to magnetic iron oxide nanoparticles, Chem. Eng. J. 236 (2014) 341-347.

[136] G. Nourmohamadi, A. Fazlavi, B. Amiri, C. Khadijeh, Investigation on adsorption of Cu^{+2} onto synthesized magnetite bentonite aano - absorbent by CCD design of experiments, Bulletin of the Georgian national academy of sciences, 8 (2014) 496-503.

[137] T. M. Attia, X. L. Hu, Y. D. Qiang, Synthesized magnetic nanoparticles coated zeolite for the adsorption of pharmaceutical compounds from aqueous solution using batch and column studies, Chemosphere, 93 (2013) 2076-2085.

[138] H. Faghihian, M. Moayed, A. Firooz, M. Iravani, Synthesis of a novel magnetic zeolite nanocomposite for removal of Cs^+ and Sr^{2+} from aqueous solution: Kinetic, equilibrium, and thermodynamic studies, J. Colloid. Interf. Sci. 393 (2013) 445-451.

[139] H. Liu, S. Peng, L. Shu, T. Chen, T. Bao, R. L.Frost, Magnetic zeolite NaA: Synthesis,characterization based on metakaolin and its application for the removal of Cu^{2+}, Pb^{2+}, Chemosphere, 91 (2013) 1539-1546.

[140] M. Fayazi, D. Afzali, M.A. Taher, A. Mostafavi, V.K. Gupta, Removal of Safranin dye from aqueous solution using magnetic mesoporous clay: Optimization study, J. Mol. Liq. 212 (2015) 675-685.

[141] S-H.Yu, H. Li, Q-Z. Yao, S-Q. Fu, G-T. Zhou, Microwave-assisted preparation of sepiolite-supported magnetite nanoparticles and their ability to remove low concentrations of Cr(VI), RSC Adv. 5 (2015) 84471-84482.

[142] H.P. Klug, L.E. Alexander, X-ray diffraction procedures, 2nd edition, Wiley & Sons, New York (1974), page 687.

[143] F. Rouquerol, J. Rouquerol, K. Sing, Adsorption by powders and porous solids, Academic Press, London, 1975.

[144] E.P. Barrett, L.G. Joyner, P.P. Halenda, The determination of pore volume and area distributions in porous substances. I. Computations from nitrogen isotherms, J. Am. Chem. Soc. 73 (1951) 373-380.

[145] B.C. Lippens, J.H. de Boer, Studies on pore systems in catalysts V. The t method, J. Catal. 4 (1965) 319-323.

[146] K. Petcharoen, A. Sirivat, Synthesis and characterization of magnetite nanoparticles via the chemical co-precipitation method, Mater. Sci. Eng. B-Adv. 177 (2012) 421-427.

[147] M. Gotić, S. Musić, Mössbauer, FT-IR and FE SEM investigation of iron oxides precipitated from FeSO4 solutions, J. Mol. Struct. 834-836 (2007) 445-453.

[148] A. Ercuta, M. Chirita, Highly crystalline porous magnetite and vacancy-ordered maghemite microcrystals of rhombohedral habit, J. Cryst. Growth, 380 (2013) 182-186.

[149] B. Stuart, Infrared Spectroscopy: Fundamentals and Applications, John Wiley& Sons Ltd. Chichester, England, 2004.

[150] M. Doula, M. Synthesis of a clinoptilolite-Fe system with high Cu sorption capacity, Chemosphere, 67 (2007) 731-740.

[151] W. Cheng, K. Tang, Y. Qi, J. Sheng, Z. Liu, One-step synthesis of superparamagnetic monodisperse porous Fe_3O_4 hollow and core-shell spheres, J. Mater. Chem. 20 (2010) 1799-1805.

[152] S. K. Behera, Facile synthesis and electrochemical properties of Fe_3O_4 nanoparticles for Li ion battery anode, J. Power Sources, 196 (2011) 8669- 8674.

[153] M. Foldvari, Handbook of thermogravimetric system of minerals and its use in geological practice, Geological Institute of Hungary, Budapest, 2011.

[154] V. Kusigerski, M. Tadić, V. Spasojević, B. Antić, D. Marković, S. Bošković, B. Matović, High coercivity of γ-Fe_2O_3 nanoparticles obtained by a mechanochemically activated solid-state displacement reaction, Scripta Mater. 56 (2007) 883-886.

[155] A. H. Morrish, The physical principles of magnetism, Wiley, New York, 1965.

[156] C. Cannas, G. Concas, D. Gatteschi, A. Falqui, A. Musinu, G. Piccaluga, C. Sangregorio, G. Spano, Superparamagnetic behaviour of γ-Fe_2O_3 nanoparticles dispersed in a silica matrix, Phys. Chem. Chem. Phys.3 (2001) 832-838.

[157] G.F. Goya, T.S. Berquo, F.C. Fonseca, M.P. Morales, Static and dynamic magnetic properties of spherical magnetite nanoparticles, J. Appl. Phys. 94 (2003) 3520-3528.

[158] R. C. Woodward, J. Heeris, T. G. St. Pierre, M. Saunders, E. P. Gilbert,M. Rutnakornpituk, Q. Zhangand, J. S. Riffle, A comparison of methods for the

measurement of the particle-size distribution of magnetic nanoparticles, J. Appl. Cryst. 40 (2007) 495-500

[159] J. Shen, A.D. Ebner, J.A. Ritter, Points of zero charge and intrinsic equilibrium constants of silica–magnetite composite oxides, J. Colloid Interf. Sci. 214 (1999) 333-343.

[160] A.A. Ahribesh, S. Lazarević, I. Janković-Častvan, B. Jokić, V. Spasojević, T. Radetić, Dj. Janaćković, R. Petrović, Influence of the synthesis parameters on the properties of the sepiolite-based magnetic adsorbents, Powder Technol. 305 (2017) 260–269.

[161] M. Ahmed, S. Ali, S. El-Dek, A. Galal, Magnetite–hematite nanoparticles prepared by green methods for heavy metal ions removal from water, Mater. Sci. Eng. B. 178 (2013) 744- 751.

[162] A.J. Habish, S. Lazarević, I. Janković-Častvan, B. Potkonjak, Đ. Janaćković, R. Petrović, The effect of salinity on the sorption of cadmium ions from aqueous medium on Fe(III)-sepiolite, Chem. Ind. Chem. Eng. Q. 21 (2015) 295-303.

[163] G. P. Jeppu, T. P. Clementa, A modified Langmuir-Freundlich isotherm model for simulating pH-dependent adsorption effects, J. Contam. Hydrol. 129–130 (2012) 46-53.

[164] O. Hamdaoui, E. Naffrechoux, Modeling of adsorption isotherms of phenol and chlorophenols onto granular activated carbon Part II. Models with more than two parameters, J. Hazard. Mater. 147 (2007) 401-411.

[165] V. Marjanović, S. Lazarević, I. Janković-Častvan, B. Potkonjak, Đ. Janaćković, R. Petrović, Chromium(VI) removal from aqueous solutions using mercaptosilane functionalized sepiolites, Chem. Eng. J. 166 (2011) 198-206.

[166] G. Gallios, M. Václavíková, Removal of chromium (VI) from water streams: a thermodynamic study, Environ Chem. Lett. 6 (2008) 235–240.

[167] S. Chowdhury, E. Yanful, Kinetics of cadmium(II) uptake by mixed maghemite-magnetite nanoparticles, J. Environ. Manage. 129 (2013) 642-651.

[168] D. Mehta, S. Mazumdar, S.K. Singh, Magnetic adsorbents for the treatment of water/wastewater-A review, J. Water Process Eng. 7 (2015) 244-265.

[169] Y. Feng, J-L. Gong, G-M. Zeng, Q-Y. Niua, H-Y. Zhang, C-G. Niua, J-H. Deng, M. Yan, Adsorption of Cd (II) and Zn (II) from aqueous solutions using magnetic hydroxyapatite nanoparticles as adsorbents, Chem. Eng. J. 162 (2010) 487-494.

[170] J-H. Deng, X-R. Zhang, G-M. Zeng, J-L. Gong, Q-Y. Niu, J. Liang, Simultaneous removal of Cd(II) and ionic dyes from aqueous solution using magnetic graphene oxide nanocomposite as an adsorbent, Chem. Eng. J. 226 (2013) 189-200.

[171] G. Zeng, Y. Liu, L. Tang, G. Yang, Y. Pang, Y. Zhang, Y. Zhou , Z. Li , M. Li, M. Lai, X. He, Y. He, Enhancement of Cd(II) adsorption by polyacrylic acid modified magnetic mesoporous carbon, Chem. Eng. J. 259 (2015) 153-160.

[172] J. Zhao, J. Liu, N. Li, W. Wang, J. Nan, Z. Zhao, F. Cui, Highly efficient removal of bivalent heavy metals from aqueous systems by magnetic porous Fe_3O_4-MnO_2: Adsorption behavior and process study, Chem. Eng. J. 304 (2016) 737-746.

[173] Y.F. Shen, J. Tang, Z.H. Nie, Y.D.Wang, Y. Ren, L. Zuo, Preparation and application of magnetic Fe_3O_4 nanoparticles for wastewater purification, Sep. Purif. Technol. 68 (2009) 312-319.

[174] S. R. Chowdhury, E. K. Yanful, Arsenic and chromium removal by mixed magnetite maghemite nanoparticles and the effect of phosphate on removal, J. Environ. Manage. 91 (2010) 2238-2247

[175] N. Mthombeni, M. Onyango,O. Aoyi, Adsorption of hexavalent chromium onto magnetic natural zeolite-polymer composite, J. Taiwan Inst. Chem. Eng. 50 (2015) 242-251.

[176] X. Lv, J. Xu, G. Jiang, J. Tang, X. Xu, Highly active nanoscale zero-valent iron (nZVI)–Fe_3O_4 nanocomposites for the removal of chromium(VI) from aqueous solutions, J. Colloid Interf. Sci. 369 (2012) 460-469.

[177] S. Bayazit, Ö. Kerkez, Hexavalent chromium adsorption on superparamagnetic multi-wall carbon nanotubes and activated carbon composites, Chem. Eng. Res. Des. 92 (2014) 2725-2733.

[178] D. Gusain, V. Srivastava, M. Sillanpaa, Y. C. Sharma, Kinetics and isotherm study on adsorption of chromium on nano crystalline iron oxide/hydroxide: linear and nonlinear analysis of isotherm and kinetic parameters, Res. Chem. Intermed . 42 (2016) 7133-7151.

[179] Y. Wei-Chun, T. Qiong-Zhi, D. Shu-Yu, C. Li-Yuan, W. Hai-Ying, Single-step synthesis of magnetic chitosan composites and application for chromate (Cr(VI)) removal, J. Cent. South Univ. 23 (2016) 317-323.

[180] C. Su, Environmental implications and applications of engineered nanoscale magnetite and its hybrid nanocomposites: A review of recent literature, J.Hazard. Mater. 322 (2017) 48–84.

[181] A. B. Savić, Dj. Čokeša, S. Lazarević, B. Jokić, Dj. Janaćković, R. Petrović, Lj. S. Živković, Tailoring of magnetite powder properties for enhanced phosphate removal: Effect of PEG addition in the synthesis process, Powder Technol. 301 (2016) 511–519

Curriculum Vitae

Date and place of birth: 25.03.1981.

Place of birth: Alkums, Libya

1988-1993: Primary school: "Elhafir school", Alkums, Libya

1994-1996: Elementary school: "Elhafir school", Alkums, Libya

1997-1999: High school: "Elhafir school", Alkoms, Libya

2000-2004: Bachelor study: University of Elmergib (Alhums, Libya), Faculty of Engineering, Chemical engineering

2006-2009: Worked as teaching assistant at the University of Elmergib, Faculty of Engineering, Chemical engineering

2010-2012: Master study: University of Belgrade, Faculty of Technology and Metallurgy, Belgrade, Serbia.

Master thesis: "The sorption of cadmium ions from the sea water and different aquatic solutions on modified zeolite".

2013-2017: PhD study: University of Belgrade, Faculty of Technology and Metallurgy, Belgrade, Serbia.

Published papers:

[1] A. Ahribesh, S. Lazarević, I. Janković-Častvan, B. Jokić, V. Spasojević, T. Radetić, Đ. Janaćković, R. Petrović, Influence of the synthesis parameters on the properties of the sepiolitebased magnetic adsorbents, Powder Technol. 305 (2017) 260-269.

[2] A. Ahribesh, S. Lazarević, B. Potkonjak, A. Bjelajac, D. Janaćković, R. Petrović, Sorption of cadmium ions from saline waters onto Fe(III)-zeolite, Hem. Ind. 69 (2015) 253-260.

[3] A. A. Ahribesh, S. Lazarević, I. Janković-Častvan, B. Jokić, Đ. Janaćković, R. Petrović: Synthesis of magnetic sepiolite nanocomposites for the removal of heavy metal ions from aqueous solutions, - Programme and the book of abstracts of the 3rd Conference of the Serbian Society for Ceramic Materials, Belgrade, 2015, p. 80.

Прилог 1.

Изјава о ауторству

Потписани-а   **Aysha Ali Ahribesh**

Број индекса или пријаве докторске дисертације   **4039/2013**

Изјављујем

да је докторска дисертација под насловом

„Синтеза, карактеризација и примена магнетних адсорбената на бази сепиолита и зеолита" (Synthesis, characterization and application of magnetic adsorbents based on sepiolite and zeolite)

- резултат сопственог истраживачког рада,
- да предложена дисертација у целини ни у деловима није била предложена за добијање било које дипломе према студијским програмима других високошколских установа,
- да су резултати коректно наведени и
- да нисам кршио/ла ауторска права и користио интелектуалну својину других лица.

Потпис докторанда

У Београду,   13.02.2017.

Прилог 2.

Изјава о истоветности штампане и електронске верзије докторског рада

Име и презиме аутора __Aysha Ali Ahribesh__

Број индекса или пријаве докторске дисертације __4039/2013__

Студијски програм __Хемијско инжењерство__

Наслов рада „Синтеза, карактеризација и примена магнетних адсорбената на бази сепиолита и зеолита" (Synthesis, characterization and application of magnetic adsorbents based on sepiolite and zeolite)

Ментор __проф. др Рада Петровић__

Потписани __Aysha Ali Ahribesh__

изјављујем да је штампана верзија мог докторског рада истоветна електронској верзији коју сам предао/ла за објављивање на порталу **Дигиталног репозиторијума Универзитета у Београду.**

Дозвољавам да се објаве моји лични подаци везани за добијање академског звања доктора наука, као што су име и презиме, година и место рођења и датум одбране рада.

Ови лични подаци могу се објавити на мрежним страницама дигиталне библиотеке, у електронском каталогу и у публикацијама Универзитета у Београду.

                                                                                    Потпис докторанда

У Београду, __13.02.2017.__

Прилог 3.

Изјава о коришћењу

Овлашћујем Универзитетску библиотеку „Светозар Марковић" да у Дигитални репозиторијум Универзитета у Београду унесе моју докторску дисертацију под насловом:

„Синтеза, карактеризација и примена магнетних адсорбената на бази сепиолита и зеолита" (Synthesis, characterization and application of magnetic adsorbents based on sepiolite and zeolite)

која је моје ауторско дело.

Дисертацију са свим прилозима предао/ла сам у електронском формату погодном за трајно архивирање.

Моју докторску дисертацију похрањену у Дигитални репозиторијум Универзитета у Београду могу да користе сви који поштују одредбе садржане у одабраном типу лиценце Креативне заједнице (Creative Commons) за коју сам се одлучио/ла.

1. Ауторство

2. Ауторство - некомерцијално

3. Ауторство – некомерцијално – без прераде

4. Ауторство – некомерцијално – делити под истим условима

5. Ауторство – без прераде

6. Ауторство – делити под истим условима

(Молимо да заокружите само једну од шест понуђених лиценци, кратак опис лиценци дат је на полеђини листа).

Потпис докторанда

У Београду, ___13.02.2017._____

1. Ауторство - Дозвољавате умножавање, дистрибуцију и јавно саопштавање дела, и прераде, ако се наведе име аутора на начин одређен од стране аутора или даваоца лиценце, чак и у комерцијалне сврхе. Ово је најслободнија од свих лиценци.

2. Ауторство – некомерцијално. Дозвољавате умножавање, дистрибуцију и јавно саопштавање дела, и прераде, ако се наведе име аутора на начин одређен од стране аутора или даваоца лиценце. Ова лиценца не дозвољава комерцијалну употребу дела.

3. Ауторство - некомерцијално – без прераде. Дозвољавате умножавање, дистрибуцију и јавно саопштавање дела, без промена, преобликовања или употребе дела у свом делу, ако се наведе име аутора на начин одређен од стране аутора или даваоца лиценце. Ова лиценца не дозвољава комерцијалну употребу дела. У односу на све остале лиценце, овом лиценцом се ограничава највећи обим права коришћења дела.

4. Ауторство - некомерцијално – делити под истим условима. Дозвољавате умножавање, дистрибуцију и јавно саопштавање дела, и прераде, ако се наведе име аутора на начин одређен од стране аутора или даваоца лиценце и ако се прерада дистрибуира под истом или сличном лиценцом. Ова лиценца не дозвољава комерцијалну употребу дела и прерада.

5. Ауторство – без прераде. Дозвољавате умножавање, дистрибуцију и јавно саопштавање дела, без промена, преобликовања или употребе дела у свом делу, ако се наведе име аутора на начин одређен од стране аутора или даваоца лиценце. Ова лиценца дозвољава комерцијалну употребу дела.

6. Ауторство - делити под истим условима. Дозвољавате умножавање, дистрибуцију и јавно саопштавање дела, и прераде, ако се наведе име аутора на начин одређен од стране аутора или даваоца лиценце и ако се прерада дистрибуира под истом или сличном лиценцом. Ова лиценца дозвољава комерцијалну употребу дела и прерада. Слична је софтверским лиценцама, односно лиценцама отвореног кода.